A.D. MDLXII

UNIVERSITY OF SASSARI

PH.D. SCHOOL IN NATURAL SCIENCE

*Dissertation for the Degree of Doctor of Philosophy in
Science and technology of minerals and rocks of industrial interest
presented at Sassari University in 2012*

XXV CYCLE

Prospecting of Industrial Minerals:
a geophysical approach

DIRECTOR: PROF. MARCO CURINI GALLETTI

COORDINATOR: PROF. GIACOMO OGGIANO

TUTOR: **PH.D. STUDENT:**

PROF. GIACOMO OGGIANO   DR. VITTORIO LONGO

Vittorio Longo - Prospecting of Industrial Minerals: a geophysical approach -
PhD Thesis in Natural Science - University of Sassari

1

Vittorio Longo - Prospecting of Industrial Minerals: a geophysical approach -
PhD Thesis in Natural Science - University of Sassari

2

Abstract

This work deals with the evaluation of the electrical resistivity method for the identification and characterization of industrial minerals deposits.

The ERT (Electrical Resistivity Tomography) technique is demonstratively applied to 4 different areas of the central and northern Sardinia.

The research focused on clays, which generally have conductivity values greater than those of the host lithotypes. In this regard, a bentonite deposit close Ozieri (N-Sardinia) was investigated by 2D and 3D ERT surveys, and a preliminary study was conducted in the northern part of Nurra (NW-Sardinia) in order to discriminate Messinian clay deposits from the underlying bedrock.

The ERT method was also tested on cineritic levels, which for their absorption properties are increasingly required as litter for pets. Potentially exploitable cineritic levels have been identified in two different sites of central Sardinia (Macomer and Zerfaliu), within the Oligo-Miocene calcalkaline volcanic sequence.

In all the 4 case studies it is attempted: 1) to define the geometry of the deposits; 2) to estimate the reserves and locate the main faults useful to decipher the ore-forming processes; 3) to evaluate the reliability of the ERT method by cross-checking the results with boreholes data.

The results indicate that ERT method may represent a relatively cheap and powerful tool to obtain high-resolution geological and stratigraphic information on clayey and cineritic bodies.

Keywords: Industrial Minerals, Electrical Resistivity Tomography (ERT), bentonitic clays, cineritic levels.

Vittorio Longo - Prospecting of Industrial Minerals: a geophysical approach -
PhD Thesis in Natural Science - University of Sassari

3

Riassunto

Questo lavoro si occupa della valutazione del metodo della resistività elettrica per l'identificazione e la caratterizzazione di depositi di minerali industriali.

La tecnica ERT (Electrical Resistivity Tomography) è stata applicata in modo dimostrativo a 4 differenti aree della Sardegna centrale e settentrionale.

La ricerca è stata focalizzata principalmente sulle argille, che presentano generalmente valori di conducibilità più elevati rispetto ai litotipi incassanti. A tal proposito, è stato investigato mediante indagini 2D e 3D ERT un deposito di argille bentonitiche in prossimità di Ozieri (N-Sardegna), e uno studio preliminare è stato condotto nella Nurra settentrionale (NW-Sardegna) al fine di discriminare alcuni depositi di argille Messiniane dal bedrock sottostante.

Il metodo ERT è stato anche testato su livelli cineritici, i quali per le loro proprietà assorbenti sono sempre più richiesti come lettiere per animali domestici. Alcuni livelli cineritici potenzialmente estraibili sono stati individuati, all'interno della sequenza vulcanica calcalcalina Oligo-Miocenica, in due differenti siti della Sardegna centrale (Macomer e Zerfaliu).

In tutti i casi di studio si è cercato di: 1) definire la geometria dei depositi; 2) stimare le riserve disponibili e localizzare le principali faglie utili a decifrare i processi di formazione delle mineralizzazioni; 3) valutare l'affidabilità del metodo ERT mediante il confronto incrociato tra i dati indiretti e i dati dei sondaggi.

I risultati indicano che il metodo ERT può rappresentare uno strumento potente e a basso costo che consente di ottenere informazioni geologiche e stratigrafiche ad alta risoluzione sui corpi argillosi e cineritici.

Parole chiave: Minerali Industriali, Tomografia Elettrica di Resistività (ERT), argille bentonitiche, livelli cineritici.

Vittorio Longo - Prospecting of Industrial Minerals: a geophysical approach -
PhD Thesis in Natural Science - University of Sassari

4

Introduction

Research and exploration of Industrial Minerals (IM) had a significant increase in Sardinia after the crisis of the metal ores sector.

The industrial minerals includes generally a wide range of solid material extracted for purpose other than energy and metals production (Manning, 1994) implying a "for use" classification and not a mineralogical one.

IM resources are used in a wide range of applications in their natural state or after beneficiation either as raw materials or as additives.

Compared to metallic ores, which generally require large-scale investment both in exploitation and beneficiation process, the deposits of IM not necessarily must imply conspicuous investment.

Prospecting and evaluating the potential mineral resources is one of basic issues for the enterprise operating in the IM field.

Some geophysical methods provide an important contribution in defining the geometric characteristics of the mineralized bodies (thickness, lateral extent, depth).

On this concern Electrical Resistivity Tomography (ERT) could represent the resolutive geophysical methodology. It is allows generating models of subsurface electrical property distributions, from which subsurface geological variations can be identified.

With the aim to test the efficacy of ERT method in prospecting and quantifying deposits of conductive IM within the Tertiary volcanic and sedimentary complexes of Sardinia, this Ph.D. thesis focused on: i) bentonitic clays derived from Tertiary volcanites, which generally have conductivity values greater than those of several host lithotypes; ii) cineritic levels, which for their absorption properties are increasingly required by the market; iii) Messinian sedimentary clays linked to a wide alluvial system.

The ERT technique is demonstratively applied to 4 different areas of the central and northern Sardinia. In all areas a preliminary geological survey was performed, with a next phase of data collection and analysis of the electrical resistivity resulting models.

The four case studies allowed evaluating the potential and limitations of the method.

The thesis is structured as follows:

Chapter 1 considers the theoretical basis of the electrical resistivity method and analyzes the advantages of the ERT compared to monodimensional resistivity surveys.

Vittorio Longo - Prospecting of Industrial Minerals: a geophysical approach -
PhD Thesis in Natural Science - University of Sassari

5

In **chapter 2** both the galvanic coupling georesistivimeter Abem Terrameter SAS1000 and the programs used for the data inversion are described.

A brief geodynamic setting of Sardinia in Cenozoic age is reported in **chapter 3**, with particular reference to calcalkaline volcanics rocks, which host the most important industrial minerals deposits.

An example of application of 2D and 3D ERT method on a bentonitic clay deposit near Ozieri (N-Sardinia) is presented in **chapter 4**.

The aim of this survey was to define the spatial patterns of the mineralized body, and to assess the available reserves in a deposit area before of the mining activity.

At Zerfaliu and Macomer (central Sardinia), the 2D ERT method was used as a guideline to prospecting exploitable cineritic deposits (**chapters 5 and 6** respectively).

Chapter 7 shows a preliminary study carried out in northern part of Nurra region (N-W Sardinia) in order to discriminate Messinian clay deposits by the underlying bedrock, and in the meantime defining the thickness and extension of the clayey body.

The thesis concludes with general considerations on the ERT method applied to Industrial Minerals research (**chapter 8**).

References

MANNING, D.A.C., 1994. *Introduction to Industrial Minerals.* Chapman and Hall Eds., 288.

Vittorio Longo - Prospecting of Industrial Minerals: a geophysical approach -
PhD Thesis in Natural Science - University of Sassari

6

Chap. 1 - The electrical resistivity method

The geoelectrical methods can be divided into two main groups: i) passive methods that use natural electric currents exist in the subsurface and ii) active methods that use artificial electrical currents placed into the ground.

Among the active methods, the Direct Current (DC) resistivity method is the traditional way of measuring the resistivity of the subsurface.

The technique employs an artificial source of direct or pseudo-direct electric current injected into the ground via galvanic contact through point electrodes, thus creating stationary current flow in the earth. By measuring potentials at the surface in the vicinity of this current flow it is then possible to determine the effective resistivity of the subsurface for a given electrode geometry (Kuras, 2002).

Electrical resistivity techniques have been used in many geological formations for characterizing the subsurface for many years (Roman, 1951; Recelli-Synder et al., 1997) because of the wide range of resistivity values found in nature.

The full theory of DC resistivity is set out in geophysical textbooks such as Parasnis, (1997); Reynolds, (1997); Telford et al., (1990) or Dobrin and Savit, (1988).

The fundamental physical law used in resistivity survey is Ohm's Law that governs the flow of current in the ground.

In 1827, Georg Simon Ohm derived empirical relationship between the resistance (**R**) of a resistor in a simple series circuit, the current passing through the resistor (**I**), and the corresponding change in potential (**ΔV**):

$$\Delta V = \ R \cdot I \qquad\qquad (1.1)$$

The units of **R**, **V**, and **I** are Ohms [Ω], Volts [V], and Amperes [A] respectively.

A simple series circuit that consists of a battery connected to a resistor (cylindrical-shaped body with uniform resistivity) by a wire demonstrates this relationship.

Through the Ohm's Law, the value of resistance (R) can easily be calculated once the voltage (**ΔV**) and current (**I**) are known in equation 1.1.

The electrical resistance is defined as "the opposite offered by a body or substance to the passage through it of a steady electric current".

The electrical resistivity method concept is based on this empirical relation (1.1), with the assumption that the resistor in the circuit is the Earth.

Vittorio Longo - Prospecting of Industrial Minerals: a geophysical approach -
PhD Thesis in Natural Science - University of Sassari

7

There is another relationship that defines resistance (**R**) as a function of geometry of a resistor and the resistivity of the cylindrical-shaped body:

$$R = \frac{\rho \cdot L}{A}$$
(1.2)

For a given material, the resistance is inversely proportional to the cross-sectional area (**A**) [m^2] and is proportional to the length (**L**) [m] of element (fig. 1.1).

A factor that defines the ease for electrical current to flow through the media is known as resistivity (ρ).
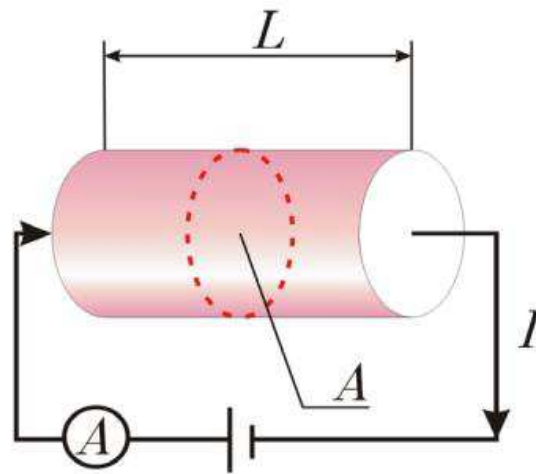
Fig. 1.1 - Electric circuit consisting of a battery and a resistor, Ohm' s Law (Muchaidze, 2008).

By rearranging equation (1.2) the resistivity can be expressed as:

$$\rho = \frac{R \cdot A}{L}$$
(1.3)

The electrical resistivity is a internal parameter of the material and the unit is Ohm-meter [Ω·m]; it quantifies how strongly the material opposes the flow of electric current.

High values of resistivity imply that the material making up the wire is very resistant to the flow of electricity. Low values of resistivity show that the wire transmits electrical current very easily (Muchaidze, 2008).

Less frequently, in geophysical investigations, the parameter of conductivity (σ) is measured. The conductivity is the inverse of resistivity (**1/ρ**), it has unit of Siemens/meter [S/m].

Vittorio Longo - Prospecting of Industrial Minerals: a geophysical approach -
PhD Thesis in Natural Science - University of Sassari

8

1.1 - Electrical properties of Earth materials

There are three ways in which electric current can be conducted through a rock: electrolytic, electronic and dielectric conduction.

- *Electrolytic or ionic conduction:* occurs by the relatively slow movement of ions within an electrolyte (i.e. groundwater) and depends upon the ion, ionic concentration and mobility, etc. The ions in the electrolyte are mobilized by an electric field, which causes a current flow and involves the physical transport of material (ions).

- *Electronic conduction:* the current flow occurs through free electrons, which are not strongly attached to atoms, as in metals. The metallic sulphides (such as pyrrhotite, galena and pirite) show this type of electrical conduction, and exhibit very low resistivity values, typically less than 1 $\Omega \cdot m$ (Bernard, 2003).

- *Dielectric conduction:* occurs in very weakly conducting materials (or insulator) when an external alternating current is applied, so causing atomic electrons to be shifted slightly with respect to their nuclei. Most minerals, show a dielectric conduction, such as some silicate, carbonate and sulphates in dry conditions.

Generally, the rocks in the natural state are permeated with pore water rich in salts, therefore the electrolytic conduction is the main mechanism of electrical conduction.

The electrical conductivity of earth materials is influenced by many factors as: mineralogical composition, porosity, saturation, presence of clayey minerals and organic materials, fracturation or fissuring etc.

The solid matrix of grains is largely semi–conducting, with notable exceptions being metallic grains and the surface of certain clay minerals which are conducting.

Groundwater filling the pore spaces of rocks, is a natural electrolyte with a considerable amount of ions. As a rule, the more porous or fissured is a rock and a more amount its groundwater content, the higher is the conductivity and the lower the resistivity.

If a water-bearing rock contains clay minerals, a relative number if ions may be released from such minerals by ion exchange processes.

Clays are hydrated minerals with high porosities and low permeabilities. The minerals themselves may not be very conductive, but their surface causes an excess of cations in the pore fluid immediately adjacent to the clay minerals surface.

The result is high conductivity near the clay minerals surface, which can dominate the overall conductance if the pore water conductivity is low.

Vittorio Longo - Prospecting of Industrial Minerals: a geophysical approach -
PhD Thesis in Natural Science - University of Sassari

9

Generally intact rocks are resistive, but many geological processes can alter a rock and significantly lower its resistivity.

Dissolutions, faulting, shearing, columnar jointing, weathering, and hydrothermal alteration usually increase porosity and fluid permeability, and hence lower the resistivity. In contrast, precipitation of calcium carbonate or silica reduces porosity and hence increases the resistivity.

Hardening of a rock by compaction and/or metamorphism will reduce porosity and permeability, and therefore increase the resistivity.

Resistivity is, therefore, an extremely variable parameter, not only from formation to formation but within a particular formation (Udphuay, 2008).

Due to many factors that influence the overall resistivity of a rock, it seems clear the impossibility to attribute unique values of resistivity for each class of rocks or soils; for these can be establish the range of resistivity values, often very large.

Generalizing, igneous and metamorphic rocks typically have high resistivity values. The resistivity of these rocks is greatly dependent on the degree of fracturing, and the percentage of the fractures filled with groundwater.

These rock type can have a large range of resistivity, from about 1000 to 10 million Ω·m, depending on whether it is wet or dry (fig. 1.2A).

Sedimentary rocks, which are usually more porous and have higher water content, normally have lower resistivity values (from 10 to about 10000 Ω·m, with most values below 1000 Ω·m) compared to igneous and metamorphic rocks (Loke, 2010).

The resistivity of common rocks and soil materials (Daniels and Alberty, 1966; Telford et al., 1990) is shown in figure 1.2A-B.

Vittorio Longo - Prospecting of Industrial Minerals: a geophysical approach -
PhD Thesis in Natural Science - University of Sassari

10

Resistivity in ohm.m

A)
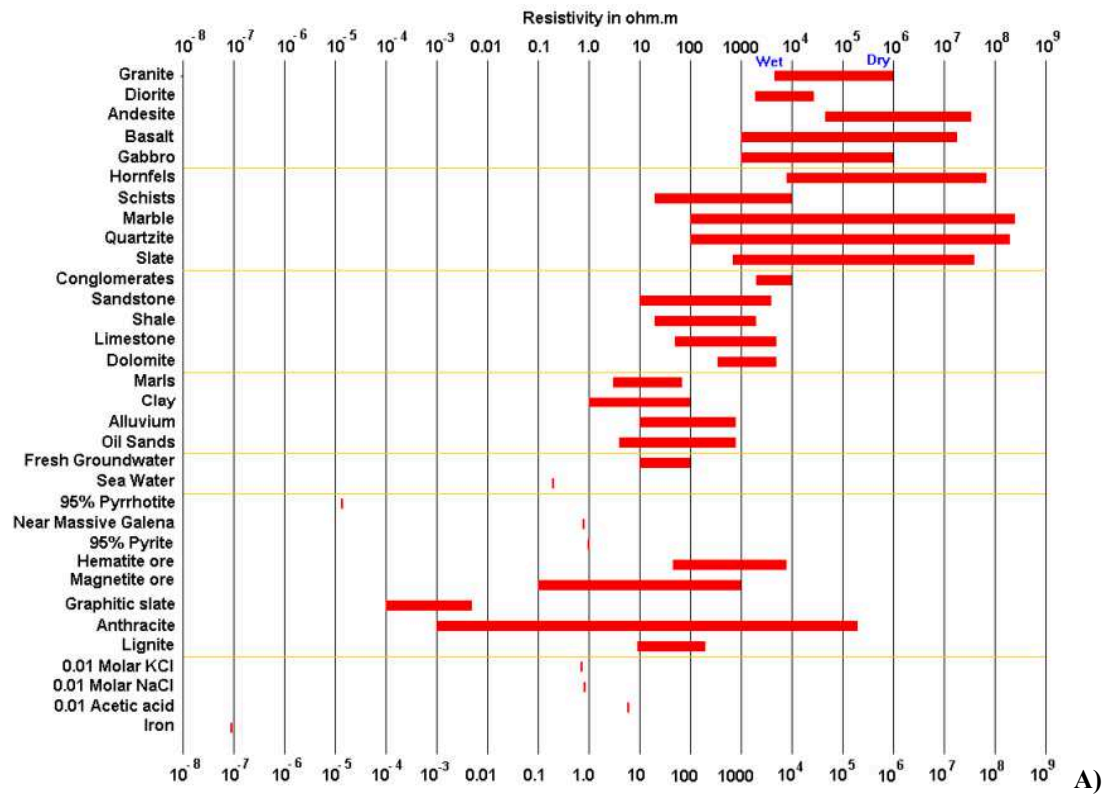
Material	Resistivity (Ω.m)	Conductivity (Ω.m)$^{-1}$
Igneous & metamorphic rocks		
Granite	$5 \times 10^3 - 10^6$	$10^{-6} - 2 \times 10^{-4}$
Basalt	$10^3 - 10^6$	$10^{-6} - 10^{-3}$
Slate	$6 \times 10^2 - 4 \times 10^7$	$2.5 \times 10^{-8} - 1.7 \times 10^{-3}$
Marble	$10^2 - 2.5 \times 10^8$	$4 \times 10^{-9} - 10^{-2}$
Quartzite	$10^2 - 2 \times 10^8$	$5 \times 10^{-9} - 10^{-2}$
Sedimentary Rocks		
Sandstone	$8 - 4 \times 10^3$	$2.5 \times 10^{-4} - 0.125$
Shale	$20 - 2 \times 10^3$	$5 \times 10^{-4} - 0.05$
Limestone	$50 - 4 \times 10^2$	$2.5 \times 10^{-3} - 0.02$
Soils and Waters		
Clay	$1 - 100$	$0.01 - 1$
Alluvium	$10 - 800$	$1.25 \times 10^{-3} - 0.1$
Groundwater (fresh)	$10 - 100$	$0.01 - 0.1$
Sea water	$0 - 15$	6.7
Chemicals and Metals		
Iron	9.074×10^{-8}	1.102×10^7
0.01 M Potassium chloride	0.708	1.413
0.01 M Sodium chloride	0.843	1.185
0.01 M acetic acid	6.130	0.163
Xylene	6.998×10^{16}	1.429×10^{-17}

B)

Fig. 1.2 - The resistivity of some common rocks, soils, minerals, chemical and metals (A - from Loke, 2010; B - after Loke, 1997).

Vittorio Longo - Prospecting of Industrial Minerals: a geophysical approach -
PhD Thesis in Natural Science - University of Sassari

11

1.2 - Basic resistivity theory

The estimation of the apparent resistivity of the Earth is relatively simple if several assumptions are made. The first assumption is that a model-Earth is uniform and homogeneous, thus it possesses constant resistivity throughout the entire Earth.

The second assumption is that the Earth is a hemispherical resistor in a simple circuit consisting of a battery and two electrodes (the source and the sink electrodes) pounded into the ground (fig. 1.3A).

The battery generates direct electrical current that enters the Earth at the source electrode connected to the positive portal of the battery. The current exits at the sink electrode coupled to the negative portal of the battery (Muchaidze, 2008).
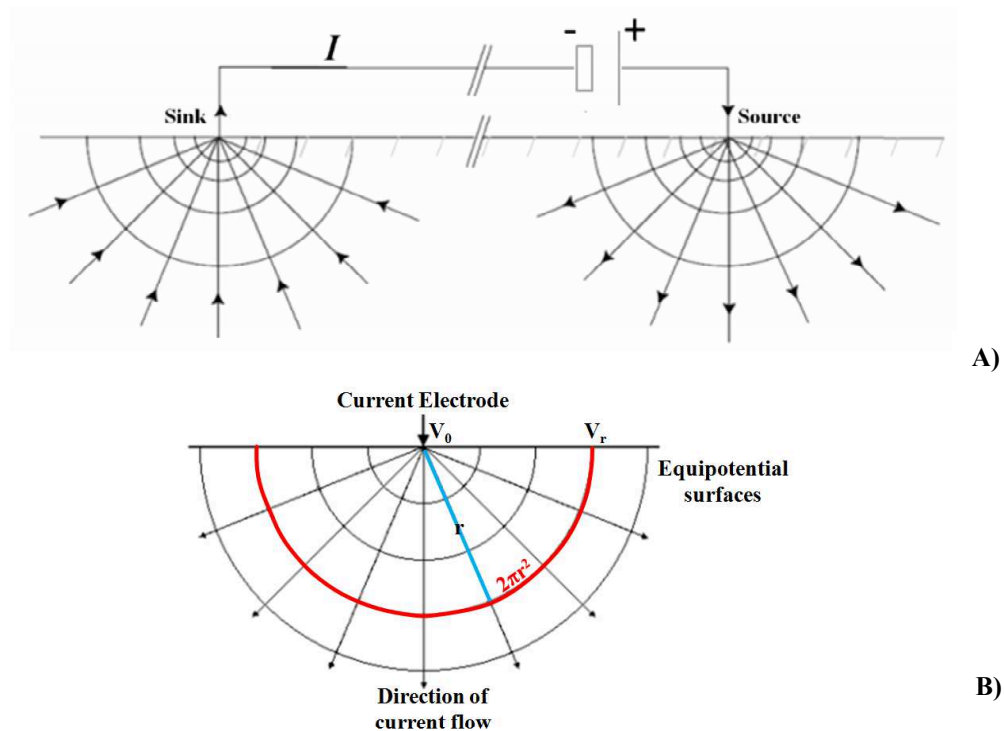
Fig. 1.3 - A) Current lines radiating from the source electrode and converging on the sink. B) The flow of current from a point current source into a homogeneous Earth and the resulting potential distribution.

When current with **I** intensity is introduced to the ground , it is compelled to mode outward from the source electrode. Since we assume that the Earth is homogeneous the current spreads in all directions from the electrode, and at each moment of time, the current front will move through a hemispherical zone (equipotential surface) (fig. 1.3B).

Vittorio Longo - Prospecting of Industrial Minerals: a geophysical approach -
PhD Thesis in Natural Science - University of Sassari

12

The hemispherical shape of equipotential surfaces can be explained by imagining to locate a current electrode deep into the ground. The current flows in this case in a radial form and the equipotential surfaces show a spherical shape.

When the current point is close to the surface, the current lines and equipotential surfaces are distorted.

Finally, when the current electrode is placed on the surface, the current lines are again radial, but affect only the portion below the surface and the equipotential surfaces take on a hemispherical shape involving only the subsoil (fig. 1.4).
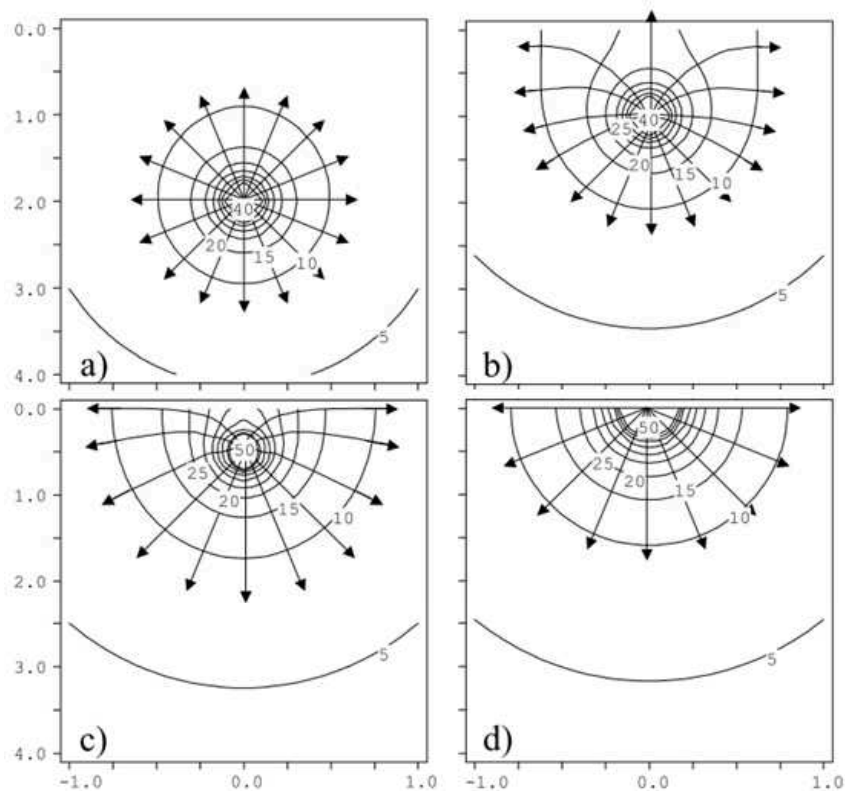
Fig. 1.4 - Current flow and equipotential surfaces for one electrode in different positions. a) electrode located 2m depth, b) electrode located 1m depth, c) electrode to 0,50cm depth, d) shallow electrode.

The area of such hemispherical zone can be found from the relationship:

$$A = 2\pi r^2 \tag{1.4}$$

where *r* is the distance from the source electrode to the point on the hemisphere surface.

Vittorio Longo - Prospecting of Industrial Minerals: a geophysical approach -
PhD Thesis in Natural Science - University of Sassari

13

By substituting equation (1.4) into equation (1.3), we can obtain an expression that defines resistance of the media at a point separated from the source by distance r:

$$R = \frac{\rho}{2\pi r}$$

(1.5)

Combining Ohm's Law expressed by equation (1.1) and equation (1.5) can be found the potential difference resulting from the flow of current through the hemispherical resistor:

$$\Delta V = \frac{I \cdot \rho}{2\pi r}$$

(1.6)

whit:

$$\Delta V = V_0 - V_r$$

(1.7)

where V_0 is a potential at the source electrode;

V_r is a potential at the surface of the hemisphere with radius r.

Since the potential (V_0) at source electrode is 0, the potential for a point located at the surface of the hemisphere with radius r (fig. 1.3B) is:

$$V_r = \frac{I \cdot \rho}{2\pi r}$$

(1.8)

This equation demonstrates, that for any point located at the hemispherical surface with radius r, the potential difference between this point and source electrode is the same.

In other words, the potential difference between a source and any point on the equipotential surface has the same numerical value.

Vittorio Longo - Prospecting of Industrial Minerals: a geophysical approach -
PhD Thesis in Natural Science - University of Sassari

14

1.2.1 - The four-electrode arrays and apparent resistivity

In the field, two electrodes are required in order to pass an electric current into the ground. The current electrodes are commonly referred to as C_1 and C_2. Other two electrodes are connected to a voltmeter and are used to measure a potential difference between two points on the surface. These are called potential electrodes and referred to as P1 and P2. This concept of a four-electrode array is show in figure 1.5:
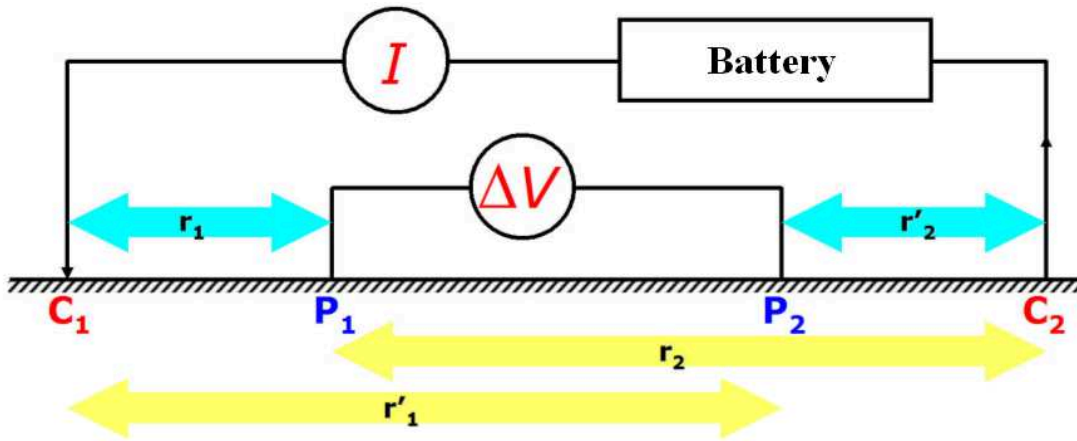
Fig. 1.5 - Scheme of four-electrode array with the interelectrode relative distances.

Since the distance between the current electrodes is necessarily finite, the potential at any surface point nearby will be affected by both.
The potential due to C_1 and C_2 observed at a potential electrode P_1 is obtained by:

$$V_{P1} = \frac{I \cdot \rho}{2\pi} * \left(\frac{1}{r_1} - \frac{1}{r_2} \right) \qquad (1.9)$$

Likewise the potential due to C_1 and C_2 observed at a potential electrode P_2 is obtained by:

$$V_{P2} = \frac{I \cdot \rho}{2\pi} * \left(\frac{1}{r'_1} - \frac{1}{r'_2} \right) \qquad (1.10)$$

Therefore, the potential difference (or voltage) observed between P_1 and P_2 is then given by the superposition of the individual potentials:

$$\Delta V_{P1P2} = \frac{I \cdot \rho}{2\pi} * \left[\left(\frac{1}{r_1} - \frac{1}{r_2} \right) - \left(\frac{1}{r'_1} - \frac{1}{r'_2} \right) \right] \qquad (1.11)$$

Vittorio Longo - Prospecting of Industrial Minerals: a geophysical approach -
PhD Thesis in Natural Science - University of Sassari

15

For a homogeneous isotropic subsurface, the potential difference ΔV can be measured for an array of known geometry and a know injection current.

In reality, the sub-surface ground does not conform to a homogeneous and isotropic medium and thus the resistivity obtained is no longer the "true" resistivity but the "apparent" resistivity (ρ_a).

The apparent resistivity of a half-space is given by solving (1.11) for ρ:

$$\rho_a = K \frac{\Delta V}{I} \tag{1.12}$$

where the term k is given by:

$$K = \frac{2\pi}{\left[\frac{1}{r_1} - \frac{1}{r_2} - \frac{1}{r'_1} + \frac{1}{r'_2}\right]} \tag{1.13}$$

and denote the geometric factor which depends on the specific configuration of current and potential electrodes.

The relationship between the "apparent" resistivity and the "true" resistivity is very complex and to determine the true resistivity from the apparent resistivity values, must be solved the "inversion" problem (Loke, 2010).

Consequently, all field resistivity data are apparent resistivity while those obtained by interpretation techniques are "true" resistivity.

Vittorio Longo - Prospecting of Industrial Minerals: a geophysical approach -
PhD Thesis in Natural Science - University of Sassari

16

1.3 - A comparison of different electrode arrays

The apparent resistivity values depends on the geometry of the electrode array used, as defined by the geometric factor **k**. Various array types are common use with DC resistivity, each of which has specific characteristics.

The choice of the "best" array for a field survey depends on the type of structure to be mapped, the sensitivity of the resistivity meter ad the background noise level (Loke, 2010).

The main characteristics of an array are:

- Depth of investigation;
- Sensitivity of the array to vertical and horizontal changes in the subsurface resistivity;
- Horizontal data coverage;
- Signal strength.

The first two characteristics can be determined from the sensitivity function of the array for a homogeneous Earth model. The sensitivity function basically tells us the degree to which a change in the resistivity of a section of the subsurface will influence the potential measured by the array.

The higher the value of the sensitivity function, the greater is the influence of the subsurface region on the measurement. Generally, the highest sensitivity values are found near the electrodes. At larger distance from the electrodes, the contour patterns are different for the different arrays. The difference in the contour pattern of the sensitivity function plot helps to explain the response of the different arrays to different types of structures (Loke, 2010).

Mathematically, the sensitivity function is given by the Frechet derivate (McGillivray and Oldenburg, 1990).

Consider the simplest possible array configuration show in figure 1.6 with just one current electrode (C1) located at the origin (0,0,0) and one potential electrode (P1) located at (a, 0, 0) which results in a potential φ observed.

Vittorio Longo - Prospecting of Industrial Minerals: a geophysical approach -
PhD Thesis in Natural Science - University of Sassari

17

Both electrodes are on the ground surface and they are **"a"** meters apart.

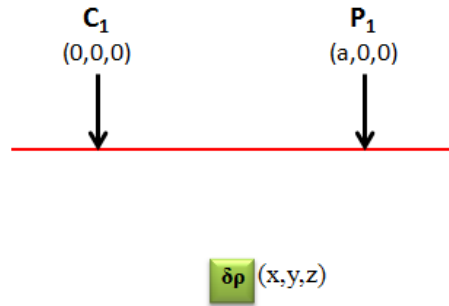C$_1$
(0,0,0)

P$_1$
(a,0,0)

δρ (x,y,z)

Fig. 1.6 - The parameters for the sensitivity function calculation at a point (x, y ,z) within a half-space.

The change the resistivity within a small volume of the ground located at (x, y, z) by a small amount **δρ**, caused a corresponding change in the potential **δφ** measured at P1.

The equation which describes this is:

$$\frac{\delta\varphi}{\delta\rho} = \int \frac{1}{4\pi^2} \cdot \frac{x\,(x-a) + y^2 + z^2}{[x^2 + y^2 + z^2]^{1.5}\,[(x-a)^2 + y^2 + z^2]^{1.5}}\, dx\,dy\,dz \quad (1.14)$$

The 3D Frechet derivate is then given by the term within the integral:

$$F_{3D}(x,y,z) = \frac{1}{4\pi^2} \cdot \frac{x\,(x-a) + y^2 + z^2}{[x^2 + y^2 + z^2]^{1.5}\,[(x-a)^2 + y^2 + z^2]^{1.5}} \quad (1.15)$$

This gives the Frechet derivative or sensitivity function for a pole-pole array consisting of just one current and one potential electrode. To obtain the Frechet derivative for a general four electrode array, the contributions from the four current-potential pair must be added.

The analysis of the sensitivity function influence the depth of investigation achieved by the various devices.

Some authors have used the maximum point as the depth of investigation of the array. However, Edwards (1977) and Barker (1989) have show that a more robust estimate is the "median depth of investigation".

To explain the relationship between the sensitivity function and the depth of investigation, a subsurface horizontal layers model and a vertical resistivity sounding is assumed.

Vittorio Longo - Prospecting of Industrial Minerals: a geophysical approach -
PhD Thesis in Natural Science - University of Sassari

18

The sensitivity function for a thin horizontal layer is obtained by integrating the 3D sensitivity function given in equation 1.15 in the x and y directions:

$$F_{1D}(z) = \frac{2}{\pi} \cdot \frac{z}{(a^2 + 4z^2)^{1.5}} \tag{1.16}$$

The above function is also known as the depth investigation characteristic and has been used by many authors to determine the properties of various arrays in resistivity sounding survey (Edwards, 1977; Barker, 1981; Merrick, 1997).

The function 1.16, if plotted in a Cartesian diagram, shows a curve with asymmetric distribution. In the curve, the maximum peak corresponding of the maximum sensitivity value and the and the median of the curve corresponds to the "median depth of investigation" (fig. 1.7)
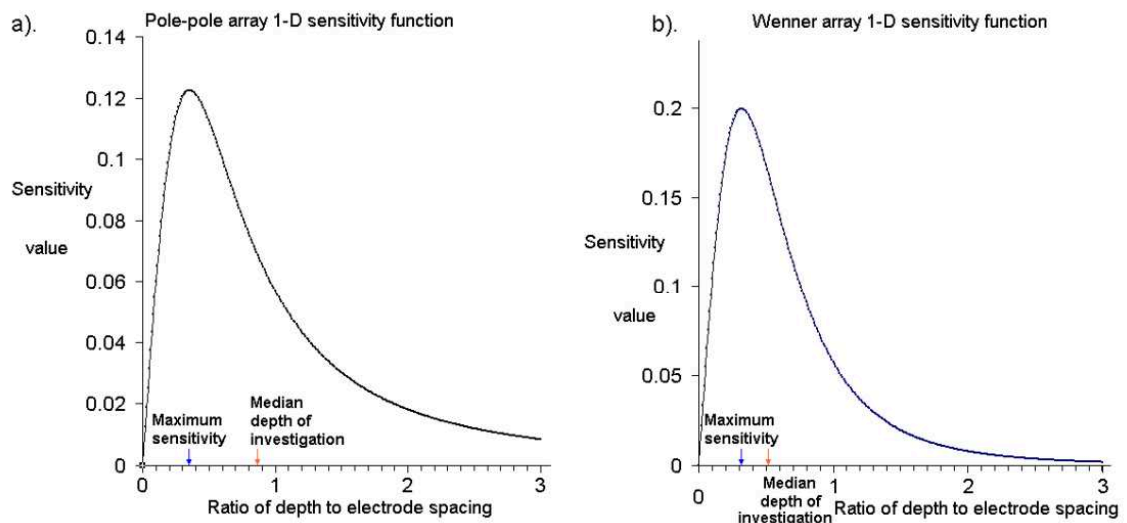
Fig. 1.7 - A plot of the 1-D sensitivity function. a) The sensitivity function for the pole-pole array. b) The sensitivity function and median depth of investigation for the Wenner array.

The "median depth of investigation" is the depth above which the area under the curve is equal to half the total area under the curve. The upper section of the Earth above the "median depth of investigation" has the same influence on the measured potential as the lower section. This tells us roughly how deep we can see with an array.

This depth does not depend on the measured apparent resistivity or the resistivity of the homogeneous Earth model. It should be noted that the depths are strictly only valid for a homogeneous Earth model, but they are probably good enough for planning field surveys (Loke, 2010).

Vittorio Longo - Prospecting of Industrial Minerals: a geophysical approach -
PhD Thesis in Natural Science - University of Sassari

19

If there are large resistivity contrasts near the surface, the actual depth of investigation could be somewhat different.

The sensitivity function for other arrays can be determine by adding up the contributions from the appropriate four pairs of current-potential electrodes.

Table 1 gives the median depth of investigation for the different arrays. To determine the maximum depth mapped by a particular survey, multiply the maximum **"a"** electrode spacing, or maximum array length **"L"**, by the appropriate depth factor **"z_e"**.

Array	z_e/a	z_e/L
Wenner α	0.519	0.173
Wenner-Schlumberger		
n = 1	0.519	0.173
n = 2	0.925	0.186
n = 3	1.318	0.189
n = 4	1.796	0.190
n = 5	2.093	0.190
n = 6	2.478	0.191
n = 7	2.863	0.191
n = 8	3.247	0.191
Dipolo-Dipolo		
n = 1	0.416	0.139
n = 2	0.697	0.174
n = 3	0.962	0.192
n = 4	1.22	0.203
n = 5	1.476	0.211
n = 6	1.73	0.216
n = 7	1.983	0.22
n = 8	2.236	0.224

Tab.1 - The median depth of investigation (z_e) for many array type (by Loke, 2010).

Therefore, the depth of investigation is a function of an array type, the physical parameters of material underlying the area of interest and the length of the array, typically ranges from one-third to one-fifth of the length of the entire array length (Edwin and Coruh, 1988).

The horizontal data coverage depends on the array type and will be discussed in detail below, in the single arrays description.

The signal strength is inversely proportional to the geometric factor used to calculate the apparent resistivity value for the arrays.

Typically, the signal strength decreases as we investigate the deeper layers. The gradient with which the signal decreases is affected by several factors as: array type, characteristic of subsurface materials and thickness of the layers.

The following will describe the arrays that are most commonly used for 2D imaging surveys.

Vittorio Longo - Prospecting of Industrial Minerals: a geophysical approach -
PhD Thesis in Natural Science - University of Sassari

20

1.3.1 - Wenner α array

In Wenner α array the distance between the various electrodes (interelectrode distance) is the same and it is equal to **"a"** according to the scheme in figure 1.8.
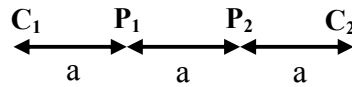

Fig. 1.8 - Wenner α array scheme.

For a four-electrode array, there are three possible permutations of the position of the electrodes (Carpenter and Habberjam, 1956). The "normal" Wenner array is technically the Wenner α array, where the potential electrodes are placed at the centre of the current electrodes.

The geometric factor for the Wenner array is **2πa**, this is smaller than the geometric factor for the other arrays. Among the common arrays, the Wenner α array has the strongest signal strength. This can be an important factor if the survey is carried in areas with high background noise.

The median depth of investigation for the Wenner α array is approximately 0.5 times the **"a"** maximum spacing used. Compared to other array, the Wenner α array has a moderate depth of investigation. The signal strength is inversely proportional to the geometric factor used to calculate the apparent resistivity value for the array.

One disadvantage of this array for 2D survey is the relatively poor horizontal coverage as the electrode spacing is increased. This could be a problem if it use a system with a relatively small number of electrodes.

In figure 1.9, the sensitivity plot for the Wenner α array has almost horizontal contours beneath the center of the array.
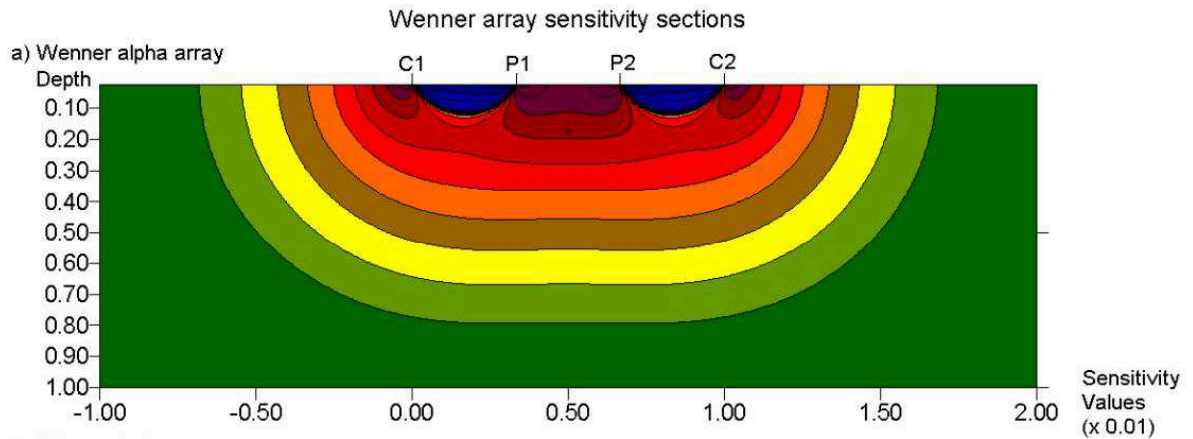
Vittorio Longo - Prospecting of Industrial Minerals: a geophysical approach -
PhD Thesis in Natural Science - University of Sassari

21

Fig. 1.9 - 2-D sensitivity section for the Wenner α array (Loke, 2010).

As a result of this property, the Wenner array is relatively sensitive to vertical changes in the subsurface resistivity below the center of the array. However, it is less sensitive to horizontal changes in the subsurface resistivity.

In general, the Wenner α is good in resolving vertical changes (i.e. horizontal structure), but relatively poor in detecting horizontal changes (i.e. narrow vertical structures).

1.3.2 - Wenner-Schlumberger array

This is a new hybrid between the Wenner and Schlumberger arrays (Pazdirek and Blaha, 1996). The arrangement of electrodes for this array is show below in figure 1.10.
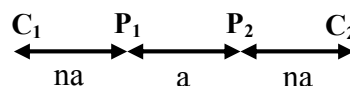
Fig. 1.10 - Wenner-Schlumberger array scheme.

The **"n"** factor for this array is the ratio of the distance between the C1-P1 (or P2-C2) electrodes to the spacing between the P1-P2 potential pair. The Wenner α array is a special case of this array where the **"n"** factor is equal to 1.

The geometric factor is: $K = \pi n (n+1)a$. Accordingly the signal strength for this array is approximately inversely proportional to the square of the **"n"** value. The signal strength is weaker than that for the Wenner array. The median depth of investigation for this array is about 10% larger than that for the Wenner array for the same distance between the outer (C1 and C2) electrodes for high **"n"** values.

The Wenner-Schlumberger arrays has a slightly better horizontal coverage than that the Wenner array. For the Wenner array each deeper data level has 3 data points less than the

Vittorio Longo - Prospecting of Industrial Minerals: a geophysical approach -
PhD Thesis in Natural Science - University of Sassari

22

previous data level, while for the Wenner-Schlumberger array there is a loss of 2 data points with each deeper data level.

The figure 1.11 shows the sensitivity pattern for this array as the **"n"** factor is increased from 1 (Wenner α array) to 6 (the classical Schlumberger array).
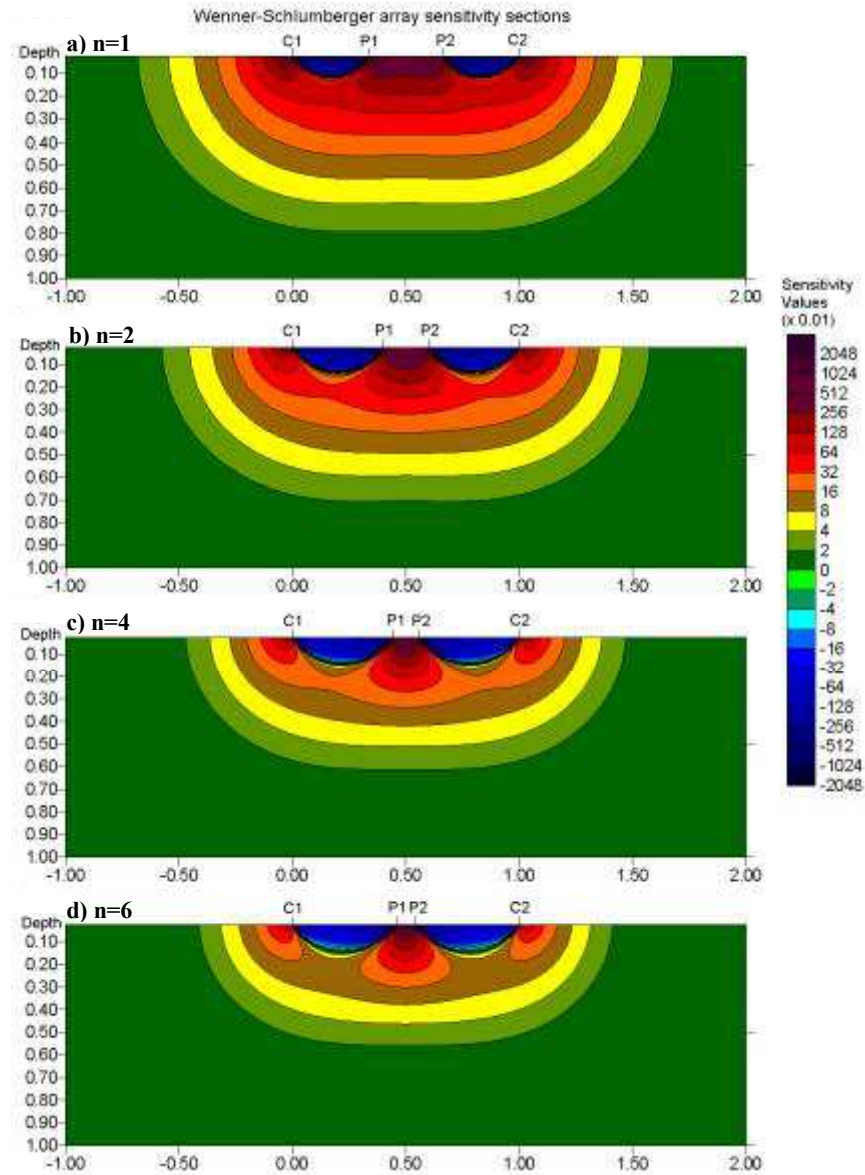
Fig. 1.11 - 2-D sensitivity sections for the Wenner-Schlumberger array. The sensitivity sections with: a) *n*=1, b) *n*=2, c) *n*=4 and d) *n*=6.

This arrays is moderately sensitive to both horizontal (for low **"n"** values) and vertical structures (for high **"n"** values). In areas where both types of geological structures are expected, this array might be a good compromise between the Wenner and dipole-dipole array.

Vittorio Longo - Prospecting of Industrial Minerals: a geophysical approach -
PhD Thesis in Natural Science - University of Sassari

23

1.3.3 - Dipole-Dipole array

For Dipole-Dipole array, the arrangement of the electrodes is shown in figure 1.12.
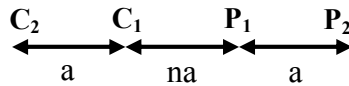
Fig. 1.12 - The Dipole-Dipole array scheme.

The spacing between the current electrodes pair, C2 - C1, is given as **"a"** which is the same as the distance between the potential electrodes pair P1 - P2. This array has another facto marked as **"n"**, this is the ratio of the distance between the C1 and P1 electrodes to the C2 - C1 (or P1 - P2) dipole length **"a"**.

The geometric factor is: $K = \pi n(n+1)(n+2)a$, therefore the voltage is inversely proportional to cube of the **"n"** factor. For the same current, the voltage measured by the resistivity meter drops by about 56 times when **"n"** is increased from 1 to 6.

One method to overcome this problem is to increase the **"a"** spacing between the C1-C2 (and P1-P2) dipole pair to reduce the drop in the potential when the overall length of the array is increased to increase the depth of investigation.

The median depth of investigation of this array depends on both the **"a"** spacing and the **"n"** factor. In general, this array has a shallower depth of investigation compared to the Wenner array (Tab. 1).

For 2D surveys, this array has better horizontal data coverage than the Wenner, this can be an important advantage when the number of nodes available with the multi-electrode system is small. The sensitivity contour pattern becomes almost vertical for **"n"** values greater than 2 (fig. 1.13).

Vittorio Longo - Prospecting of Industrial Minerals: a geophysical approach -
PhD Thesis in Natural Science - University of Sassari

24
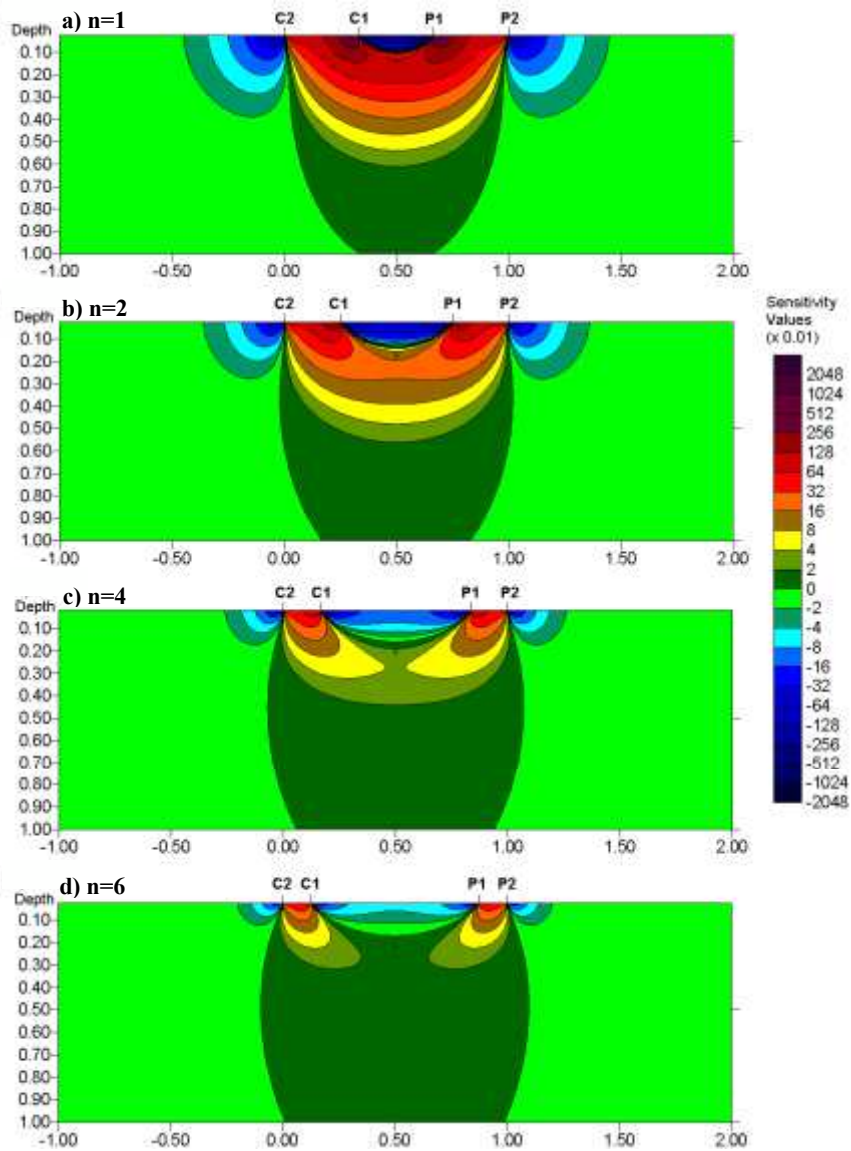
**Fig. 1.13 - 2-D sensitivity sections for the dipole-dipole array with: a) n=1, b) n=2, c) n=4 and n=6.**

Thus the dipole-dipole array is very sensitive to horizontal changes in resistivity, but relatively insensitive to vertical changes in the resistivity. Thus it is good in mapping vertical structures, such as dykes and cavities, but relatively poor in mapping horizontal structures such as sills or sedimentary layers.

Vittorio Longo - Prospecting of Industrial Minerals: a geophysical approach -
PhD Thesis in Natural Science - University of Sassari

25

1.4 - Monodimensional resistivity surveys: Vertical Electrical Sounding and electrical profiling

Traditionally, there are two basic monodimensional resistivity surveys which have been used in connection with four-point arrays: Vertical Electrical Sounding (VES) and resistivity profiling or Horizontal Electrical Sounding (SEO).

Vertical electrical sounding is employed if variations of resistivity with depth are of interest, while resistivity profiling are used to study lateral contrast or localized anomalies. However, the information obtained is a function either of depth or lateral distance only.

The procedure involved in VES is primarily based on the assumption that the subsurface has a horizontal stratigraphy. It consist of discrete, homogeneous and isotropic layers.

For VES the measurement are taken with gradually increasing distances of the electrodes.

As the distance between current probes is increased, there is also an increased in the depth of investigation. In this way, an estimate of the vertical resistivity distribution below the centre of the array is determined (fig. 1.14A). The result of a VES survey is a curve of apparent resistivity as a function of depth (fig. 1.14b).

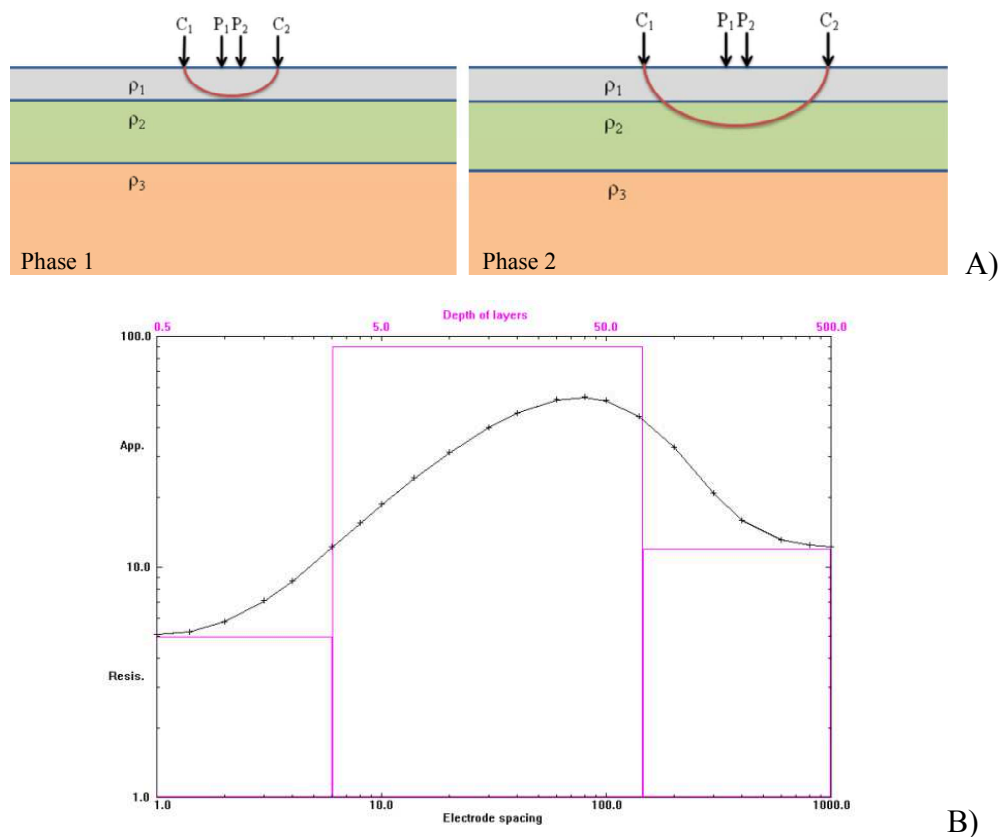

Fig. 1.14 - A) Scheme of electrode positioning on the field for VES survey. B) VES curve of apparent resistivity as a function of depth.

Vittorio Longo - Prospecting of Industrial Minerals: a geophysical approach -
PhD Thesis in Natural Science - University of Sassari

26

It can be interpreted by 1D layered earth models, however these are inherently non-unique.

The technique is useful in determining thickness of overburden, depth, structure and resistivity of flat-lying sedimentary beds or depth to water-bearing layers.

The SEO involves the lateral movement of an electrode array of fixed size, i.e. with a constant electrode separation. If a progression is along a single line, the result is a profile of apparent resistivity with distance (fig. 1.15).
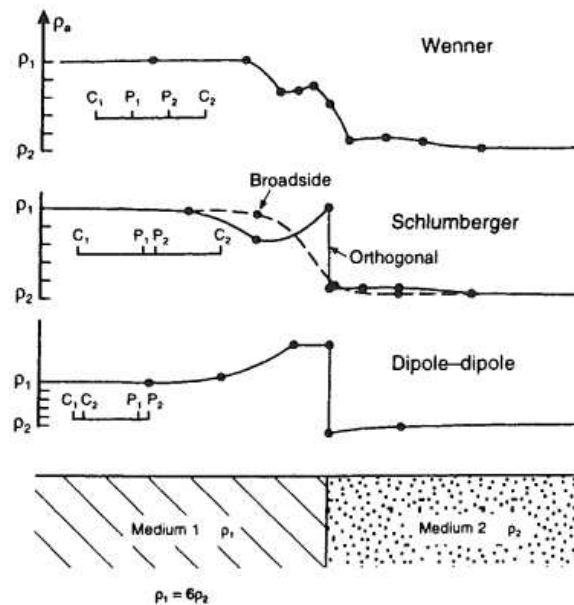
Fig. 1.15- Apparent resistivity profiles measured over a vertical boundary using different electrode arrays (by Reynolds, 1997).

Values are usually plotted against the position of the array midpoint on the profile. Lateral variations in apparent resistivity indicate anomalous areas along the profile.

This acquisition method allows to detect vertical discontinuities such as dykes, faults and vertical tectonic contacts along the line of investigation.

1.5 - 2D Electrical Resistivity Tomography: multi-electrode systems

A limitation of the monodimensional resistivity surveys is that their quantitative interpretation is restricted to simple geological structures such as a 1D layered Earth or lateral contrast such as vertical boundaries. Although these basic techniques have turned out to be extremely useful in some geological application, they are insufficient in areas of complex geology and mostly inapplicable in a site investigation context where the subsurface is often highly heterogeneous and includes localized anomalous feature (Kuras, 2002).

Vittorio Longo - Prospecting of Industrial Minerals: a geophysical approach -
PhD Thesis in Natural Science - University of Sassari

27

In this case, two-dimensional (2D) or three-dimensional (3D) Earth models must be considered. The construction of 2D and 3D images of the subsurface from resistivity data is commonly known as Electrical Resistivity Tomography (ERT).

The ERT provides more accurate subsurface imaging because, generally, the resistivity varies in both the vertical direction and the horizontal direction along the survey line.

In the 2D case, it is assumed that subsurface resistivity does not change in the direction perpendicular to the survey line. In theory, a full 3D resistivity survey and interpretation should be even more accurate.

However, 2D surveys are the most practical economic compromise between obtaining accurate images and keeping the survey cost down (Dahlin, 1996).

ERT surveys are nowadays conducted with multiplex computer-controlled systems using a large number of electrodes connected to multicore cables at regular spacing (Barker, 1981; Griffiths and Turnbull, 1985; Griffiths et al., 1990).

Data acquisition is then entirely automatic with a computer-controlled switching unit collecting data from a predefined sequence of electrode arrays with varying geometries.

If resistivity data are acquired using multiple array separations on the same profile, the resulting dataset contains information about both lateral and vertical variations of resistivity.

Measurements are carried out between current electrodes pairs and potential electrode pairs. An increase in the distance between two electrode pairs given the apparent resistivity data at greater depth. The usual form of display is then to plot apparent resistivity on a section of profile distance versus depth (fig.1.16).
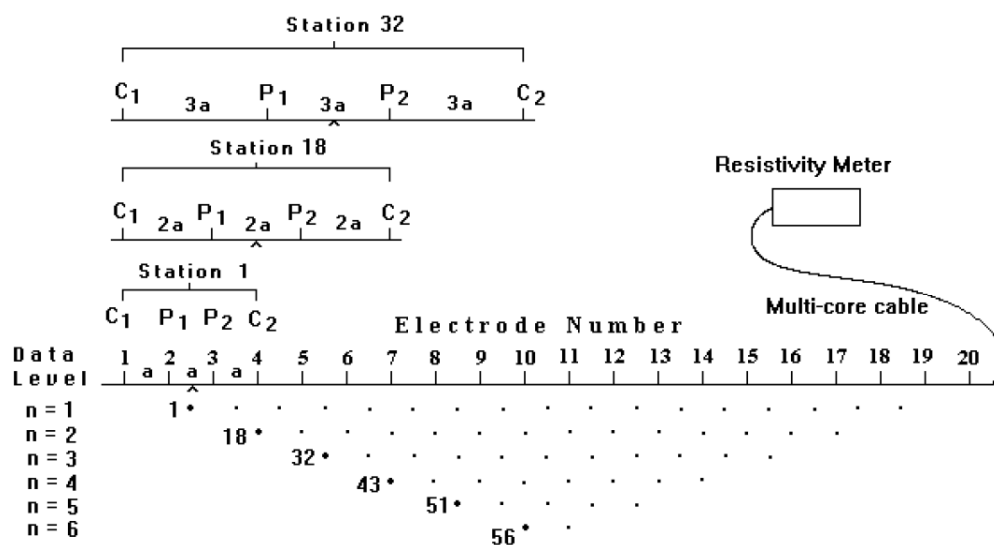

Fig. 1.16 - The arrangement of electrodes for a 2-D electrical survey and the sequence of measurements used to build up a pseudosection (by Loke and Barker, 1996).

Vittorio Longo - Prospecting of Industrial Minerals: a geophysical approach -
PhD Thesis in Natural Science - University of Sassari

28

This is referred to as a pseudosection since it is indicative of resistivity variations with distance and depth, but does not necessarily correspond to the true distribution of resistivity in the form of a cross-section.

To plot the data from a 2D imaging survey, the pseudosection contouring method is normally used. Generally, the horizontal location of the point is placed at the mid-point of the set of electrodes used to make that measurement. The vertical location of the plotting point is placed at a distance that is proportional to the separation between the electrodes (Loke, 2010).

Just for the dipole-dipole array, apparent resistivity data are plotted at the intersection of the two lines draw at a 45° angle to the horizon from the center of the current (C_1-C_2) and the potential (P_1-P_2) dipole pairs (fig. 1.17).
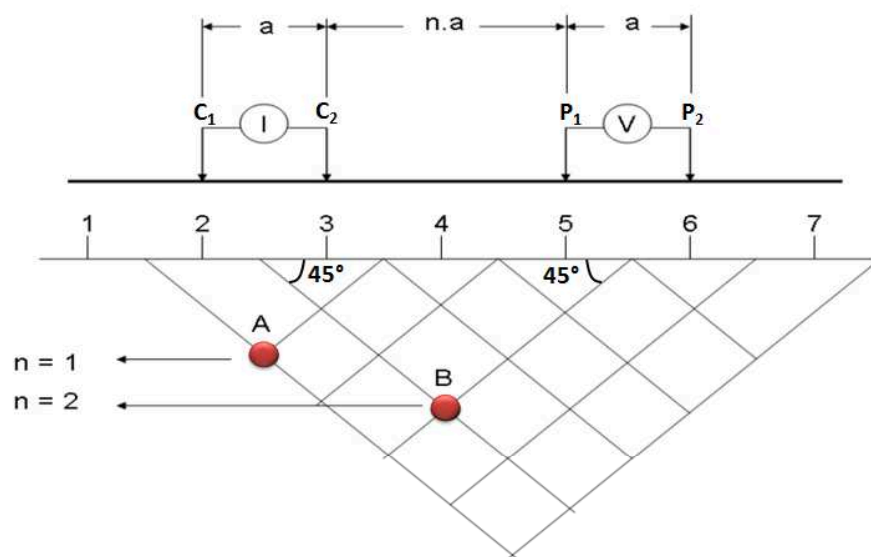
Fig. 1.17 - Classical method of plotting dipole-dipole data on a pseudosection. (A) is a plotting for Dipole 1-2 and Dipole 3-4 measurement. (B) is plotting for Dipole 2-3 and Dipole 5-6 measurement.

It is important to emphasize that this is merely a plotting convention, and it does not imply the current flow or isopotential lines have a 45°angle with the surface in an inhomogeneous earth model (Loke, 2010).

To extend horizontally data coverage, the roll-along survey technique is now widely used in resistivity survey. After completing the initial sequence of measurements, the cable is moved past one end of the line by several unit electrode spacing. All the measurement that involve the electrodes on part of the cable that do not overlap the original end of the survey line are repeated (fig.1.18)

Vittorio Longo - Prospecting of Industrial Minerals: a geophysical approach -
PhD Thesis in Natural Science - University of Sassari

29

Fig. 1.18 - The use of the roll-along method to extend the area covered by a 2-D survey (Loke, 2010).

If the overlap area is half of the total length of the electrical line, the data coverage is not complete. In this case the lower portion of tomography shows a triangular area where the resistivity values are not detected (fig. 1.19).

During data processing, in this triangular area is greater the degree of uncertainty.

Fig. 1.19 - Schematization of a roll-along investigation to 64 electrodes. The overlap area is half of the total length of the electrical line (32 electrodes). The red area show uncovered area from the measures.

Vittorio Longo - Prospecting of Industrial Minerals: a geophysical approach -
PhD Thesis in Natural Science - University of Sassari

30

References

BARKER, R.D., 1981. *The offset system of electrical resistivity sounding and its use with a multicore cable*: Geophysical Prospecting, 29, 1, 128-143.

BARKER, R.D., 1989. *Depth of investigation of collinear symmetrical four-electrode arrays.* Geophysics, 54, 8, 1031-1037.

BERNARD, J. 2003. *Short notes on the principles of geophysical methods for groundwater investigations*. www. Terraplus.com, 8.

CARPENTER, E.W. AND HABBERJAM, G.M., 1956. *A tri-potential method of resistivity prospecting.* Geophysical Prospecting, 21, 2, 455-469.

DAHLIN, T., 1996. *2D resistivity surveying for environmental and engineering applications.* First Break, 14, 7, 275-283.

DANIELS, F., AND ALBERTY, R.A., 1966. *Physical Chemistry.* John Wiley and Sons, Inc. 365.

DOBRIN, M. B., AND SAVIT, C.H., 1988. *Introduction to Geophysical Prospecting.* McGraw-Hill College. 867.

EDWARDS, L.S., 1977. *A modified pseudosection for resistivity and IP.* Geophysics, 42, 5, 1020-1036.

EDWIN, R.S., AND CORUH, C., 1988. *Basic Exploration Geophysics*. Virginia Polymeric Institute and State University, 445-478.

GRIFFITHS, D.H., TURNBULL, J., AND OLAYINKA, A.I., 1990. *Two-dimensional resistivity mapping with a computer-controlled array*. First Break, 8, 4, 121-129.

GRIFFITHS, D.H., AND TURNBULL, J., 1985. *A multi-electrode array for resistivity surveying* . First Break, 3, 7, 16-20.

KURAS, O., 2002. *The Capacitive Resistivity Technique for Electrical Imaging of the Shallow Subsurface*. PhD Thesis, University of Nottingham, 286.

LOKE, M.H., Barker, R.D., 1996. *Rapid least-squares inversion of apparent resistivity pseudosections by a quasi-Newton method.* Geophysical Prospecting, 44, 1, 131–152.

LOKE, M.H., 1997. *Electrical imaging surveys for environmental and engineering studies - A practical guide to 2D and 3D survey*, Penang, Malaysia, Sains Malaysia University, unpublished short training course lecture note, 61.

LOKE, M.H., 2010. *Tutorial: 2-D and 3-D electrical imaging suveys.* Unpublished report: www.geoelectrical.com. 145.

MCGILLIVRAY, P.R., AND OLDENBURG, D.W., 1990. *Methods for calculating Frechet derivatives and sensitivities for the non-linear inverse problem: a comparative study.* Geophysical Prospecting, 38, 5, 499-524.

MERRICK, N.P., 1997. *A new resolution index for resistivity electrode arrays.* Exploration Geophysics, 28, 2, 106-109.

Vittorio Longo - Prospecting of Industrial Minerals: a geophysical approach -
PhD Thesis in Natural Science - University of Sassari

31

MUCHAIDZE, I., 2008. *Imaging in Karst terrain using electrical resistivity tomography*. Thesis for degree in master of science in geological engineering. Missouri University of Science and Technology, 68.

OHM, G.S., 1827. *Die galvanische Kette: mathematisch bearbeitet* (*The Galvanic Circuit Investigated Mathematically*). Graph. Darst, Riemann, Berlin, 245.

PARASNIS, D.S., 1997. *Principles of Applied Geophysics.* Chapman and Hall, 400.

PAZDIREK, O., AND BLAHA, V., 1996. *Examples of resistivity imaging using ME-100 resistivity field acquisition system.* EAGE 58th Conference and Technical Exhibition Extended Abstracts, Amsterdam.

RECCELLI-SNYDER, H.L., STAHL, B., LEBERFiNGER, A., WARREN, P.G., AND WARREN, J.J., 1997. *Electrical imaging: A Method for Identifying Potential Collapse and other Karst Features Near Roadways.* Science Applications International Corporation, Middletown, Pennsylvania. 50th Annual Highway geology symposium.

REYNOLDS, J.M., 1997. *An introduction to applied and environmental geophysics.* John Wiley and Sons, Inc, England, 796.

ROMAN, I., 1951. *Resistivity reconnaissance in American Society of testing and materials. Symposium on surface and subsurface reconnaissance.* American society of testing materials special technical publication, 122, 171-220.

TELFORD, W.M., GELDART, L.P., SHERIFF, R.E., 1990. *Applied Geophysics, (2nd ed.).* Cambridge University Press, Cambridge, 527–529.

UDPHUAY, S., 2008. *3-D Electrical Resistivity Tomography for Cliff Stability Assessment at Pointe du Hoc in Normandy, France.* PhD Thesis , Geophysics, Texas A&M University, 138.

Vittorio Longo - Prospecting of Industrial Minerals: a geophysical approach -
PhD Thesis in Natural Science - University of Sassari

32

Chap. 2 - Materials and methods

2.1 - Galvanic coupled resistivity system: Abem Terrameter SAS1000

The geoelectrical surveys were carried out by a Terrameter SAS1000 device, a single-channel georesistivimeter developed by ABEM Instruments (Sweden), based on the use of metal electrodes for galvanic coupling.

This device allows to get a complete set of geoelectrical measurement: Vertical Electrical Sounding, resistivity profiles, 2D and 3D Electrical Resistivity Tomography, measurement of Induced Polarization (IP) and Self Potential (SP).

The control unit Terrameter SAS1000 encloses both the energizing unit and the receiver unit.

The electrically isolated transmitter sends out well-defined and regulated signal currents, it can be set to values from 1 mA up to 1000 mA. The maximum voltage at the current electrodes is 400V.

The receiver measures the response voltage signal at discrete time intervals and discriminates noise and measures voltage correlated with transmitted signal current.

The Terrameter SAS1000 is combined to LUND system which consist of Electrode Selector ES10-64 and multi-conductor cables (fig. 2.1).

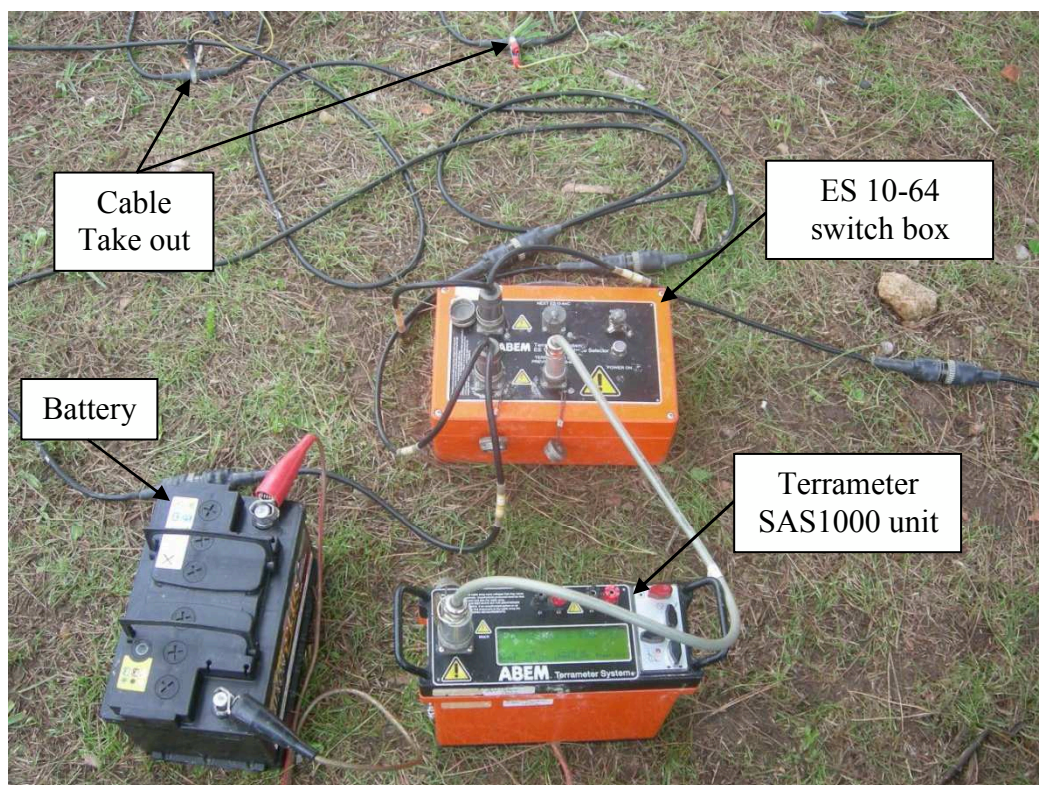**Fig. 2.1 - Arrangement for data acquisition with Abem Terrameter SAS1000 and Lund multi-electrode resistivity survey.**

Vittorio Longo - Prospecting of Industrial Minerals: a geophysical approach -
PhD Thesis in Natural Science - University of Sassari

33

The ES 10-64 is a multi-channel relay matrix switch for high-resolution 2D and 3D resistivity surveys, which allows the automatic control of the electrode arrays.

Field system use a multicore cable to which 64 electrodes are connected at takeouts moulded on at predetermined equal intervals (fig. 2.2). The cable is directly connected to a ES 10-64 switching module and to stainless steel electrodes hammered in the ground.
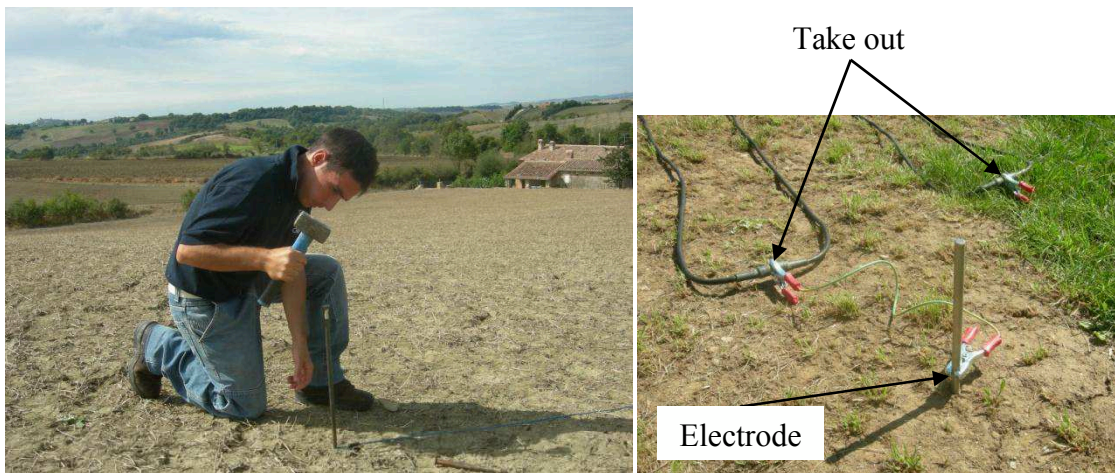

Take out

Electrode

Fig. 2.2 - Positioning of the electrodes in the field at equal intervals (left) and connecting of metal electrode with multicore cable (right).

With this system, any electrodes may be switched to act as either current or potential electrodes and so within the constraints of the electrodes emplaced, any electrode arrangement can be employed (Barker et al., 2001).

The 12V external battery is required for measurements during ABEM Lund Imaging survey to ensure sustainable energy during data acquisition.

2.1.1 - Communication between Abem Terrameter and PC computer

The ABEM Terrameter SAS1000 communicates with PC compatible computer through the serial cable. It is set to the RS232 communication mode so that it is ready to an external PC computer. Data are displayed on the computer screen and the specific file can be imported to the PC by marking it in the checkbox.

Files in the Terrameter are saved in binary formats with the file extension.s4k. This format is not compatible with the many inversion programs so it has to be converted to a convenient format. The conversion program is automatic and readily converts the data without any inputs from the operator.

Vittorio Longo - Prospecting of Industrial Minerals: a geophysical approach -
PhD Thesis in Natural Science - University of Sassari

34

2.2 - Inversion programs

The converted data from a survey line are arranged in the form of an apparent resistivity pseudosection.

The pseudosection plot obtained by contouring the apparent resistivity values is a convenient means to display the raw data resistivity. The pseudosection gives a very approximate picture of the true subsurface resistivity distribution beneath the survey lines; however they provide only a distorted picture of the subsurface because the shape of the contours depends on the type of array (Loke, 2010).

The pseudosection is useful as a means to present the measured apparent resistivity values in a pictorial form, and as an initial guide for further quantitative interpretation. One common mistake made is to try to use the pseudosection as a final picture of the true subsurface resistivity (Loke, 2010).

In fact, after the data from a survey line are arranged in the form of an apparent resistivity pseudosection (fig. 2.3A), an inversion of the data set is required to obtain an high-resolution subsurface geological model or Electrical Resistivity Tomography (ERT) (fig.2.3B).
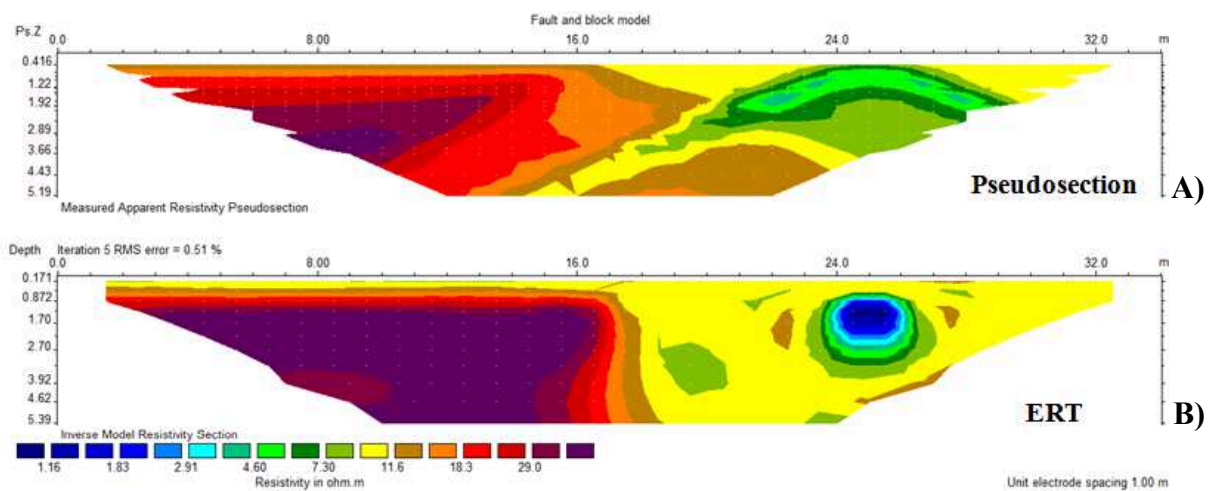
Fig. 2.3 - Example of inversion result using the RES2DINV software (Geotomo). A) The apparent resistivity pseudosection and B) Electrical Resistivity Tomography.

Due to the large variety of data sets collected over various geological environments, no single inversion method will give the optimum results in all cases.

In geophysical inversion, trying to find a model that gives a response that is similar to the true spatial distribution of intrinsic resistivity in the region of interest from an apparent resistivity dataset (pseudosection) (Loke, 2010).

Vittorio Longo - Prospecting of Industrial Minerals: a geophysical approach -
PhD Thesis in Natural Science - University of Sassari

35

Modern inversion techniques can deal with arbitrary resistivity distributions, are fully automated and frequently use non-linear optimization methods to iteratively improve simple starting models in an attempt to achieve a "best fit" between model and measured data.

One of most popular general geophysical inversion techniques is the Gauss-Newton least-squares inversion (Lines and Treitel, 1984) due to its robustness and variety of applications. One particular incarnation of this method, known as Occam's inversion, demands smoothness of the model as a general constraint (Constable et al., 1987; deGroot-Hedlin and Constable, 1990).

Loke and Barker, (1996) have developed a fast and particularly versatile implementation of the smoothness-constrained least-squares inversion. A quasi-Newton method is used to estimate the Jacobian matrix of partial derivates during each iteration, resulting in a dramatic reduction of processor time and memory requirements.

For inversion dataset, in this thesis, were employed the RES2DINV (Loke, 2001) and RES3DINV (Loke 2004) programs which using a non-linear smoothness-constrained least-squares optimization techniques (Loke and Barker, 1996) with the equation as follows:

$$(J^TJ + \lambda F)p_i = J^Tg$$

In which $F = f_x f_x^T + f_z f_z^T$
f_x = filter from horizontal structures
f_z = filter from vertical structures
J = matrix of partial derivatives
λ = damping factor
p_i = model perturbation factor
g = discrepancy vector

One advantage of this method is that the damping factor and flatness filters can be adjusted to suit different types of data.

In this software the subsurface is divided into a lot of rectangular blocks, and the number of blocks is approximately equal to the number of data points in the apparent resistivity pseudosection and arranged in a similar manner (fig. 2.4).
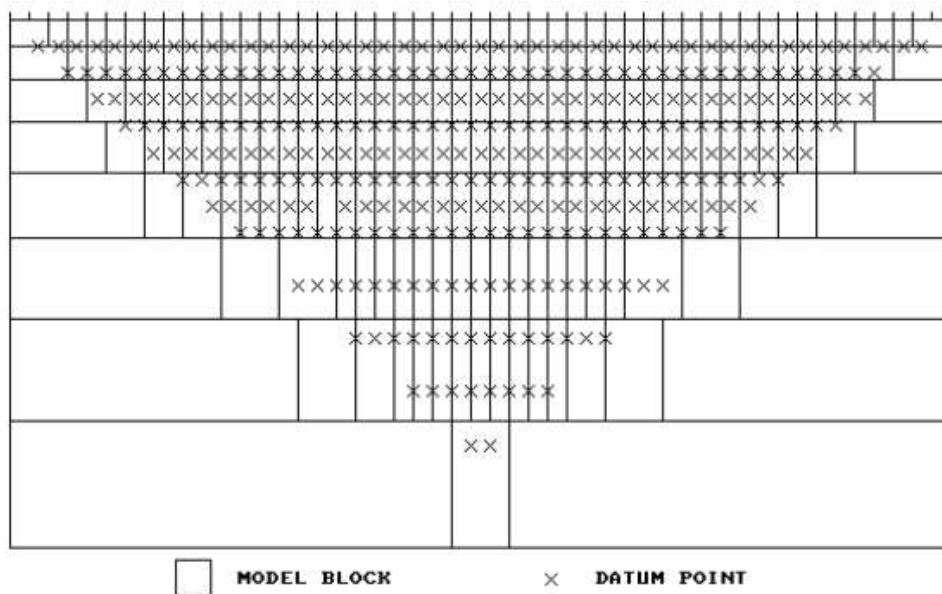
Vittorio Longo - Prospecting of Industrial Minerals: a geophysical approach -
PhD Thesis in Natural Science - University of Sassari

36

Fig.2.4 - Arrangement of the blocks used in a model together with the datum pints in the pseudosection (Loke, 2010).

The model parameters are the resistivity values of the model blocks while the data are the apparent resistivity values.

The optimization method tries to reduce the difference between the calculated and measured apparent resistivity values by adjusting the resistivity of the model blocks.

The model is considered to be appropriate when the calculated values and the measured ones are best fitted.

The measure of this difference is given by the root mean square (RMS) error.

The model with the lowest possible RMS error can sometimes show large unrealistic variations in the model resistivity values and might not always be the best model from geological perspective (Loke, 2010).

The root mean square (RMS) is calculated from the difference between the logarithms of the measured and calculated apparent resistivity values. The RMS decreases after each iteration with the largest reductions in the first three iterations.

Both their 2D and 3D algorithms have proven to be robust under many circumstances and have been successfully applied to complex dataset obtained during environmental and engineering site investigations (Chambers et al., 1999;Ogilvy et al., 2002).

The inversion programs RES2DINV (Loke, 2001) and RES3DINV (Loke, 2004) allows to set some parameters to optimize the final models.

The options used for inversion of each datasets will be described in every case study.

Vittorio Longo - Prospecting of Industrial Minerals: a geophysical approach -
PhD Thesis in Natural Science - University of Sassari

37

In all case, to obtain a good resistivity model the data must be of equally good quality. Bad data points can be described as "systematic" and "random" noise.

- Systematic noise is usually caused by some sort of failure during the survey, example include breaks in the cable, very poor ground contact at an electrode, connecting the cables in the wrong direction etc.

- Random noise include effect such telluric currents that affect all the reading, and the noise can cause the readings to be lower or higher than the equivalent noise-free readings. This noise is usually more common with arrays that have very large geometric factors.

In this work, before carrying out the inversion of a data set, were deleted the bad data point.

In profile form, the systematic noise show up as spots with unusually low or high values (Fig. 2.5) and can be easily removed manually for the data set.

In the RES2DINV (Loke, 2001) program, choose the "Edit data" on the top menu bar followed by the "Exterminate bad data points" option. The bad data points can be removed by clicking them with the mouse.
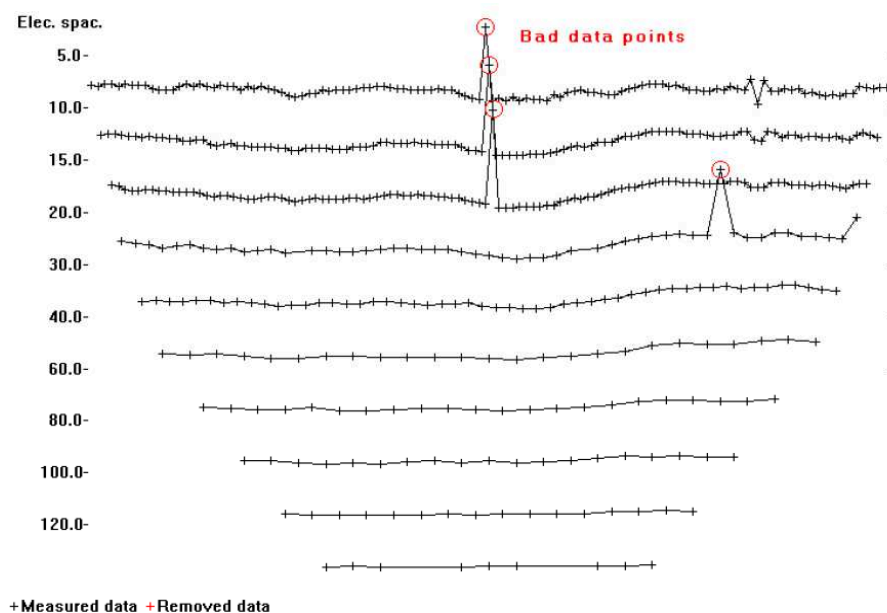
Fig. 2.5 - An example of a field data set with a few bad data points.

When the noise is of a more random nature, the noisy data points are not as obvious, so it might not be practical to remove them manually. In this case, a preliminary inversion of the data set is first carried with all the data points. After that, with "RMS error statistic" the error distribution is show in the form of a bar chart (fig. 2.6).

Vittorio Longo - Prospecting of Industrial Minerals: a geophysical approach -
PhD Thesis in Natural Science - University of Sassari

38
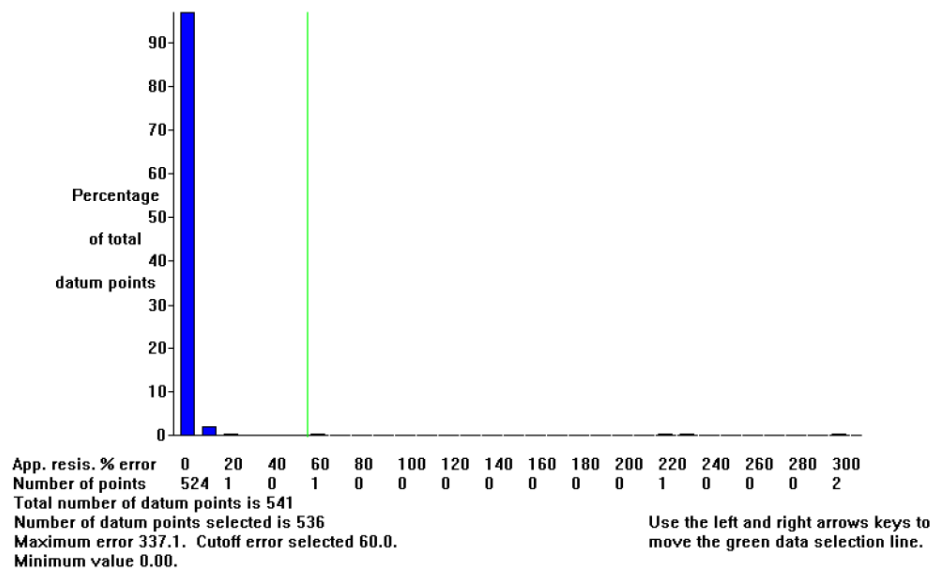
Fig. 2.6 - Error distribution bar chart from a trial inversion of the data set with five bad data points (Loke, 2010).

Normally, the highest bar is the one with the smallest errors, and the heights of the bars should decrease gradually with increasing error values.

The bad data points can be easily removed from the data set by moving the green cursor line to the left of the percentage error bar.

Vittorio Longo - Prospecting of Industrial Minerals: a geophysical approach -
PhD Thesis in Natural Science - University of Sassari

39

References

BARKER, R.D., VENKATESWARA, R.T. AND THANGARAJAN M., 2001. *Delineation of contaminant zone through electrical resistivity imagine technique.* Current science, 81, 3, 277-283.

CHAMBERS, J., OGILVY, R., MELDRUM, P., AND NISSEN, J., 1999. *3D resistivity imaging of buried oil- and tar-contaminated waste deposits:* European Journal of Environmental and Engineering Geophysics, 4, 1, 3-14.

CONSTABLE, S.C., PARKER, R.L. AND CONSTABLE, C.G., 1987. *Occam's inversion: A practical algorithm for generating smooth models from electromagnetic sounding data.* Geophysics, 52, 289-300.

DEGROOT-HEDLIN, C., AND CONSTABLE, S., 1990. *Occam's inversion to generate smooth, two-dimensional models form magnetotelluric data.* Geophysics, 55, 1613-1624.

LINES, L.R., AND TREITEL, S., 1984. Tutorial: *A review of least-squares inversion and its application to geophysical problems.* Geophysical Prospecting, 32, 159-186.

LOKE, M.H., 2001. *RES2DINV ver. 3.4: Rapid2-D Resistivity & IP inversion using the least-squares method.* www.terraplus.com, 98.

LOKE, M.H., 2004. *RES3DINV ver. 2.14: Rapid 3D Resistivity & IP inversion using the least squares methods.* www.geoelectrical.com, 90.

LOKE, M.H., 2010. *Tutorial: 2-D and 3-D electrical imaging suveys.* Unpublished report: www.geoelectrical.com, 145.

LOKE, M.H., AND BARKER, R.D., 1996. *Practical techniques for 3D resistivity surveys and data inversion.* Geophysical Prospecting, 44, 499-523.

OGILVY, R.D., MELDRUM, P.I., CHAMBERS, J.E., AND WILLIAMS, G.M., 2002. *The Use of 3D Electrical Resistivity Tomography to Characterize Waste and Leachate Distribution within a Closed Landfill, Thriplow, UK* European Journal of Environmental and Engineering Geophysics, 7, 1, 11-18.

Vittorio Longo - Prospecting of Industrial Minerals: a geophysical approach -
PhD Thesis in Natural Science - University of Sassari

40

Chap. 3 - Geodynamics of Sardinia and evolution of Cenozoic volcanism

Sardinia is located in the Mediterranean Sea between two marine basins, which have a crustal structure from transitional to oceanic-type. Together with Corsica, Sardinia forms a microcontinent with a continental crust about 30 to 35 km thick.

In Sardinia the Pre-Cenozoic is represented by a Paleozoic basement made up of low- to high-grade Hercynian metamorphic rocks belonging to different tectonic units and affected by several deformation phases (Carmignani et al., 1982). The basement was intruded by Late-Hercynian granitoids.

Carboniferous–Permian volcanic and sedimentary rocks and Mesozoic carbonate rocks (Carmignani et al., 1992) unconformably overlay the more ancient terrains.

During Cenozoic, Sardinia was involved, even if marginally, in some orogenic events. Due its position, between the Pyrenean orogen and the North Apennine, this sector of European crust recorded both compressive and extensional events referable to the geodynamics of the Western Mediterranean realm.

Two main hypotheses concern the role played by Sardinia-Corsica crustal Block.

In the classical reconstructions the crust of this micro-plate firstly played as the foreland of the Alpine Chain and then, after its counter-clockwise drift and rotation, acted as hinterland of the Northern Apennine chain (Boccaletti et al, 1971; Boccaletti & Guazzone, 1974; Boccaletti et al, 1990). This point of view implies the following consequences:

i) the nappe stack of NE Corsica is a segment of the alpine chain with Europe-directed vergence;

ii) starting from the Oligocene, a subduction flip beneath the southern margin of the European plate must be invoked, in order to explain the Adria-vergence of Northern Apennine and the calcalkaline Oligo-Miocene volcanic activity in the present-day Sardinia and on the western shelf of Corsica;

iii) the Sardinia-Corsica crust evolved as an Andean-type arc, which migrated ocean-ward leading to the opening of the Gulf of Lion-Liguro-Provençal back-arc basin.

The rotation of the Sardinia-Corsica crustal block ended because of its collision with Adria that lasted until the Tortonian (Giglia, 1973).

Starting from the late 80's, a new hypothesis regarding Sardinia-Corsica crust as the mere hinterland of Northern Apennine arrived, so excluding an Oligocene subduction flip (Principi and Treves, 1984; Carmignani et al. 1995; Lahondere et al. 1999; Oggiano et al. 2009).

This hypothesis required:

Vittorio Longo - Prospecting of Industrial Minerals: a geophysical approach -
PhD Thesis in Natural Science - University of Sassari

41

i) the nappe building of Northern Corsica is the consequence of the accretionary wedge deformation, which generated at the active margin of south Europe. This margin experienced subduction since mid-Cretaceous, and so, flip is required to explain the eastern vergence of North Apennine.

ii) collision between Adria and Europe plates started in Oligocene generating a chain with both Europe and Adria-verging tectonic units (Principi and Treves 1984; Carmignani et al. 1995, fig. 3.1). The European hinterland was affected by strike-slip tectonics.
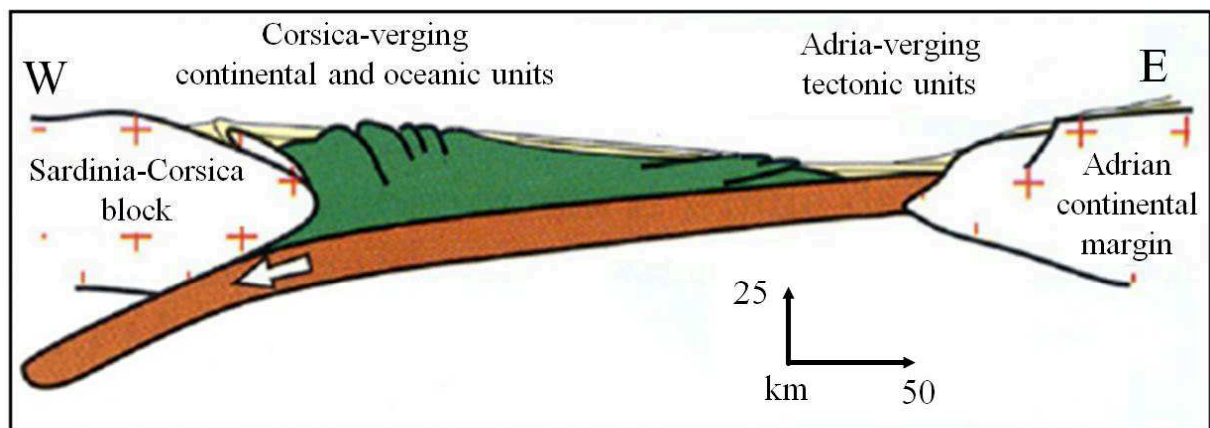

Fig. 3.1 - Scheme of Adria plate subduction and consequent formation of Europe- and Adria-verging tectonic units. After Carmignani et al. (2001), modified.

According to this hypothesis, strike-slip faults at late Oligocene generated the Aquitanian strike-slip basins that strike ENE in northern Sardinia and NW in southern Sardinia.

This evidence rules out the case of Oligocene-Aquitanian E-W extension (in present day coordinates) that led to a N-S trending "Sardinian Rift". East-west extension in Sardinia started from mid-upper Burdigalian and pursued until Pliocene.

During Burdigalian time, back arc spreading and rotation of the Sardinia-Corsica block followed this geodynamic context (Boccaletti and Guazzone, 1972).

According to Beccaluva et al. (1987) most of the volcanic activity is concentrated between 21 and 17 Ma, time during which the drift of Sardinia (Vigliotti and Langenheim, 1995) and the related opening of the Balearic back arc basin (Malinverno and Ryan, 1986, fig. 3.2) occurred.
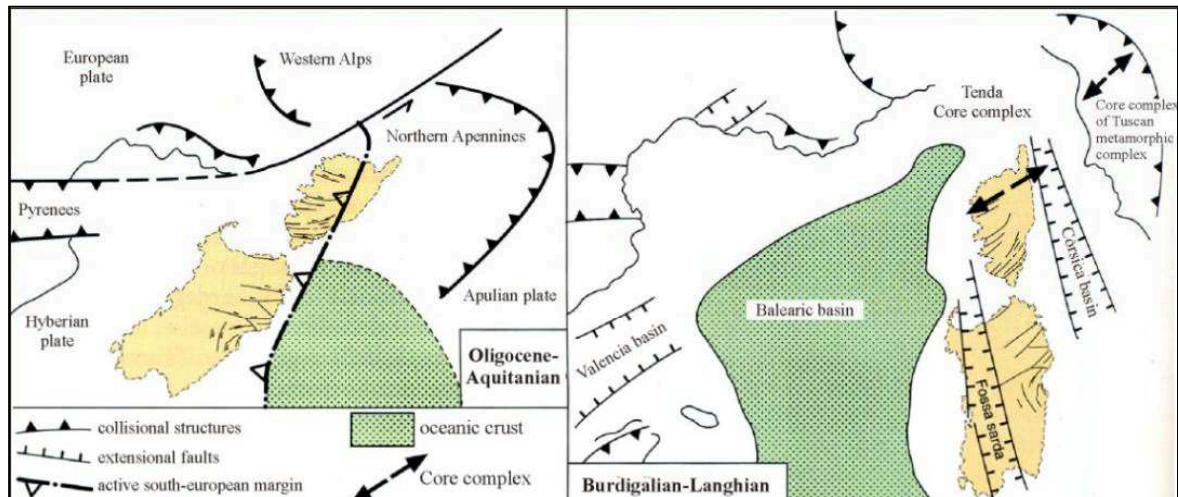
Vittorio Longo - Prospecting of Industrial Minerals: a geophysical approach -
PhD Thesis in Natural Science - University of Sassari

42

Fig. 3.2 – Scheme of Sardinia-Corsica block rotation and its position in Mediterranean area at Oligocene-Aquitanian (a) and Burdigalian-Langhian (b). After Carmignani et al. (2001), modified.

In this complex geodynamic scenario, the island of Sardinia experienced an intense igneous activity with calcalkaline to high-K calcalkaline magmatism (Lecca et al., 1997; Lustrino et al., 2004).

The volcanic products comprise pyroclastic flow deposits, lava flows and domes; their compositions are dominated by dacites and rhyolites, with subordinate andesites and very scarce basalts.

These volcanic rocks, outcrop over an area of about 10,000 km^2 in the island, and hosting the most important Industrial Mineral (IM) deposits as bentonite, kaolin, zeolite, and potassium feldspar mineralizations.

All deposits have generally derived from the alteration of the most acidic members of the Cenozoic volcanic rocks (rhyolites to rhyodacites), but differences among the associated ore-forming phenomena are recognized. Hydrothermal sensu stricto, deuteric alteration and weathering are the most important processes involved in ore formation.

The extent and type of occurrences are mainly controlled by the local geological and structural features, and the environmental geochemical conditions.

Vittorio Longo - Prospecting of Industrial Minerals: a geophysical approach -
PhD Thesis in Natural Science - University of Sassari

43

References

BECCALUVA, L., BROTZU, P., MACCIOTTA, G., MORBIDELLI, L., SERRI, G., AND TRAVERSA, G., 1987. *Caenozoic tectono-magmatic evolution and inferred mantle sources in the sardo-tyrrhenian area.* In: Borani, A., Bonafede, M., Piccardo, G.B. and Vai, G.B. (Eds), The lithosphere in Italy. Advances in earth science research. Accademia Nazionale dei Lincei, 229-248.

BOCCALETTI, M., ELETER, P., AND GUAZZONE, G., 1971. *Plate tectonic models for the development of the Western Alps and Northern Apennines.* Nature, 234, 108-111.

BOCCALETTI, M., AND GUAZZANE, G., 1972. *Gli archi appenninici, il Mar Ligure ed il Tirreno nel quadro della tettonica dei bacini retro-arco.* Memorie della Società Geologica Italiana, 11, 201-216.

BOCCALETTI, M., AND GUAZZONE, G., 1974. *Remnant arcs and marginal basins in the Cainozoic development of the Mediterranean.* Nature Physics, 252, 18-21.

BOCCALETTI, M., CIARANFI, N., COSENTINO, D., DEIANA, G., GELATI, R., LENTINI, F., MASSARI, F., MORATTI, G., PESCATORE, T., RICCI LUCCHI, F., AND TORTORICI, L., 1990. *Palinspastic restoration and paleogeogaphic reconstruction of the peri-Tyrrehenian area during Neogene.* Palaeogeography Palaeoclimatology Palaeoecology, 77, 41-50.

CARMIGNANI, L., COCOZZA, T., GHEZZO, C., PERTUSATI, P.C., AND RICCI, C.A.,1982. *Lineamenti del basamento sardo.* Bollettino della Societa` Geologica Italiana, Special Issue, Guida alla Geologia del Paleozoico Sardo, Guide Geologiche, 11–23.

CARMIGNANI, L., BARCA, S., CAPPELLI, B., DI PISA, A., GATTIGLIO, M., OGGIANO, G., AND PERTUSATI, P.C., 1992. *A tentative geodynamic model for the Hercynian basement of Sardinia.* In: Carmignani, L., Sassi, F.P., (Eds.), Contribution to the Geology of Italy With Special Regard to the Paleozoic Basement. I.G.C.P. 276, Newsletter, 5, 61–82.

CARMIGNANI, L., DECANDIA, F.A., DISPERATI, L., FANTOZZI, P.L., LAZZAROTTO, A., LIOTTA, D. AND OGGIANO, G., 1995. *Relationschip between the Tertiary structural evolution of the Sardinia-Corsica-Provençal Domain and the Northern Apennines.* Terra Nova, 7, 128-137.

GIGLIA, G., 1973. *L'insieme Corsica-Sardegna e i suoi rapporti con l'Appennino settentrionale: rassegna dei dati cronologici e strutturali.* In: Paleogeografia del Terziario Sardo nell'ambito del mediterraneo occidentale. Rendiconti Seminario Facoltà di Scienze Università di Cagliari, suppl., 43, 245-275.

LAHONDERE, D., ROSSI, P. AND LAHONDERE, J.C., 1999. *Structuration alpine d'une marge continentale externe: le massif du Tenda (Haute-Corse). Implications géodynamiques au neveau de la transversale Corse-Apennins.* Geologie de la France, 4, 27-44.

LECCA, L., LONIS, R., LUXORO, S., MELIS, F., SECCHI, F., AND BROTZU, P., 1997. *Oligo-Miocene volcanic sequence and rifting stages in Sardinia.* ARSVIEW, 66, 7–61.

LUSTRINO, M., MORRA, V., MELLUSO, L., BROTZU, P., D'AMELIO, F., FEDELE, L., FRANCIOSI, L., LONIS, R. AND PETTERUTI LIEBERCKNECHT, A.M., 2004. *The Cenozoic igneous activity of Sardinia.* Periodico di Mineralogia, 73, 105-134.

Vittorio Longo - Prospecting of Industrial Minerals: a geophysical approach -
PhD Thesis in Natural Science - University of Sassari

44

MALINVERNO, A., AND RYAN, W.B.F., 1986. *Extension in the Tyrrhenian Sea and shortening in the Apennines as a result of arc migration driven by sinking of the lithosphere.* Tectonics, 5, 227-245.

OGGIANO, G., FUNEDDA, A., CARMIGNANI, L., AND PASCI, S., 2009. *The Sardinia–Corsica microplate and its role in the Northern Apennine Geodynamics: new insights from the Tertiary intraplate strike-slip tectonics of Sardinia.* Bollettino della Società Geologica Italiana 128, 227-239.

PRINCIPI, G. AND TREVES, B., 1984. *Il sistema corso-appenninico come prisma d'accrezione. Riflessi sul problema generale del limite Alpi-Appennini.* Memorie della Società Geologica Italiana, 28, 549-576.

VIGLIOTTI, L., AND LANGENHEIM, V.E., 1995. *When did Sardinia stop rotating? New paleomagnetic results.* Terra Nova, 7, 424-435.

Vittorio Longo - Prospecting of Industrial Minerals: a geophysical approach -
PhD Thesis in Natural Science - University of Sassari

45

Chap. 4 - Application of 2D and 3D ERT method on a bentonitic clay deposit in Northern Sardinia

4.1 - Introduction

Bentonite can be considered the most important Sardinian industrial mineral occurrences as for number of deposits.

The potential clay reserves are evaluated by the minerals industry using conventional methods, which include structural and stratigraphic studies, direct investigations (boreholes) and trenches.

Currently, some geophysical methods provide an important contribution not only in prospecting but also in defining the geometric characteristics of the mineralized bodies (thickness, lateral extent, depth).

Particularly, the geoelectrical resistivity methods have been applied successfully to identify and characterize conductive clay bodies (Sinha, 1980; Ferguson et al., 1999; Giao et al., 2003).

The effectiveness of this technique is related to the high-resistivity contrast between mineralized body and the host rocks.

In fact, the electrical resistivity of clays is generally lower than that of several host lithotypes (Parasnis, 1973), and ranges from 1 to 100 $\Omega \cdot m$ (Reynolds, 1997; Loke, 1999).

Particularly for bentonitic clays have been measured resistivity values lower than 4 $\Omega \cdot m$ in relation to the smectite minerals content and to high Cation Exchange Capacity (CEC) (Kaufhold and Penner, 2006).

In the last two decades, the traditional one-dimensional investigations of electrical resistivity (sounding and profiling) were partially replaced by the application of new techniques of acquisition calls Resistivity Imaging (RI) and Electrical Resistivity Tomography (ERT).

The great advantage of the ERT survey is that it is a low-cost non-invasive method which allows to create rapidly 2D resistivity models of the subsurface.

In the interpretation of data from 2D imaging surveys, it is assumed that the subsurface geology does not change significantly in the direction that is perpendicular to the survey line.

In areas with very complex geology, significant variations in the subsurface resistivity in this direction occur. The assumption made for the 2D ERT surveys may introduce significant errors, and the resulting 2D images can contain significant distortions (Loke, 2001a; Bentley and Gharibi, 2004).

Vittorio Longo - Prospecting of Industrial Minerals: a geophysical approach -
PhD Thesis in Natural Science - University of Sassari

46

For this reason to investigate complex three-dimensional structures (Aizebeokhai and Olayinka, 2010; Neyamadpour et al., 2009), to map sites contaminated by pollution (Chambers et al., 2006), or to estimate the volume of materials potentially extracted in quarries or mines is preferable to make acquisitions 3D ERT (Chambers et al., 2008).

3D resistivity model can be obtained by different acquisition methods: i) an ideal 3D survey with the electrodes arranged in a rectangular grid and with measurements in all possible directions (Loke and Barker, 1996); ii) from the measurement made in the two directions along the grid lines, iii) or intersection of several 2D lines (Chambers et al., 2002; Bentley and Gharibi, 2004; Chambers et al., 2006; Aizebeokhai and Olayinka, 2010), iv) and from measurement in only one direction along a series of parallel 2D survey lines (Chambers et al., 2008; Neyamadpour et al., 2009).

In this paper an example of application of 2D and 3D ERT method to investigate a bentonitic clays deposit near Ozieri (N-Sardinia) is presented.

The aim of this investigation was to define the spatial patterns of the mineralized body, and to assess the available reserves in the deposit area which will start mining activity.

The resistivity data integrated with boreholes information have been displayed in virtual 3D space using geologic modeling software.

Vittorio Longo - Prospecting of Industrial Minerals: a geophysical approach -
PhD Thesis in Natural Science - University of Sassari

47

4.2 – Study area and geological setting

The study area is located about 13 Km to the north-west of the town of Ozieri (SS), northern Sardinia.

The site, named "Monte Furros", lies at the base of a morphological step culminating at N-W with Monte Pittu (48 metres above sea level) and at S-W with Monte Cheja (407 metres above sea level) (fig. 4.2).

At base of the morphological step, the flat area forms a large basin slopping down eastward, with variable altitudes from 300 to 315 metres above sea level.

The considered bentonite deposit, as the most important industrial minerals deposits of northern Sardinia, derives from the alteration of the pyroclastic sequences associated with the Oligo-Miocene calcalkaline volcanic cycle.

Tertiary volcanic successions in northern Sardinia, are mainly constituted by alternating lavas and pyroclastics flows, with composition variable from andesitic-basaltic to rhyolitic.

These volcanic successions, which host many types of regional-scale epithermal mineralizations (Mameli, 2000; Padalino et al., 2003; Oggiano and Mameli, 2012), fill several basins of Oligo-Miocene age characterized by different structural directions.

The oldest basins develop in the E-NE direction and have been interpreted as strike-slip basins associated with the north Apenninic collision of Oligo-Aquitanian age (Oggiano et al., 1995); while the Burdigalian basins, typically with N-NW trending, have been interpreted as half-graben associated with the Appennines post-collisional distension phase and with the opening of the Balearic basin.

The study area is located in the north-western margin of one of the most representative and well preserved Sardinians Oligo-Aquitanian strike-slip basins: the Chilivani-Berchidda basin (fig. 4.1). This basin provides an exemplary case of a strike-slip basin formed along a sinistral strike-slip fault (Olbia Fault) in correspondence with a left bend, hence a releasing bend, which generated local NW-SE extension on the western advancing side (Oggiano et al., 1995).

To the south-west of the study area, the Chilivani-Berchidda basin is intersected by faults from NNW to meridian trending that delimit the adjacent Burdigalian Logudoro basin (fig. 4.1). Both basins host volcano-sedimentary successions consisting mainly of pyroclastic flow products with lacustrine epiclastics intercalated (Cerri and Oggiano, 2002).

The lithotypes outcropping in the examined area, are attributable to the Oligo-Miocene volcano-sedimentary sequence and to Holocene deposits.
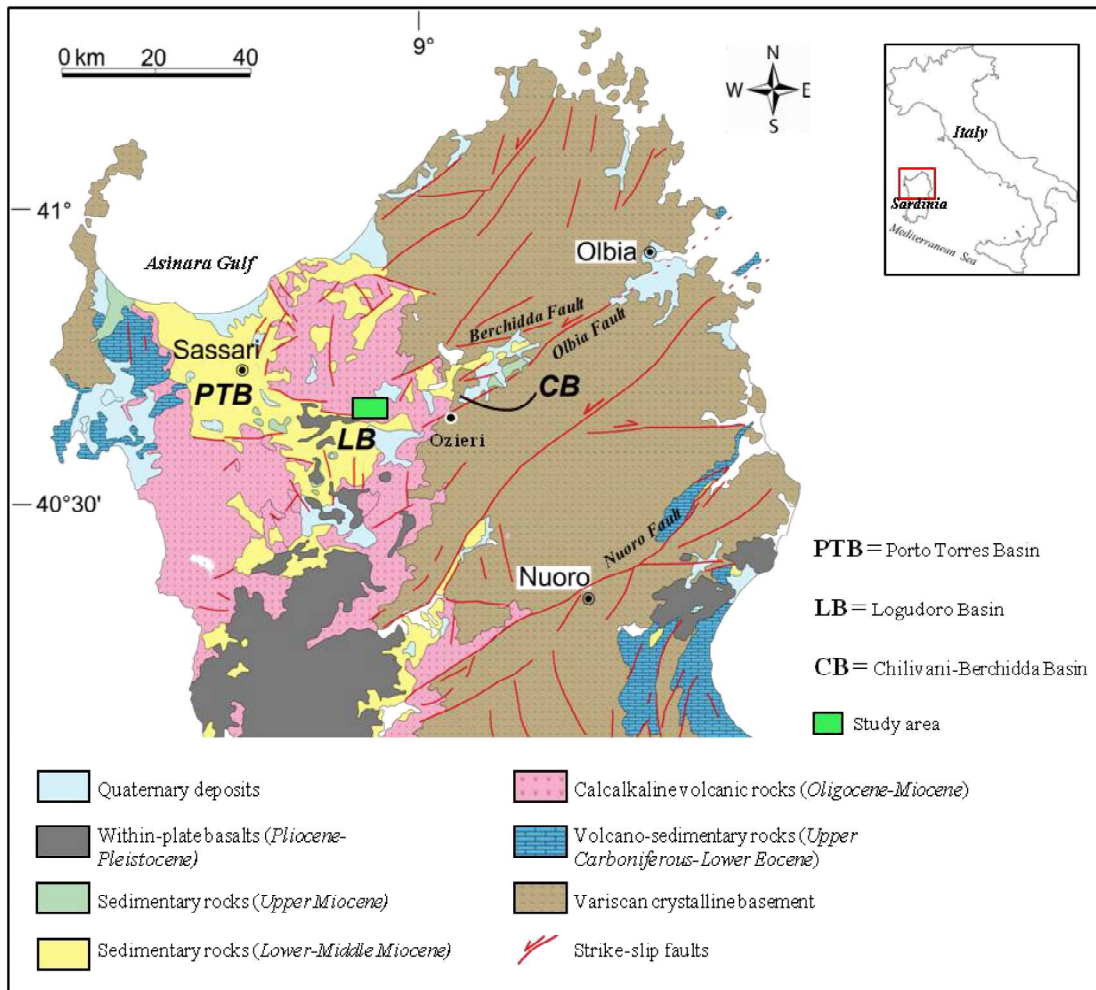
Vittorio Longo - Prospecting of Industrial Minerals: a geophysical approach -
PhD Thesis in Natural Science - University of Sassari

48

Fig. 4.1 - Geological sketch map of northern Sardinia. The study area is highlighted with green box.

Figure 4.2 shows the 1:10000 geological map obtained with permission from Minersarda S.p.a. company.

The lithologies outcropping in the site, from bottom to top, can be described as follows:

- Epiclastic deposits composed of finely laminated tuffites (**12**) characterized by alternating laminae of pumice- and ash-rich layers. These levels outcrop in the western sector of the geological map, to the west of M. Pittu.

- Andesitic autoclastic breccias with porphyritic structure. These units were dominated by pyrolusite and silica important mineralizations and outcropping in the northern sector (outside of the limits of the geological map).

- Poorly welded pyroclastic fall-out deposits (**10**) are pink in colour and they outcrop sporadically at west of M. Pittu and at east of M. Cheja.

- Strongly welded pyroclastic flow deposits with rhyolitic composition (**9**) and red-purple in colour. This is the main lithotype of study area and shows a less welded horizon with not collapsed pumice lenses and interbedded smectictic clays.

Vittorio Longo - Prospecting of Industrial Minerals: a geophysical approach -
PhD Thesis in Natural Science - University of Sassari

49

- Mildly welded pyroclastic fall-out deposits, pink in colour (**8**) are found in the western and southern parts of the work area, usually close to the faults or fractures.

- Epiclastic deposits consists of medium to fine sandstones with traces of bioturbation, brownish silt and green sandstones deposited in lacustine environment. These lithologies do not outcrop in the study area.

- The sedimentary sequence associated with the Burdigalian transgression is absent and the Tertiary volcanic rocks are directly overlain by blackish-brown clayey soils smectitic minerals-rich (**2**).

At the base of the main morphological steps, originated by faults, there is a detritus sediment consisting of cemented angular clasts rich in clay matrix of Oligocene age.
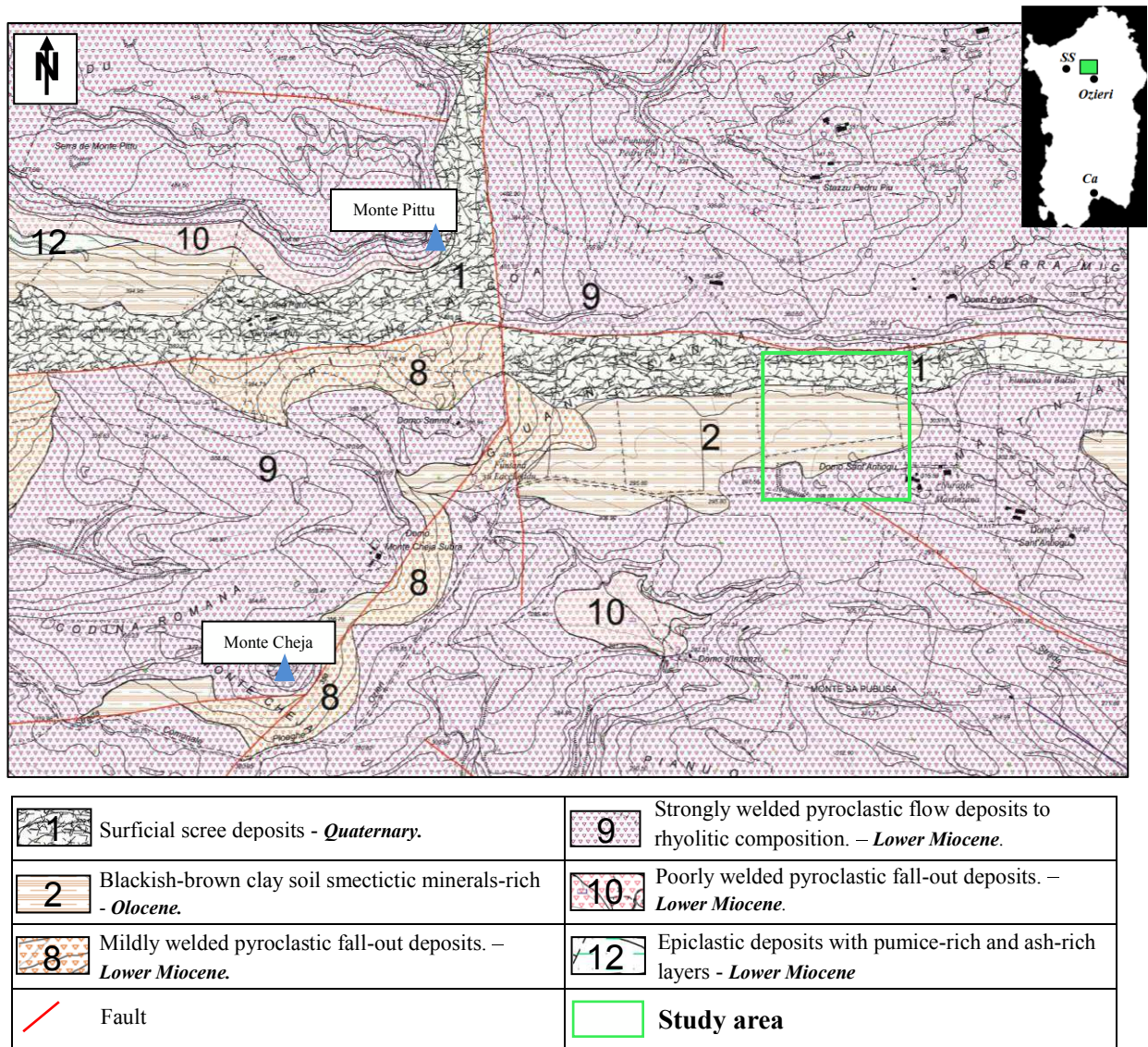

1 Surficial scree deposits - *Quaternary.*		**9** Strongly welded pyroclastic flow deposits to rhyolitic composition. – *Lower Miocene*.	
2 Blackish-brown clay soil smectictic minerals-rich - *Olocene.*		**10** Poorly welded pyroclastic fall-out deposits. – *Lower Miocene*.	
8 Mildly welded pyroclastic fall-out deposits. – *Lower Miocene.*		**12** Epiclastic deposits with pumice-rich and ash-rich layers - *Lower Miocene*	
Fault		**Study area**	

Fig. 4.2 - Geological map (1:10000 scale). Green box show the study area.

Vittorio Longo - Prospecting of Industrial Minerals: a geophysical approach -
PhD Thesis in Natural Science - University of Sassari

50

4.2.1 - Hypothesis on the genesis of the clay deposit

The examined bentonite deposit has similar characteristics to some accumulations of clays found in nearby areas (Locality Sa Coa and near Nuraghe Ruiu) from previous studies (Fois, 2002). The "Monte Furros" deposit shows the features of hydrothermal deposit.

The different types of Sardinian bentonite deposits can be related to the chemical, physical and mineralogical condition under which the alteration of the source rock occurs.

In these deposits the alteration occurs just after the deposition of poorly welded pyroclastic units (pomiceous-ash-rich layers) and the clay formation is favored from the action of meteoric waters and juvenile fluids in hydrothermal environments.

In the "Monte Furros" deposit, the alteration process also has been controlled by hydrothermal fluids circulating along the main faults or fractures systems.

Although the pyroclastic volcanic materials outcrop everywhere in the examined area, it is significant that these mineralized rocks are found only in correspondence of the faults, namely an important E-W trending strike-slip fault and a N-S trending normal fault (fig. 4.2).

Vittorio Longo - Prospecting of Industrial Minerals: a geophysical approach -
PhD Thesis in Natural Science - University of Sassari

51

4.3 - Location of geoelectrical profiles and intrusive site investigation

The geoelectrical surveys have been carried out by a multi-electrode system (Dahlin, 1996), consisting of Abem Terrameter SAS1000 control unit combined with ES 10-64 electrode selector (par.2.1).

For each 2D electrical line, 64 stainless steel electrodes were strung and anchored into the ground surface with constant spacing and connected to a multicore cable.

The Wenner-Schlumberger array was used for data acquisition. This configuration is a hybrid between Wenner and Schlumberger arrays (Loke, 2000) and it is moderately sensitive to both horizontal and vertical structures.

A complete scheme of ERTs location is presented in figure 4.3A.

The OZ1 profile, with 2°N direction, was performed perpendicularly to the E-W trending strike-slip fault, in order to evaluate the clay/bedrock resistivity contrasts and to define the geometry of the mineralized body in deep. In the line the electrodes were spaced every 6 metres, giving a total length of 378m and a maximum investigation depth of 60m.

The OZB1 and OZB2 profiles were located to the south of the E-W trending fault. For both lines was used inter-electrode spacing of 4m, obtaining an unit length of 252m and a maximum investigation depth of 40m.

These 2D electrical lines were performed in correspondence of some pre-existing boreholes for evaluate the reliability of the method.
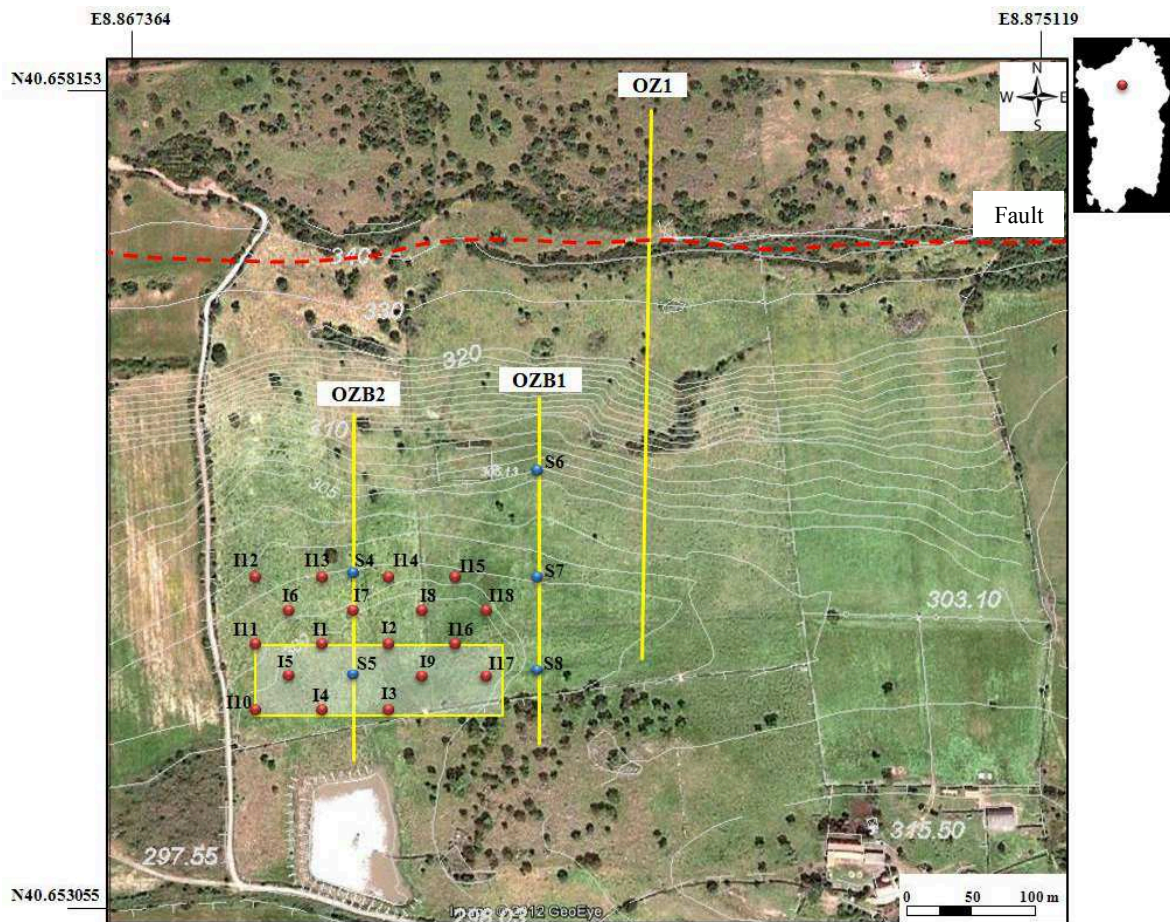
The 3D ERT survey covered a rectangular surface of 189m (*x-axis*) by 54m (*y-axis*) in the south-western part of study area (fig. 4.3B).

Data were collected only in x-direction along a series of 7 west-east parallel 2D electrical lines positioned at 9m intervals. For each line the electrode spacing of 3m was used, giving a unit length of 189m.

The aim of 3D ERT survey was to provide a reliable resistivity model to estimate the volume of exploitable clay in a test area.
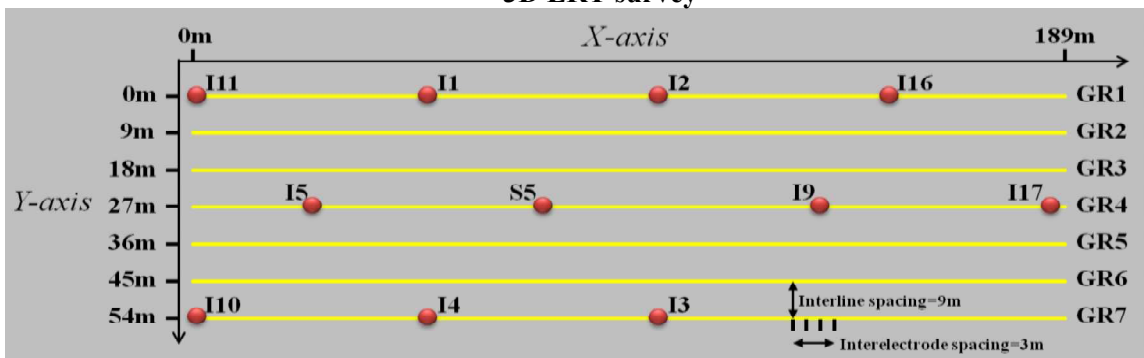
All lines have been placed in the map through GPS points collected in the field (fig. 4.3A). For each line were measured the coordinates relative to the first electrode, at the centre of the profile and the last electrode.

The topography, essential for a correct interpretation of tomographies, was rebuilt through the altitudes measured with an inclinometer.

Vittorio Longo - Prospecting of Industrial Minerals: a geophysical approach -
PhD Thesis in Natural Science - University of Sassari

52

A)

B)

Fig. 4.3 - A) Satellite image of the study area including boreholes (S logs in red colour and I logs in blue colour) and ERT survey lines position (yellow lines). B) Detail of the investigated area by 3D ERT survey.

In addition to the ERT surveys, two phases of intrusive investigation have been undertaken (fig. 4.3 A-B). The first phase was carried out before the ERT surveys and involved only few sample points (S4-S5-S6-S7-S8).

The second intrusive investigation phase (from I1 to I18), subsequent electrical investigations, was focused in and around the 3D ERT survey area. This phase included a total number of 18 boreholes placed according to a regular grid with a reciprocal distance of 50m.

Vittorio Longo - Prospecting of Industrial Minerals: a geophysical approach -
PhD Thesis in Natural Science - University of Sassari

53

4.4 - Data processing

The apparent resistivity values for each electrical line were downloaded from the Terrameter SAS 1000 control unit to the PC, and then were converted in a format that is acceptable by the RES2DINV inversion software (Loke, 2001a).

All 2D apparent resistivity data, were inverted using the *L2-norm* implementation (smoothness-constrained) of the regularized least-squares optimization method (Ellis and Oldeburg, 1994a).

This methods tends to produce models with a smooth spatial variation in resistivity values, and it is more suitable where the true subsurface geology exhibits a gradual change in the electrical proprieties (Loke et al., 2003).

The L2-method is based on the following equation:

$$(\mathbf{J_i^T J_i} + \lambda_i \mathbf{C^T C})p_i = \mathbf{J_i^T g_i} - \lambda_i \mathbf{C^T}Cr_{i-1} \qquad \text{(Eq. 4.1)}$$

where $\mathbf{J_i}$ is the Jacobian matrix of partial derivates, $\mathbf{J_i^T}$ represent the transpose of $\mathbf{J_i}$, $\mathbf{g_i}$ is the discrepancy vector which contains the difference between the logarithms of calculated and observed apparent resistivity values, p_i is the perturbation vector to the model parameters, λ is a damping factor (or Lagrange multipier) used to reduce the amplitude of p_i, $\mathbf{C}$ is a flatness-filter matrix used to minimize the roughness of p_i.

The second term on the right-hand side of equation 4.1 applies the smoothness constrain directly on the model resistivity vector, r_{i-1}. This guarantees that the model will be smooth subject to the damping factor used. It also reduces the oscillations in the model resistivity values (Ellis and Oldenburg, 1994b; Olayinka and Yaramanci, 2000).

The forward problem was solved using the finite-element method (Silvester and Ferrari 1990), in which node positions were adjusted to allow topography to be taken into account in the inversion process (Loke, 2001a).

Standard Gauss-Newton optimization methods was used whit a convergence limit of 0.005, the Jacobian matrix was recalculated for the first two iterations and the finer model with the cell width of half the minimum electrode spacing was used.

2D resisitivity data set were examined and the "bad data points" were removed in some cases manually and pre-inversion, in other cases automatically and post-inversion (par. 2.2)

For 3D ERT survey conducted in the test area, the data from each 2D electrical line, were initially inverted independently with RES2DINV to give 2D cross-sections.

Vittorio Longo - Prospecting of Industrial Minerals: a geophysical approach -
PhD Thesis in Natural Science - University of Sassari

54

To produce a single 3D data set, all 2D survey data files were rearranged using option entitled "collate data into Res3dinv format" in the file menu of RES2DINV software.

Data integration gave rise a grid size of 64 x 7 electrodes in the x-and y-direction respectively, and it provided 7.203 data points.

The collated 3D data set were inverted using *L2-norm* implementation method by RES3DINV software (Loke and Barker, 1996; Loke, 2004), which automatically produces the subsurface horizontal depth slices.

To reduce the inversion time, the *Incomplete Gauss-Newton* method with a convergent limit of 0,012 was used, and the forward problem was solved using the finite element method (Silvester and Ferrari, 1990).

The Jacobian matrix was recalculated for first five iterations and initial damping factor of 0,160 was used. After each iterating process, the inversion subroutine generally reduced the damping factor used; a minimum limit of 0,015 was set to stabilize the inversion process.

A model blocks where the three top layers are divided by half in the horizontal directions was used. The final 3D resistivity model consisted of 16 layers in the vertical directions, resulting in a total of 4.914 model cells.

4.5 - Graphical representation of the resistivity models

In addition to parameters involved in the inversion process, was used a graphical representation of the tomographies that offers a ready understanding of the search geological levels.

Figure 4.4 shows an appropriate scale of resistivity values with relative colours assigned to the interest lithologies, and a representative stratigraphic column derived from calibration boreholes.

Pyroclastic layers show a wide range of resistivity values from 13 to up 200 $\Omega \cdot m$ in relation to the fracturing and alteration conditions.

The bedrock, consisting of welded pyroclastics, is shows violet-red in colours ($\rho > 50$ $\Omega \cdot m$), while pyroclastic levels altered by hydrothermal fluids are represented by yellow-orange colours ($13 < \rho < 40$ $\Omega \cdot m$).

The bentonitic clays, according to Kaufhold and Penner (2006), have low resistivity value ranging between 1 and 4 $\Omega \cdot m$, and are represented by blue-green colours.

Vittorio Longo - Prospecting of Industrial Minerals: a geophysical approach -
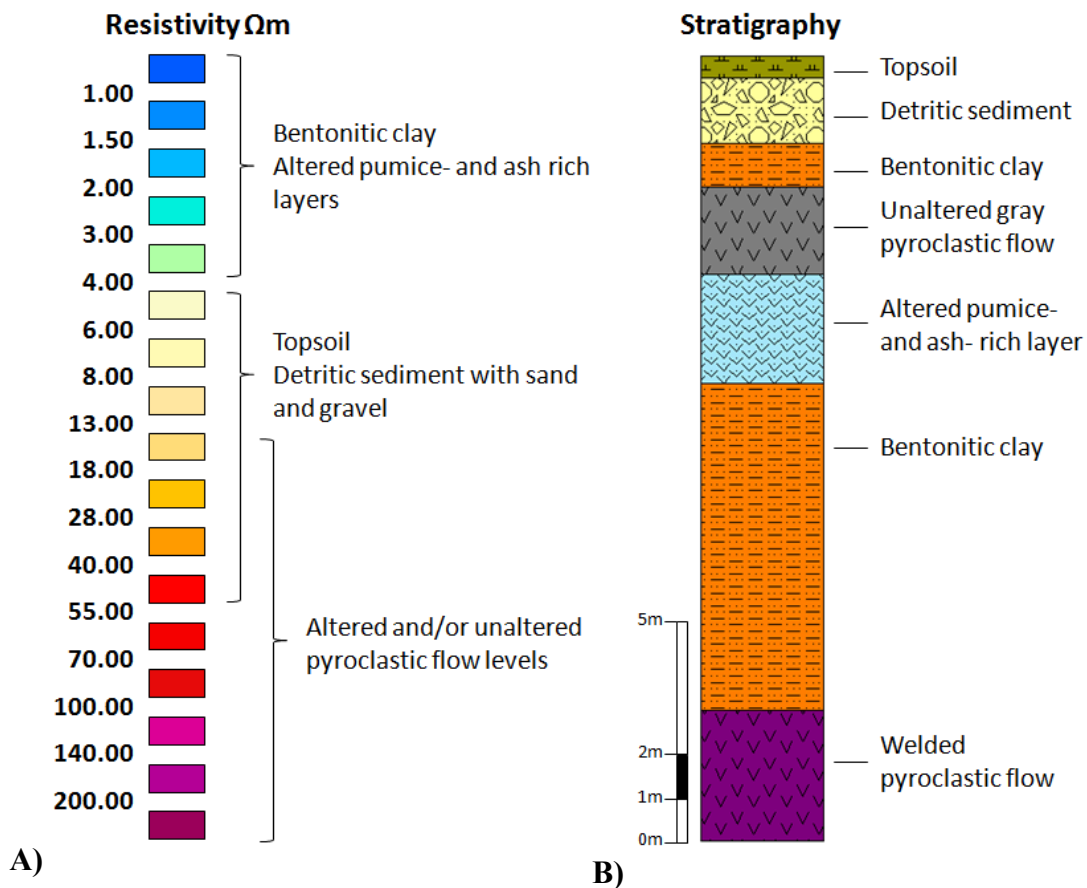PhD Thesis in Natural Science - University of Sassari

55

Fig. 4.4 - A) Scale of resistivity value with relative colours assigned to the interest lithologies. B) Representative stratigraphic column derived by boreholes.

The "overburden", that consist of a thin topsoil and a detritic sandy-gravelly deposit, has resistivity values ranging from 6 to 50 Ω·m.

This wide range is related to the heterogeneity of the deposit and the percentage of clayey component.

Pyroclastic fall-out deposits (pumice- and ash-rich layers) was also detected, interlayer within bentonitic levels. Through ERT methods, isn't possible distinguish these levels due the similar resistivity values than the bentonitic clays.

Vittorio Longo - Prospecting of Industrial Minerals: a geophysical approach - PhD Thesis in Natural Science - University of Sassari

56

4.6 - 2D ERT results

- *OZ1 tomography*

ARRAY	WENNER-SCHLUMBERGER n = 3
MEASURED RESISTIVITY POINTS	1089
ARRAY LENGTH	378 m
INTERELECTRODE SPACING	6 m
MAXIMUM INVESTIGATION DEPTH	60 m
GPS POINTS	ELECTRODE 1 - 40°39'17.37"N; 8°52'17.73"E
	ELECTRODE 32 - 40°39'23.48"N; 8°52'17.99"E
	ELECTRODE 64 - 40°39'29.56"N; 8°52'18.31"E

The OZ1 tomography was acquired perpendicular to the fault which lies in northern part of investigated area (fig. 4.5).

During the acquisition, the instrument recorded several negative measurements, which significantly reduce the data quality, and are typically caused by poor contact between the electrodes and the soil.

During processing, the negative values and measurements with high standard deviations (> 5%) have been removed. In this way the resistivity points used for the inversion process are 873 respect to the 1089 acquired and the RMS error associated is 30.6 %.

In the 2D resistivity model, at the station at 285m (*x-direction*), the presence of the fault plane causes a sudden horizontal variation of the resistivity values.

Welded pyroclastics outcrop at north of the fault and have high resistivity values ($\rho > 140$ $\Omega \cdot m$), while the pyroclastics rocks at south of the fault are altered by the action of hydrothermal fluids and have lower resistivity values ($\rho < 140$ $\Omega \cdot m$), depending of the alteration conditions.

In the southern sector, a bentonitic clay level with low resistivity values ($\rho < 4$ $\Omega \cdot m$ and blue-green in colour) is clearly defined. This continuous level is deepens towards the fault plane and from south to north show a thickness ranging from 20 to 5m.
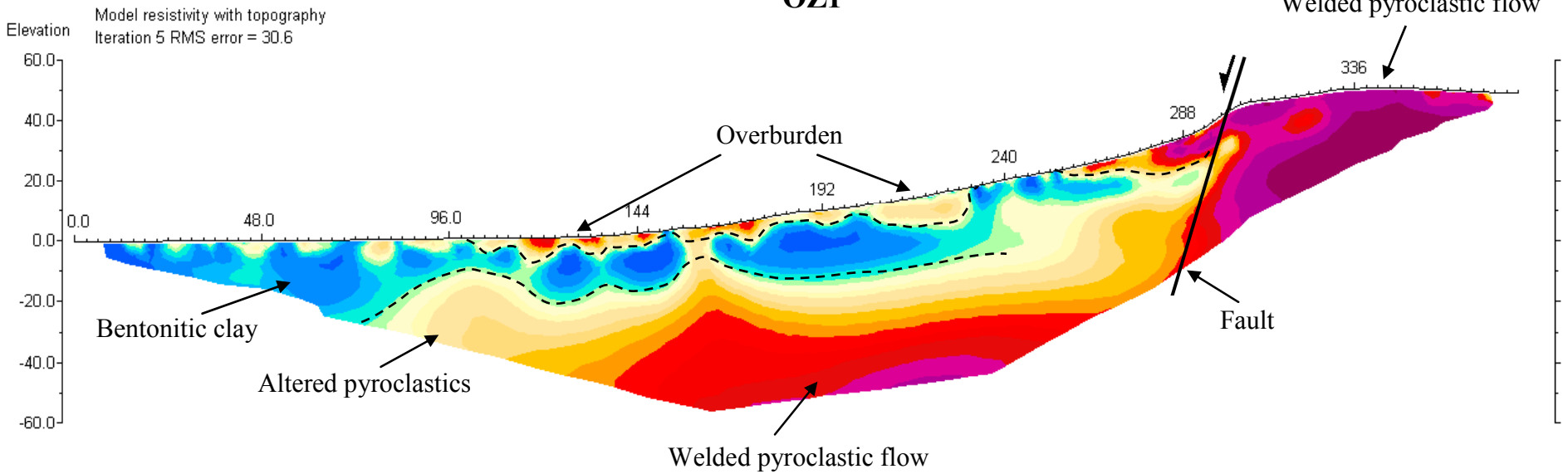
The conductive level is capped by a sandy-gravelly slope deposit rich in clay matrix, with resistivity values ranging between 6 and 50 $\Omega \cdot m$ and variable thickness from 2 to 12m.

The bedrock, detected in the deeper section of tomography, shows resistivity values which gradually increase with the depth to exceed 50 $\Omega \cdot m$ at 30m deep. Such variations are index of altered bedrock which becomes more compact in depth.

Vittorio Longo - Prospecting of Industrial Minerals: a geophysical approach -
PhD Thesis in Natural Science - University of Sassari

57

Fig. 4.5 - OZ1 tomography.

Vittorio Longo - Prospecting of Industrial Minerals: a geophysical approach -
PhD Thesis in Natural Science - University of Sassari

58

- *OZB1-OZB2 tomographies*

ARRAY	WENNER-SCHLUMBERGER n=2
MEASURED RESISTIVITY POINTS	923
ARRAY LENGTH	252 m
INTERELECTRODE SPACING	4 m
MAXIMUM INVESTIGATION DEPTH	35 m
GPS POINTS	**OZB1** *ELECTRODE 1*-40°39'15.01" N; 8°52'14.96" E *ELECTRODE 32*-40°39'19.09" N; 8°52'14.99" E *ELECTRODE64*-40°39'23.19" N; 8°52'15.01" E **OZB2** *ELECTRODE 1*-40°39'14.57" N; 8°52'9.10"E *ELECTRODE 32*-40°39'18.68" N; 8°52'09.15" E *ELECTRODE 64*-40°39'22.79" N; 8°52'9.14" E

In OZB1 and OZB2 tomographies (fig. 4.7) a good convergence between the observed and model resistivity data was achieved after five iterations with a RMS error lower than 5%.

From the ERTs analysis it's possible to recognize three sub-horizontal levels:

- Debris slope deposits with intermediate resistivity (6-50 Ω·m).
- Conductive clayey level ($\rho < 4$ Ω·m).
- Resistive pyroclastic bedrock (20-200 Ω·m).

In both profiles the debris slope deposit is conform with topographic profile and it increases in thickness towards the north.

The clayey level is clearly detected in the first part of the tomographies (from 32m to 128m in *x-direction*) where it is sub-outcropping.

Proceeding northwards, are not found the resistivity values assigned to clayey level below the debris slope deposits, even if between 10 and 25m in deep, are recorded lower resistivity values compared to the ones measured in surface and in depth.

Vittorio Longo - Prospecting of Industrial Minerals: a geophysical approach -
PhD Thesis in Natural Science - University of Sassari

59

The welded pyroclastic flow deposits were detected in the deeper portion of the ERTs at a depth of 15-20m, except in the southern sector where they outcrop (fig. 4.6).
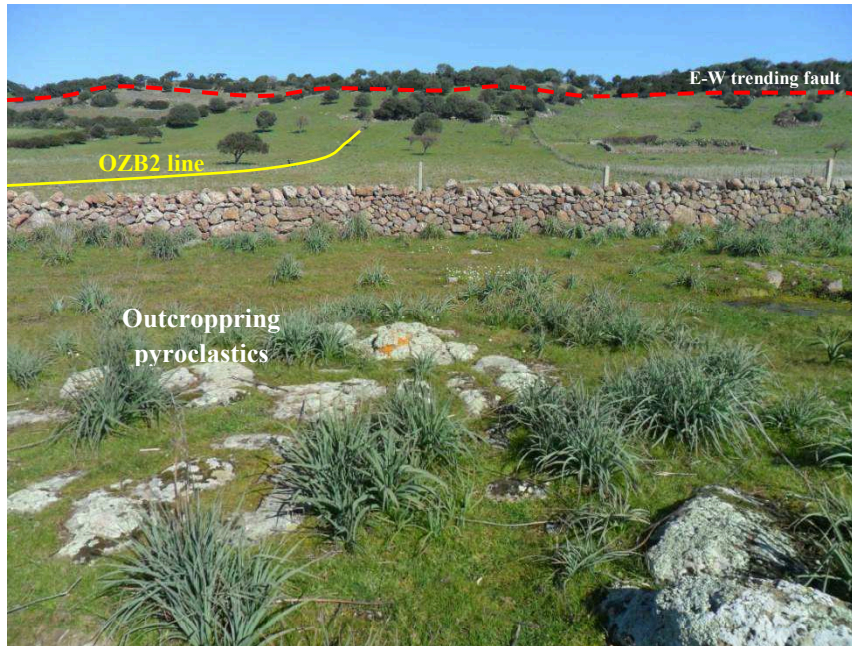

Fig. 4.6 - Southern sector of the studied area where the pyroclastics outcrop. OZB2 ERT trace (yellow line) and E-W trending fault (red line).

The borehole logs located in correspondence of the ERTs profiles confirm the presence of bentonitic clays for the whole length of the electrical surveys (fig. 4.7).

Particularly, the S8-S7 logs (50m and 122m in *x-direction* respectively) in the OZB1 line and S5-I7 logs (62m and 116m in *x-direction* respectively) in the OZB2 line show a good correspondence with the resistivity data.

Conversely, regarding S6 and S4 logs (202m in the OZB1 line and 146m in the OZB2 line in *x-direction* respectively) there is no a good corresponding between stratigraphic data and resistivity values (fig.4.7).

In these cases the presence of a thick resistive body, upper or intercalated, to the clayey level determines some difficulties in resolving properly this level.

This situation will be demonstrated by the synthetic models in 4.6.1 paragraph.

Vittorio Longo - Prospecting of Industrial Minerals: a geophysical approach -
PhD Thesis in Natural Science - University of Sassari

60
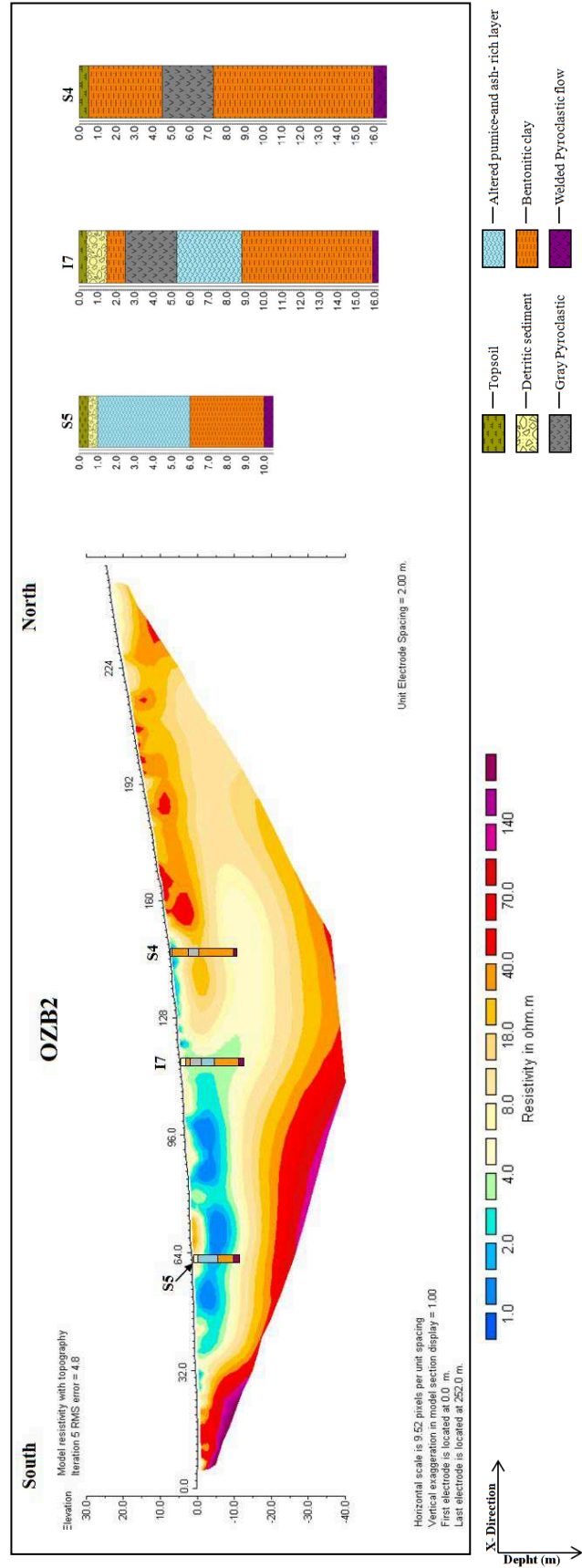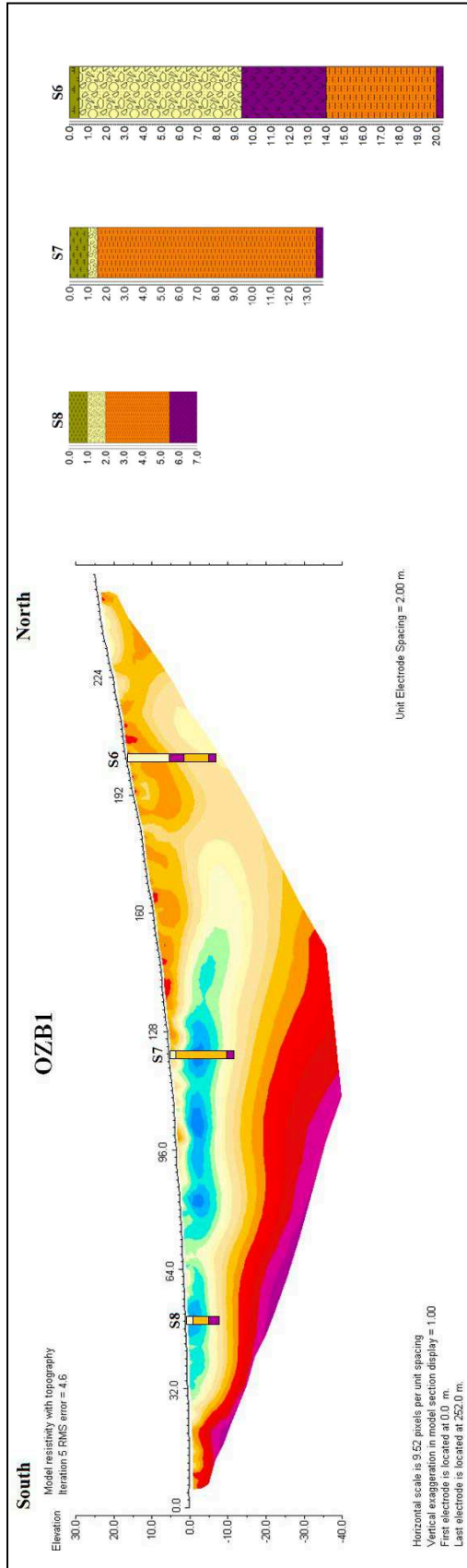
Fig. 4.7 - OZB1 and OZB2 tomographies with borehole location and relative stratigraphy columns.

Vittorio Longo - Prospecting of Industrial Minerals: a geophysical approach -
PhD Thesis in Natural Science - University of Sassari

61

Several months after the execution of the ERTs, Minersarda S.p.a. has begun work on the extraction of clays in the studied area.

During excavation activities in the SW sector (about 50m to the west of OZB2 ERT) was found a 80°N direction fault plane that define an horizontal contact between the bentonitic clays and welded ignimbrites (fig. 4.8).

The fault is represented by a sudden change of horizontal resistivity values in both resistivity models (OZB1 and OZB2 ERTs), at the station at 32m (*x-direction*) (fig. 4.7).

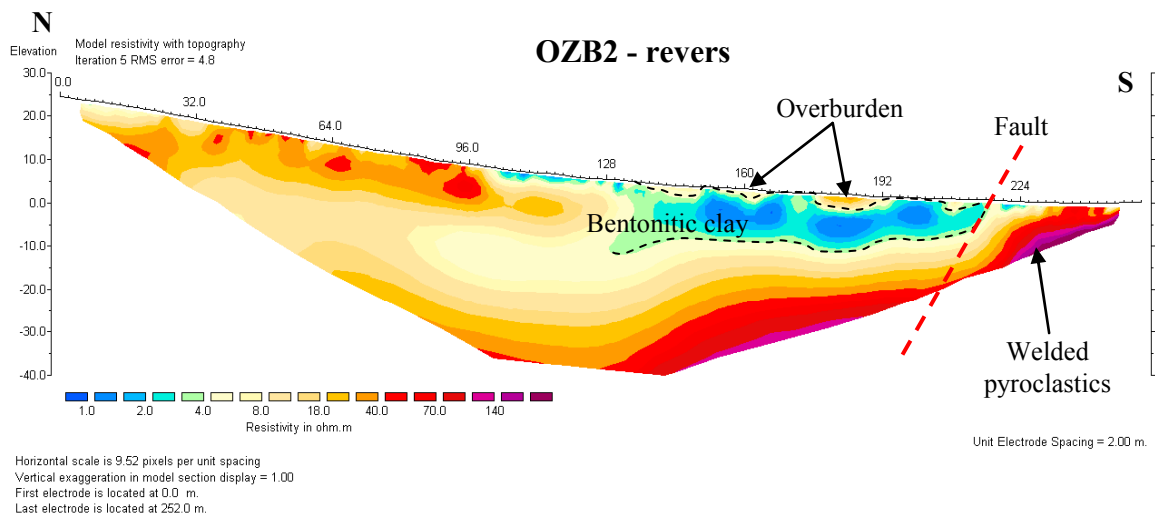**Fig. 4.8 - A) Picture of the S-W area during the excavation activity. B) OZB2 tomography performed about 50m to east of the excavation.**

Vittorio Longo - Prospecting of Industrial Minerals: a geophysical approach -
PhD Thesis in Natural Science - University of Sassari

62

4.6.1 - Synthetic simulation models

In order to illustrate how a conductive layer (clay), beneath a resistive overburden with variable thickness, is resolved in the ERT data inversion, a synthetic simulation model approach is proposed using RES2DMOD software package (Loke, 2001b).

RES2DMOD v.3.0 is a forward modeling program that calculates the apparent resistivity pseudosection for a user defined 2D subsurface model.

This method is based on finite difference modeling schemes, it works by dividing the subsoil into a series of rectangular cells and the electrical potential difference between the grid nodes is calculated respect to the resistivity values assigned to the grid rectangles (Loke, 2001b).

For each model, the apparent resistivity values are calculated considering a Wenner-Schlumberger array (*n=2 factor*), 64 electrodes spaced every 4 m and an overall length of 252m.

The synthetic apparent resistivity data were then inverted using RES2DINV v.3.4 software with *L2-norm* implementation (smoothness-constrained) of the regularized least-squares optimization method. This is the same method used for the acquired field data (OZB1 and OZB2 ERTs).

The reference model, characterized by three horizontal homogeneous levels, is shown in figure 4.9.

The first layer represents the sedimentary covering (overburden) with variable thickness (h_1) and resistivity value of 20 $\Omega \cdot m$. The second level has a thickness (h_2) of 6m and a resistivity value of 2 $\Omega \cdot m$ and represents the conductive clayey level. The third layer is the bedrock and it has an undefined thickness and a resistivity value of 100 $\Omega \cdot m$.

Eight synthetic models were elaborated using a h_1 thickness variable ranging from 0 to 14m.

The inversion results and the related synthetic models are shown in figure 4.9b.

When the overburden thickness (h_1) is less than or equal to 6m, the clay conductive level is correctly resolved despite the inversion process produces small variations in resistivity values (Kilner et al., 2005).

Conversely, when the thickness (h_1) is higher than 6m, the resistivity values of the clayey level results higher ($\rho > 6$ $\Omega \cdot m$) than whose assigned in the synthetic models ($\rho = 2$ $\Omega \cdot m$).

The depth and the thickness of the clayey layer cannot be correctly identified because its lower limit (interface clay/bedrock) is smeared and deeper than that assigned in the models.

The interface overburden/clay is clearer and more defined than the interface clay/bedrock in all obtained tomographies.
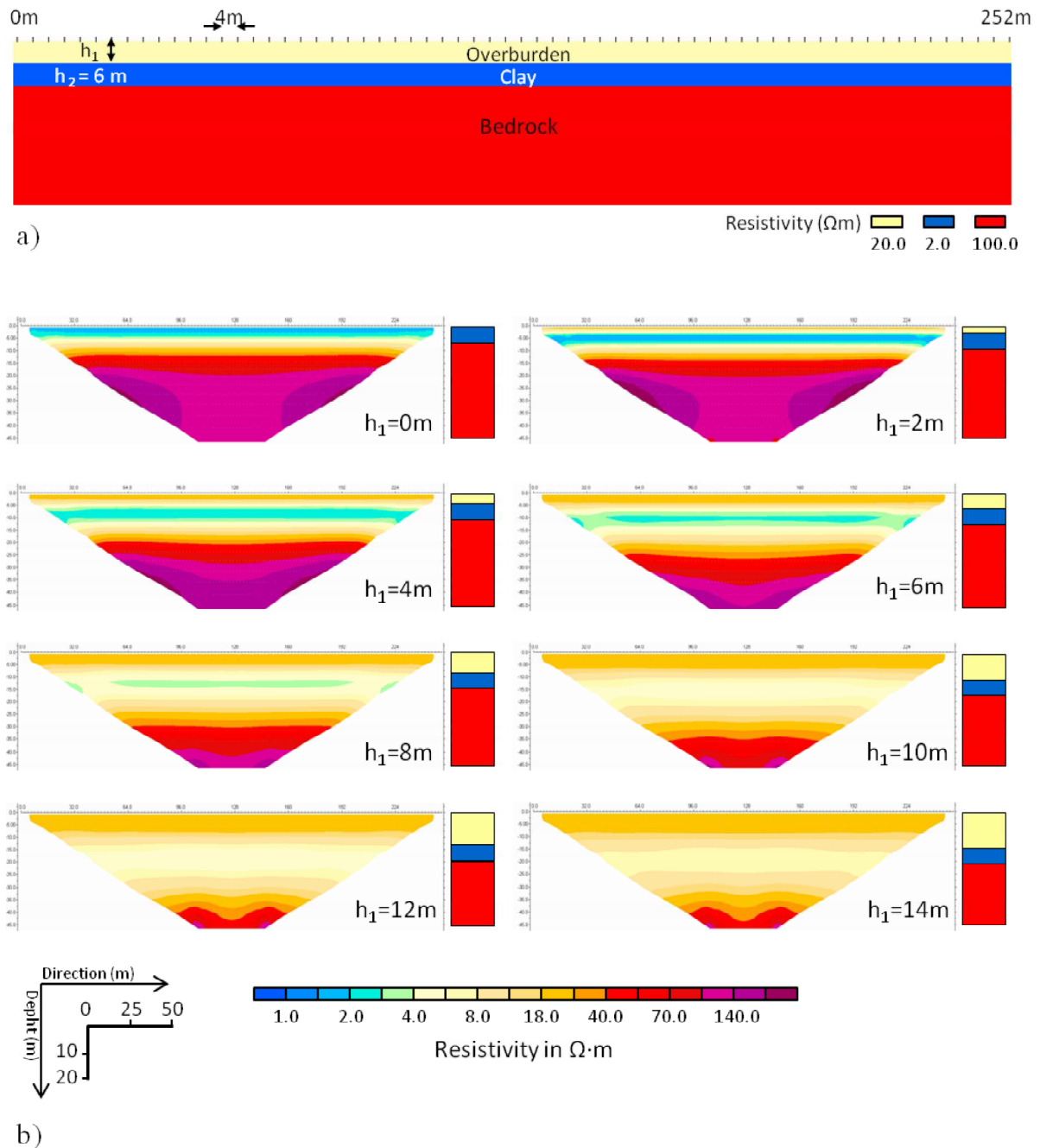
Vittorio Longo - Prospecting of Industrial Minerals: a geophysical approach - PhD Thesis in Natural Science - University of Sassari

63

Fig. 4.9 - a) Reference model with three horizontal levels represented by: overburden, clay level and bedrock. b) Inversion results for each h_1 value ranging from 0 to 14m.

The limitations discussed above are related to electrical current behavior at resistivity boundaries. When the electrical flow lines pass from the resistive level to the conductive one, they converge in correspondence of the limit (Telford et al., 1990). The result is that the current density in this boundary is increased, and so the potential gradient increase across the boundary.

Increased potential gradient leads to improve resolution in the inverted images, i.e. a sharp interface between resistive (overburden) and conductive (clay) levels.

Vittorio Longo - Prospecting of Industrial Minerals: a geophysical approach -
PhD Thesis in Natural Science - University of Sassari

64

Conversely when the current flow lines pass through clay\bedrock interface tends to diverge (Telford et al., 1990). The result is a decrease in current density and a decrease in potential gradient across the boundary. This is responsible for the smeared and deep boundary observed. The models and the respective tomographies, show that the clay layer resolvability is directly related to the overburden thickness (h_1).

In ERT survey an index of measurement accuracy at different depths is provided by the distribution of sensitivity function. The sensitivity function shows the degree to which a change in the resistivity of a section of the subsurface will influence the potential measured by the array. The higher the sensitivity value, the more reliable is the model resistivity value (Loke, 2010).

The figure.4.10 shows the models sensitivity distribution calculated for h_1=0m and h_1=14m tomographies. In the sensitivity model where the overburden is not present (h_1=0m), the cells near the surface have higher sensitivity values. For this reason the clay level present in this area is successfully solved in the tomography.

Whereas in the model where the overburden is 14 m thick, the boundary of clay level is not correctly solved due to the low values of sensitivity in the corresponding zone.

The results obtained by synthetic models have provided a useful guide to a more accurate interpretation of field survey, particularly in areas where the overburden has high thickness like S6 borehole (located at 202m in *x-direction* of OZB1 line) (fig. 4.7).
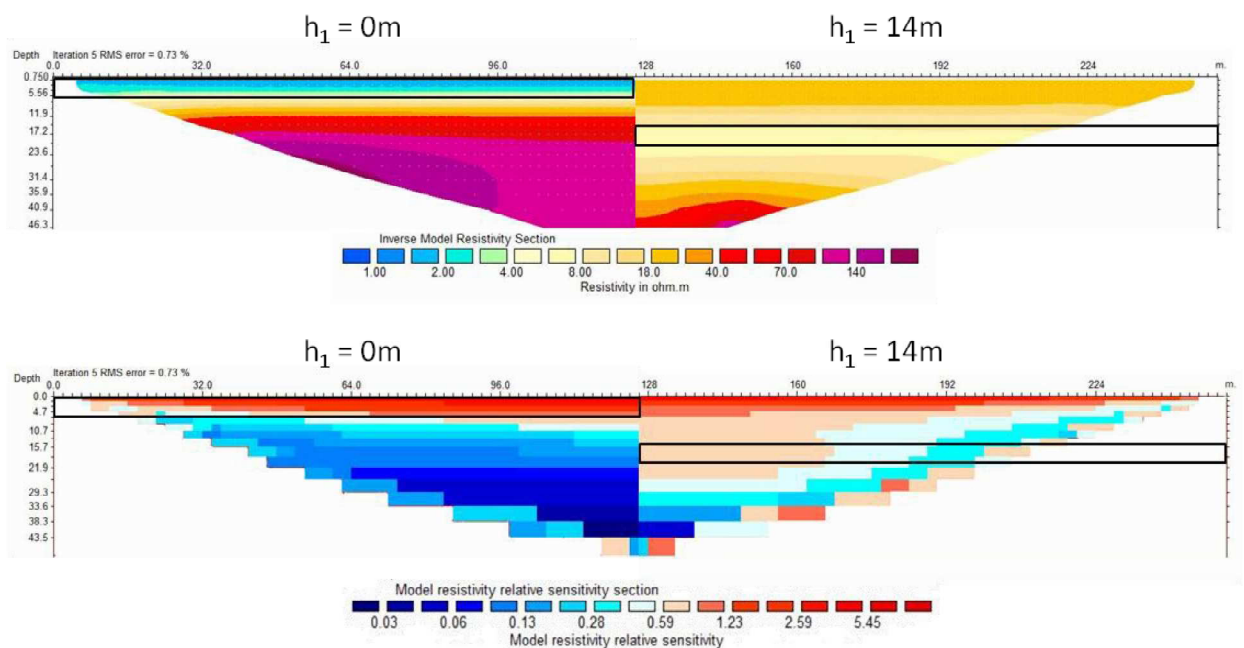

Fig. 4.10 - The top image shows the tomography related to synthetic models with h_1=0m (left) and h_1=14m (right). Below are reported the respective models of the sensitivity values distribution.

Vittorio Longo - Prospecting of Industrial Minerals: a geophysical approach -
PhD Thesis in Natural Science - University of Sassari

65

4.7 - 3D ERT results

ARRAY	WENNER-SCHLUMBERGER n = 2
MEASURED RESISTIVITY POINTS	7203
ARRAY LENGTH	189 m
INTERELECTRODE SPACING	3 m
MAXIMUM INVESTIGATION DEPTH	35 m
GPS POINTS	NW VERTEX - 40°39'17.53"N; 8°52'5.83"E
	NE VERTEX - 40°39'17.57"N; 8°52'13.86"E
	SE VERTEX - 40°39'15.75"N; 8°52'13.81"E
	SW VERTEX - 40°39'15.79"N; 8°52'5.80"E

In this paragraph are examined the 2D cross sections and 3D horizontal depth slices of the resistivity surveys performed in the test area (189x54m) located in the SW part of the site (fig.4.3).

The data collected for each of the 7 parallel electrical lines have been inverted individually using the RES2DINV software to obtain 2D resistivity models shown in figure 4.11.

A good convergence between the measured resistivity data and calculated resistivity data was reached after 5 iterations. For all tomographies the RMS error does not exceed 6,6%.

Analyzing the 2D resistivity sections, the subsurface can be approximated as consisting of three layers, according to the previous tomographies.

The intermediate level (clay) shows resistivity values lower than top layer (overburden) and bottom layer (pyroclastic bedrock).

The clayey body has been successfully resolved with an interelectrode spacing of 3 meters and a Wenner-Schlumberger array. The boreholes data validated ERT measurements.

The conductive level appears continuous in the west-east direction (*x-axis*) in all tomographies, with a narrow resistivity range between 1 and 4 Ω·m. The thickness of this layer ranged from 3 to 14 meters, in relation to the trend of the underlying bedrock.

In 2D cross sections in NS direction (y-axis), the bedrock has resistivity values greater than 50Ω·m and outcrops at the station at 150m (x-axis) in GR7 line.

In the western part of the GR1 and GR2 tomographies the conductive layer shows the maximum thickness. At the 48m station (*x-axis*) of GR1 line, the I1 log confirmed the presence of bentonitic clays interbedded with clayey tuff in a depth ranged from 2 to 12,5m.

Conversely in GR3, GR4, GR5 tomographies the conductive layer reaches the maximum thickness in the eastern sector, from 96 to 144 meters (*x-axis*).

Vittorio Longo - Prospecting of Industrial Minerals: a geophysical approach -
PhD Thesis in Natural Science - University of Sassari

66

The I9 log at the 125m station (*x-axis*) of the GR4 line confirmed the presence of bentonite and clayey tuff from 2m to about 14m in deep.

Some levels of glassy ignimbrite are present, but they are not detectable with resistivity surveys due to small thicknesses.

In the GR6 and GR7 ERT surveys the conductive layer has the minimum detected thickness (3-4m). The I10 (x =0m, y =50m), I4 (x = 50m, y = 50) and I3 (x =100m, y =50m) logs detect the clay/bedrock interface at an average depth of 7,5m.

The horizontal depth slices, obtained by a 3D data set inversion, are shows in figure 4.12.

A good convergence between the measured and calculated resistivity data was reached after 6 iterations with RMS error of 11,5%.

The subsurface has been divided into 16 XY levels, from the surface to a maximum depth of 35,5m.

In the 1 and 2 layers (depth between 0m and 3,07m) we can distinguish the overburden (**O**) with a resistivity ranged from 6 to 50 Ω·m. This shallow layer is constant with exception of the northeastern (x = from 174m to 189m; y = from 0m to -45m) and southwestern (x = from 0m to 18m; y = from 0m to -54m) edges, where conductive anomalies attributable to clays are detected.

The "banding" effect, caused by the resistivity data interpolation along the *y-axis*, is visible in the first layers and creates the resistivity anomalies with shapes elongated in this direction (Loke, 2010).

In layer 4 (depth ranged from 4,73m and 6,47m), the conductive body appears continuous and uniform, with exception of the south-eastern area where a resistive anomaly identifies the welded pyroclastics (**WP**).

From layer 5 to layer 9 (depth ranged from 6,47m to 16,5), the clayey body covers an area gradually smaller.

In the deeper horizontal slices (from layer 10 to layer 16) the highest resistivity values of the pyroclastics are measured in the south-east area (**WP**), while the lowest resistivity values are found in the central and northern portions (**AP**), according to the 2D cross section.

The uncertainty resistivity data in a 2D or 3D ERT survey increase in the edge and deepest parts.

Vittorio Longo - Prospecting of Industrial Minerals: a geophysical approach -
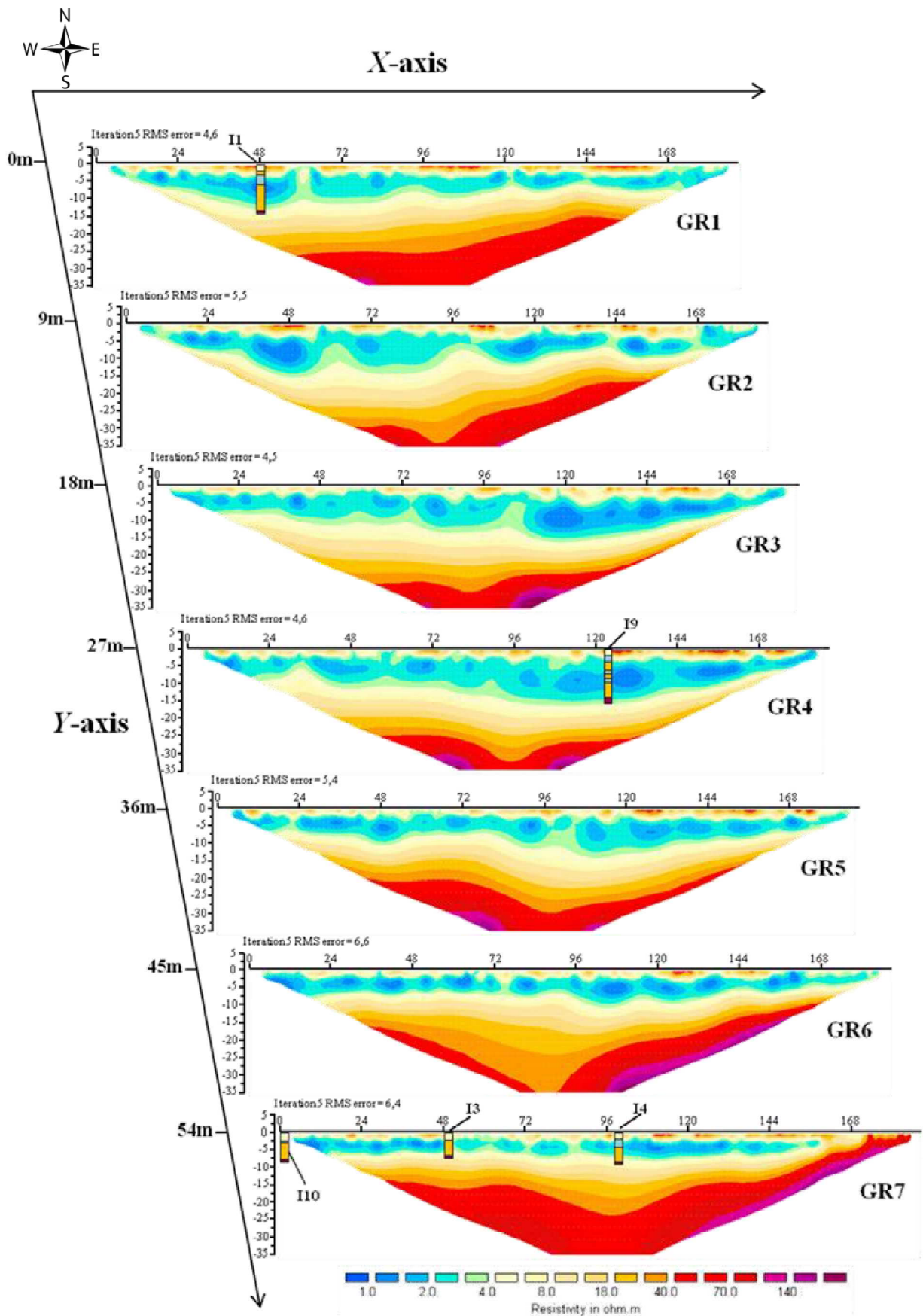PhD Thesis in Natural Science - University of Sassari

67

Fig. 4.11 - 2D parallel electrical resistivity cross sections carried out in the test area. Some boreholes were projected in correspondence to the lines.

Vittorio Longo - Prospecting of Industrial Minerals: a geophysical approach -
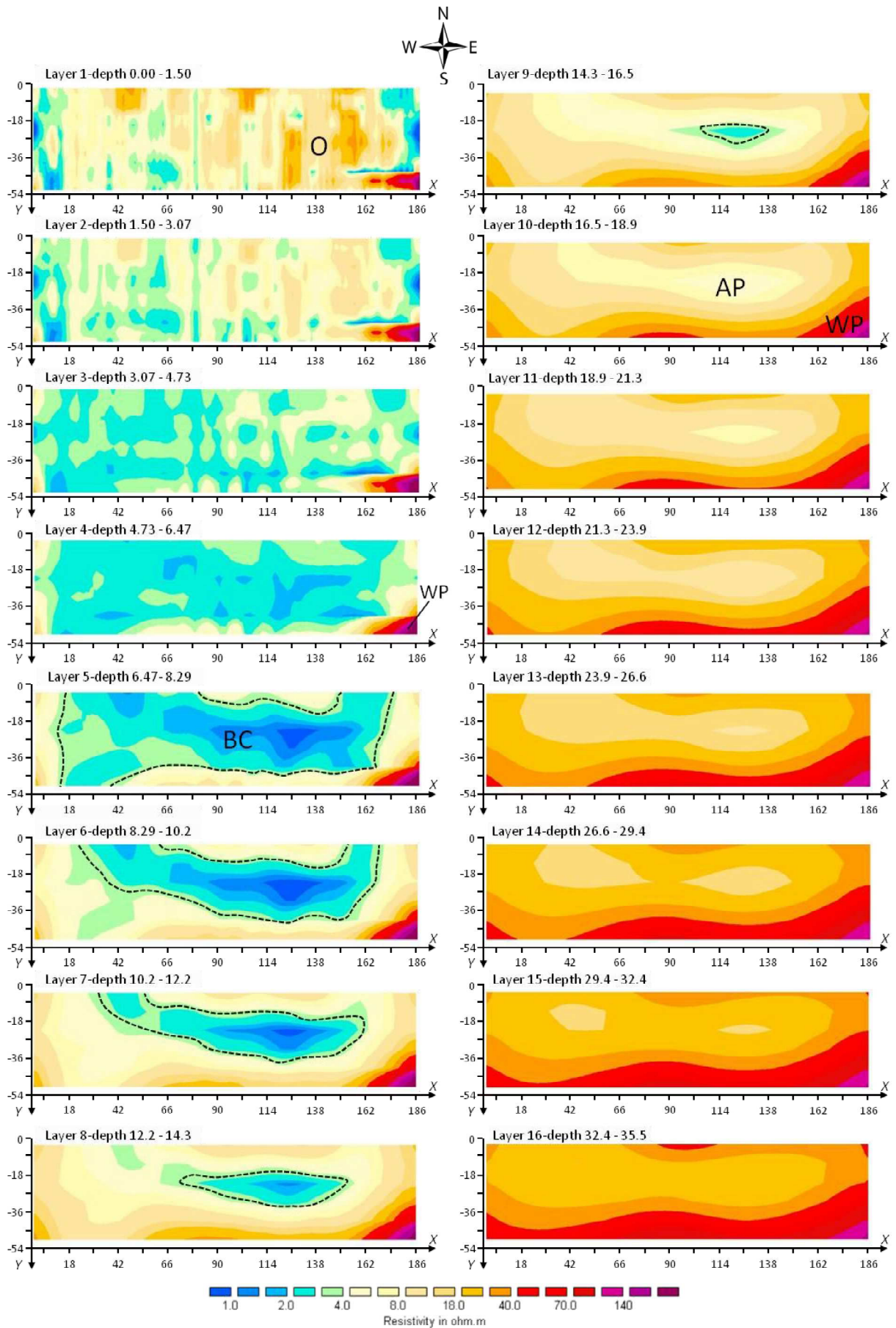PhD Thesis in Natural Science - University of Sassari

68

Fig. 4.12 - Electrical horizontal depth slices obtained by collated of 2D resistivity cross section of the test area.

Vittorio Longo - Prospecting of Industrial Minerals: a geophysical approach -
PhD Thesis in Natural Science - University of Sassari

69

4.7.1 - Integrated 3D models and visualization

In the test area, a 3D integrated models has been created with the geologic modeling software (RockWorks v.2009.3.23). Borehole logs have been included along with the resistivity model in a dynamic 3D representation of the site.

Drilling and ERT survey produce strongly contrasting types of information. On the one hand, borehole provide very detailed and very high resolution (centimeter to decimeter scale) information for vertical profiles at discrete locations, but on the other hand it provide very poor lateral resolution.

This occurs even for dense drilling grids, as in regarded case, where the separation is typically on the scale of at least tens of metres between holes. Moreover, drilling can provide direct samples of subsurface materials.

Conversely, 3D ERT provides high resolution (meter scale) spatially continuous volumetric subsurface models but provides indirect information on material properties.

Crucially, intrusive sampling is also essential for the calibration and validation of geophysical images. These two approaches are therefore complementary.

The 3D resistivity model output from RES3DINV has been gridded using a node spacing of 1m in the x, y and z directions, resulting in a model comprising 347.360 voxels.

Interpolation was carried out using an inverse-distance method, by which a weighted average of the closest data point from each 90° sector around each node was calculated.

The resulting models are shown in figures 4.13A and 4.13B.

The data deriving from 11 boreholes, performed into the test area, are in accordance with the stratigraphic relationships and the depth of the limits identified by resistivity variations.

The lower resistivity values ($\rho < 4$ $\Omega \cdot$m) assigned to the bentonitic clays were isolated (fig. 4.14), and the volume of potentially extractable materials was estimated.

The volume of conductive layer obtained by means the RockWorks software is 73.453m^3.

This value multiplied by the specific weight of material (1,9 t/m^3) and for safety factor (k=0,8) allowed to estimate of the extractable material in 111.648t.

Based only the direct surveys (borehole data) resources were estimated at 116.348t, considering covering surface (10.206m^2) X average thickness of mineralized layer (7,5 m) X specific weight of material (1,9 t/m^3) and for safety factor (k=0,8).

The calculated volume by both methods are comparable, confirming the good quality of geoelectrical data.

Vittorio Longo - Prospecting of Industrial Minerals: a geophysical approach -
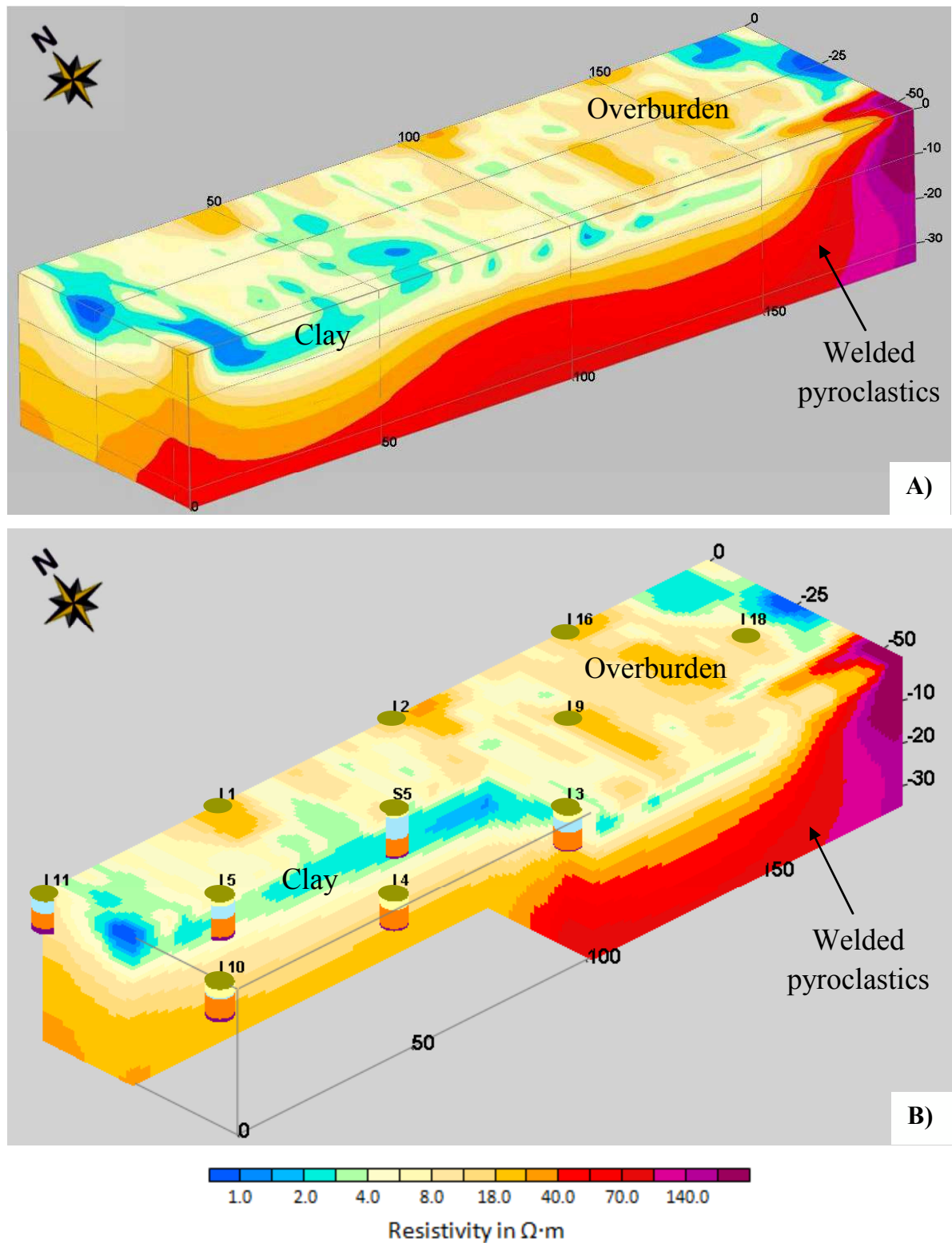PhD Thesis in Natural Science - University of Sassari

70

Fig. 4.13 - A) 3D ERT model obtained by 2D electrical resistivity cross sections interpolation. B) Integrated 3D ERT model along with borehole logs. The cut-outs allows viewing of some boreholes in 3D space.
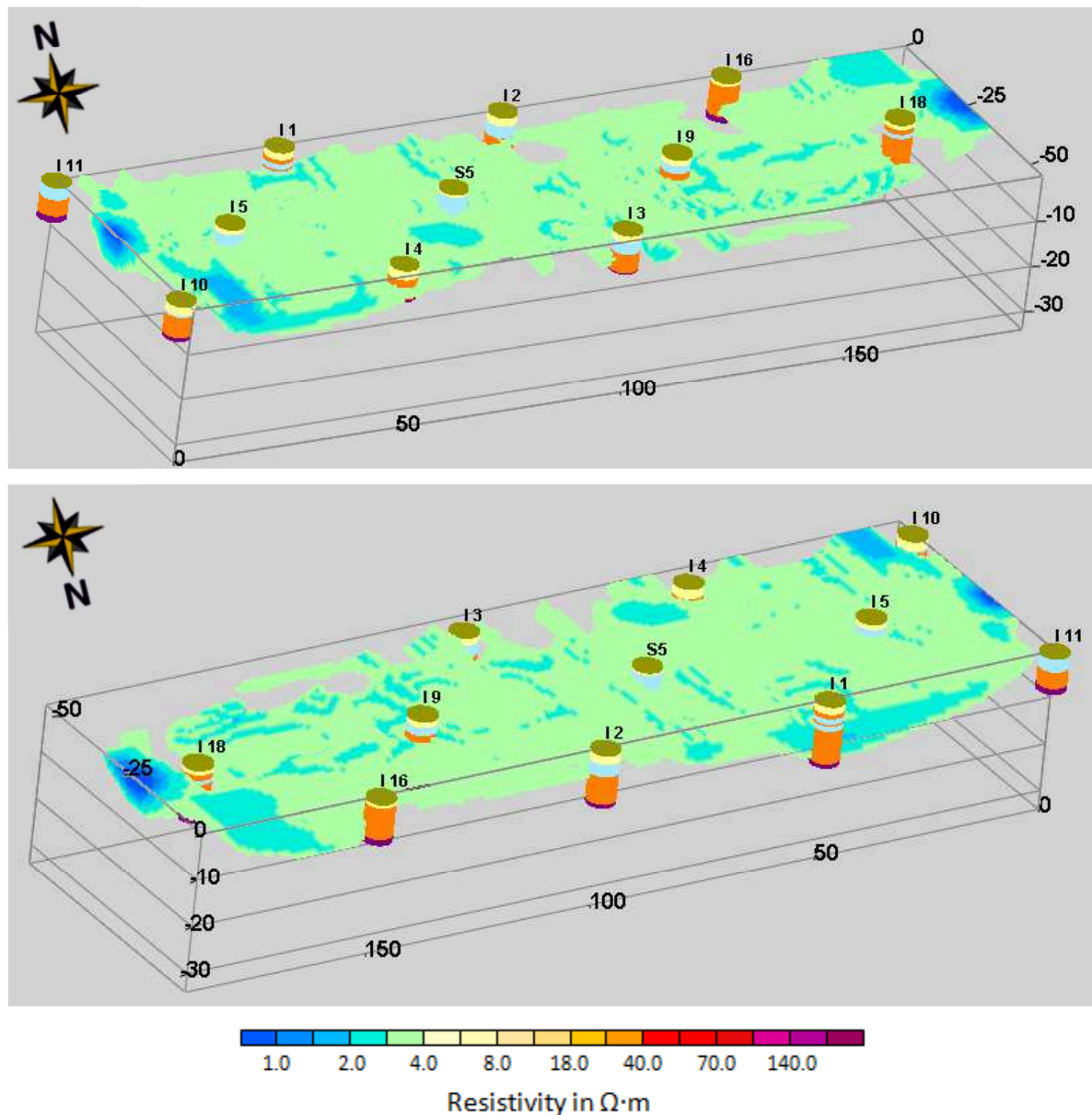
Vittorio Longo - Prospecting of Industrial Minerals: a geophysical approach -
PhD Thesis in Natural Science - University of Sassari

71

Fig. 4.14 - Integrated 3D models where the resistivity values lower than 4 Ω·m were isolated.

4.8 - Discussion and conclusions

The 2D and 3D geoelectrical survey conducted in loc. "Monte Furros" (Ozieri) confirm that this methodological approach can be successfully used for mineral exploration in geological contexts where an high-conductivity contrast exists between the mineral deposits and host rocks.

Particularly in the study area, the high resistivity contrast between the bentonitic clays and pyroclastic rocks allowed the ERT method to provide valuable indications about the locations, lateral continuity and in depth development of clayey body.

The resistivity data were calibrated based on stratigraphic constraints and borehole logs.

Vittorio Longo - Prospecting of Industrial Minerals: a geophysical approach -
PhD Thesis in Natural Science - University of Sassari

72

These information were crucial for a correct interpretation of resistivity tomographies.

As confirmed by geoelectrical surveys, the genesis and the geometry of clayey body is tectonically controlled.

In the OZ1 tomography, the E-W trending fault was well evidenced and the conductive clays body, originated by hydrothermal alteration, appears continuous.

A horizontal layers structure was identified consisting of: top layer (overburden), intermediate layer (clayey body) and bottom layer (pyroclastic bedrock).

The clayey layer has been successfully resolved by ERT method, when the overburden thickness was minor than that of the clay. Conversely, where the overburden is much thicker than the clayey layer, there is a loss in definition of the conductive layer.

These aspects have been demonstrated with synthetic models.

The 3D ERT survey revealed a relatively low cost, noninvasive and rapid mean to generate 3D model which is reliable for volume calculation of the exploitable clays.

The clay volumes estimated, by electrical and borehole data are very similar, hence an accurate 3D survey can conveniently replace direct borehole-based investigations.

References

AIZEBEOKHAI, A.P., AND OLAYINKA, A.I., 2010. *Anomaly effects of array for 3d geoelectrical resistivity imaging using orthogonal or parallel 2d profiles.* African Journal of Environmental Science and Technology, 4, 7, 446-454.

BENTLEY, L.R., AND GHARIBI, M., 2004. *Two- and three-dimensional electrical resistivity imaging at a heterogeneous remediation site.* Geophysics, 69, 674-680.

CERRI, G., AND OGGIANO, G. 2002. *Le epiclastiti zeolitizzate del Logudoro orientale: un livello guida all'interno della successione vulcano-sedimentaria della Sardegna centrosettentrionale.* Bollettino della Società Geologica Italiana, 121, 3-10

CHAMBERS, J.E., KURAS, O., MELDRUM, P.I., OGILVY, R.D., AND HOLLANDS, J., 2006. *Electrical resistivity tomography applied to geologic, hydrogeologic, and engineering investigations at a former waste-disposal site.* Geophysics, 71, 231-239.

CHAMBERS, J.E., OGILVY, R.D., KURAS, O., CRIPPS, J.C., AND MELDRUM, P.I., 2002. *3D electrical imaging of known targets at a controlled environmental test site.* Environmental Geology, 41, 690-704.

CHAMBERS, J.E., WIKINSON, P.B., WELLER, A.L., AUMONIER, J., OGILVY, R.D., WILLIAMS, J. D.O., MELDRUM, P.I., AND KURAS, O., 2008. *Determining Reserves of Aggregates by Non-invasive Electrical Tomography (DRAGNET): MIST Project MA/6/1/008.* British Geological Survey Commissioned Report, CR/08/040, 64.

Vittorio Longo - Prospecting of Industrial Minerals: a geophysical approach -
PhD Thesis in Natural Science - University of Sassari

73

DAHLIN, T., 1996. *2D resistivity surveying for environmental and engineering applications.* First Break, 14, 7, 275–283.

ELLIS, R.G., AND OLDENBURG, D.W., 1994a. *Applied geophysical inversion.* Geophysics Journal International, 116, 5–11.

ELLIS, R.G., AND OLDENBURG, D.W., 1994b. *The pole–pole 3D DC resistivity inverse problem: a conjugate-gradient approach.* Journal International, 119, 187–194.

FERGUSON, I.J., RISTAU, J.P., MARIS, V.G., AND HOSAIN, I., 1999. *Geophysical imaging of a kaolinite deposit at Sylvan, Manitoba, Canada.* Journal of Applied Geophysics, 41, 105–129.

FOIS, M., 2002. *Rilevamento geologico del Sassu di Chiaramonti. Stratigrafia, Tettonica e Georisorse.* Tesi di Laurea, Università di Sassari, 91.

GIAO, P.H., CHUNG, S.G., KYM, D.Y., AND TANAKA, H., 2003. *Electric imaging and laboratory resistivity testing for geotechnical investigation of Pusan clay deposits.* Journal of Applied Geophysics, 52, 157–175.

KAUFHOLD, S., AND PENNER, D., 2006. *Applicability of the SER method for quality control of clays from the German "Westerwald".* Applied Clay Science, 32, 53–63.

KILNER, M., WEST, L., AND MURRAY, T., 2005. *Characterization of glacial sediments using geophysical methods for groundwater source protection.* Journal of Applied Geophysics 57, 293–305.

LOKE, M.H., 1999. *Electrical imaging survey for environmental and engineering studies.* Unpublished report: www.geoelectrical.com.

LOKE, M.H., 2000. *Topographic modelling in electrical imaging inversion.* EAGE 62nd Conference and Technical Exhibition, Glasgow, UK.

LOKE, M.H., 2001a. *Res2Dinv software users manual, version 3.4.* Geotomo Software, Penang, Malaysia, 98.

LOKE, M.H., 2001b. *Res2DMod software users manual, version 3.0.* Geotomo Software, Penang, Malaysia, 28.

LOKE, M.H., 2004. *RES3DINV ver. 2.14: Rapid 3D Resistivity & IP inversion using the least squares methods.* M.H.Loke on www.geoelectrical.com, 90.

LOKE, M.H., 2010. *Tutorial: 2-D and 3-D electrical imaging suveys.* Unpublished report: www.geoelectrical.com. 145.

LOKE, M.H., ACWORTH, I., AND DAHLIN, T., 2003. *A comparison of smooth and blocky inversion methods in 2D electrical imaging surveys.* Exploration Geophysics 34, 182–187.

LOKE, M.H., AND BARKER, R. D., 1996. *Practical techniques for 3D resistivity surveys and data inversion techniques.* Geophysical Prospecting 44, 3, 499–524.

MAMELI, P., 2000. *Rilevamento e caratterizzazione mineralogica del caolino della Sardegna Settentrionale e proposta di impiego del materiale in settori non convenzionali.* PhD Thesis, 12° Cycle, Università di Sassari, 125.

Vittorio Longo - Prospecting of Industrial Minerals: a geophysical approach -
PhD Thesis in Natural Science - University of Sassari

74

NEYAMADPOUR, A., TAIB, S., AND WAN ABDULLAH, W.A.T., 2009. *An application of three-dimensional electrical resistivity imaging for the detection of an underground waste-water system.* Studia Geophysica et Geodaetica, 53, 389-402.

OGGIANO, G., AND MAMELI, P., 2012. *Tectonic and litho-stratigraphic controls on kaolin deposits within volcanic successions: Insights from the kaoliniferous district of north-western Sardinia (Italy).* Ore Geology Reviews, 48, 151–164.

OGGIANO, G., PASCI, S., AND FUNEDDA, A., 1995. *Il bacino di Chilivani-Berchidda: un esempio di struttura trastensiva. Possibili relazioni con la geodinamica cenozoica del Mediterraneo occidentale.* Bollettino della Società Geologica Italiana, 114, 465-475.

OLAYINKA, A.I., AND YARAMANCI, U., 2000. *Assessment of the reliability of 2D inversion of apparent resistivity data.* Geophysical Prospecting, 48, 2, 293–316.

PADALINO, G., PALOMBA, M., AND SIMEONE, R., 2003. *Mineralogia e geo-chimica isotopica delle facies di alterazione nei sistemi epitermali delle aree di Romana e Tresnuraghes (Sardegna NW, Italia). Applicazioni per l'esplorazione mineraria.* Bollettino della Società Geologica Italiana, 122, 139–145.

PARASNIS, D.S., 1973. *Mining Geophysics.* Elsevier, Amsterdam., 395.

REYNOLDS, J.M., 1997. *An introduction to applied and environmental geophysics.* John Wiley and Sons, Inc, England. 796.

SILVESTER, P.P., AND FERRARI, R.L., 1990. *Finite elements for electrical engineers (2nd. ed.).* Cambridge University Press, 516.

SINHA, A.K., 1980. *Overburden characteristics in the Alfred–Hawkesbury area, Ontario, obtained by D.C. Electrical Soundings.* Current Research, Part C: Geol. Surv. Can. Paper 80, 1C, 1–12.

TELFORD, W.M., GELDART, L.P., AND SHERIFF, R.E., 1990. *Applied Geophysics, (2nd ed.).* Cambridge University Press, Cambridge, 527–529.

Vittorio Longo - Prospecting of Industrial Minerals: a geophysical approach -
PhD Thesis in Natural Science - University of Sassari

75

Chap.5 - ERT method as a guideline for prospecting volcanic ash deposits: the Zerfaliu case study

5.1 - Introduction

Geoelectrical surveys have been conducted near Zerfaliu (OR), in central-western Sardinia as tool for strategic prospecting.

The main objective was to use the ERT method as a guideline to identify cinerite deposits that could potentially be exploited by mining.

Since there are no detailed geological maps of the area under examination (sheet 528 "Oristano" in preparation), another objective was to define the stratigraphic position of the cinerite levels within the Miocene marine sedimentary succession, and meantime evaluate the extent of the deposits.

Applications and therefore markets exist for both raw and popped or bloated ash products. Uses for refined ash include filtrate media, plaster wallboard, thermal (low-temperature) insulation, and lightweight fireproof acoustic tile.

Markets for raw ash include: ceramic components, glass products, mild abrasives, road construction, concrete aggregate, and as a component of granular fertilizer. Both bloated and raw ash are used as absorbents and inert filters, in the treatment of oils and production of cat litters. The absorption properties of volcanic ash are generally due to the presence of smectitic and zeolitized minerals.

Before this near-surface product can be marketed, viable means must be developed for estimated volumes, geometries, and characteristics of the ash deposits. Most important is the development of cost-effective techniques for locating, sampling (for assay), and delineating volcanic ash deposits with great enough certainty to allow the accurate resource projections necessary for securing long-term contracts based on known reserves and thereby deliverable product (Xia et al., 2010).

In the study area the calibration of the ERT method has been performed in a sample area, where cinerites have been identified in outcrops.

In order to ascertain the nature of the main conductive electrical anomalies observed in the tomographies, 3 boreholes have been performed.

Vittorio Longo - Prospecting of Industrial Minerals: a geophysical approach -
PhD Thesis in Natural Science - University of Sassari

76

5.2 - Study area and geological setting

The study area is located in the central-western sector of Sardinia, in the province of Oristano. The surveys have been conducted in a flat area of the lower valley of river Tirso, approx. 5 km NE of the town of Zerfaliu and 2 km NW of Villanova Truschedu (fig. 5.1)
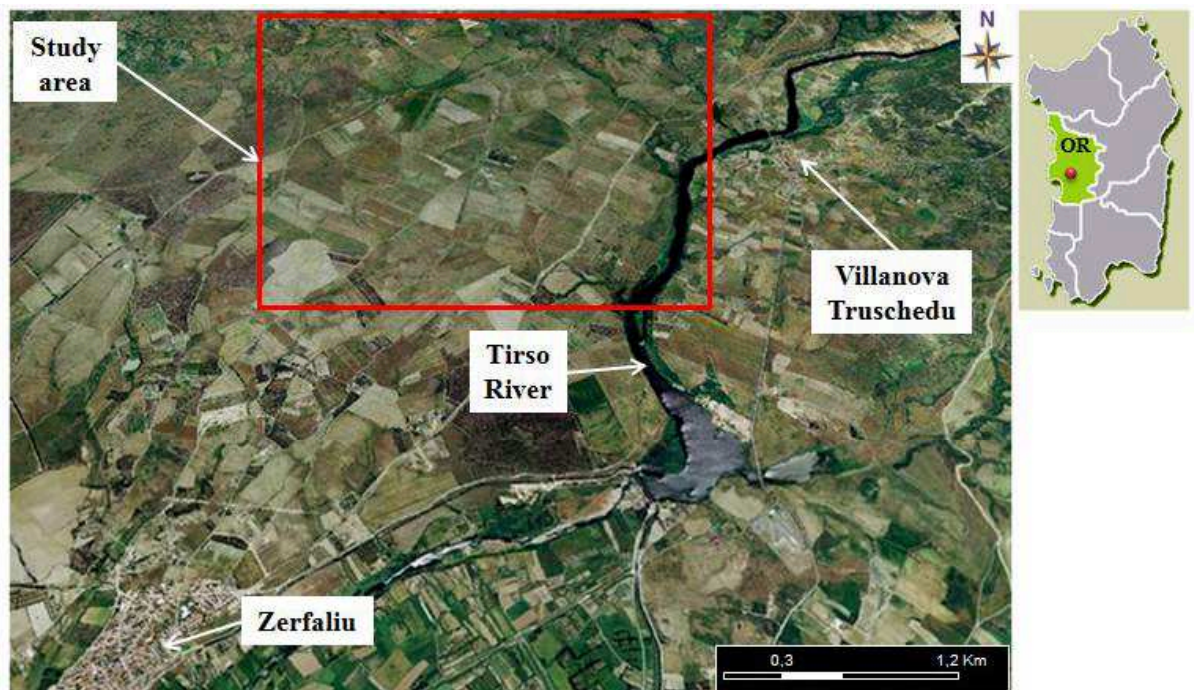

Fig. 5.1 - Location of study area.

The Tirso is the most important water course in Sardinia, both in terms of length and basin width. Its alluvial cone is the predominant element in the morphology of the "Campidano of Oristano". The original apex of the alluvial cone has been identified by Vardabasso (1956), at the outspill of the water course from the basalt gullies at Villanova Truschedu, approx. 20km in the hinterland.

The choice of study area has been dictated by three fundamental factors: i) some outcrops of material of interest in the northern sector, useful to calibrate the method, ii) geological-stratigraphic features supporting the presence of strata of interest, iii) logistics conditions favorable for the implementation of possible extraction activities.

The oldest lithologies outcropping in the study area are volcanites of the Oligo-Miocene calcalkaline cycle (**12**) (Assorgia et al., 1995). The main basic-intermediate effusive events are Aquitanian alternating layers of andesites (in domes and veins) and andesitic breccias, outcropping to the south of Paulilatino (fig. 5.2).
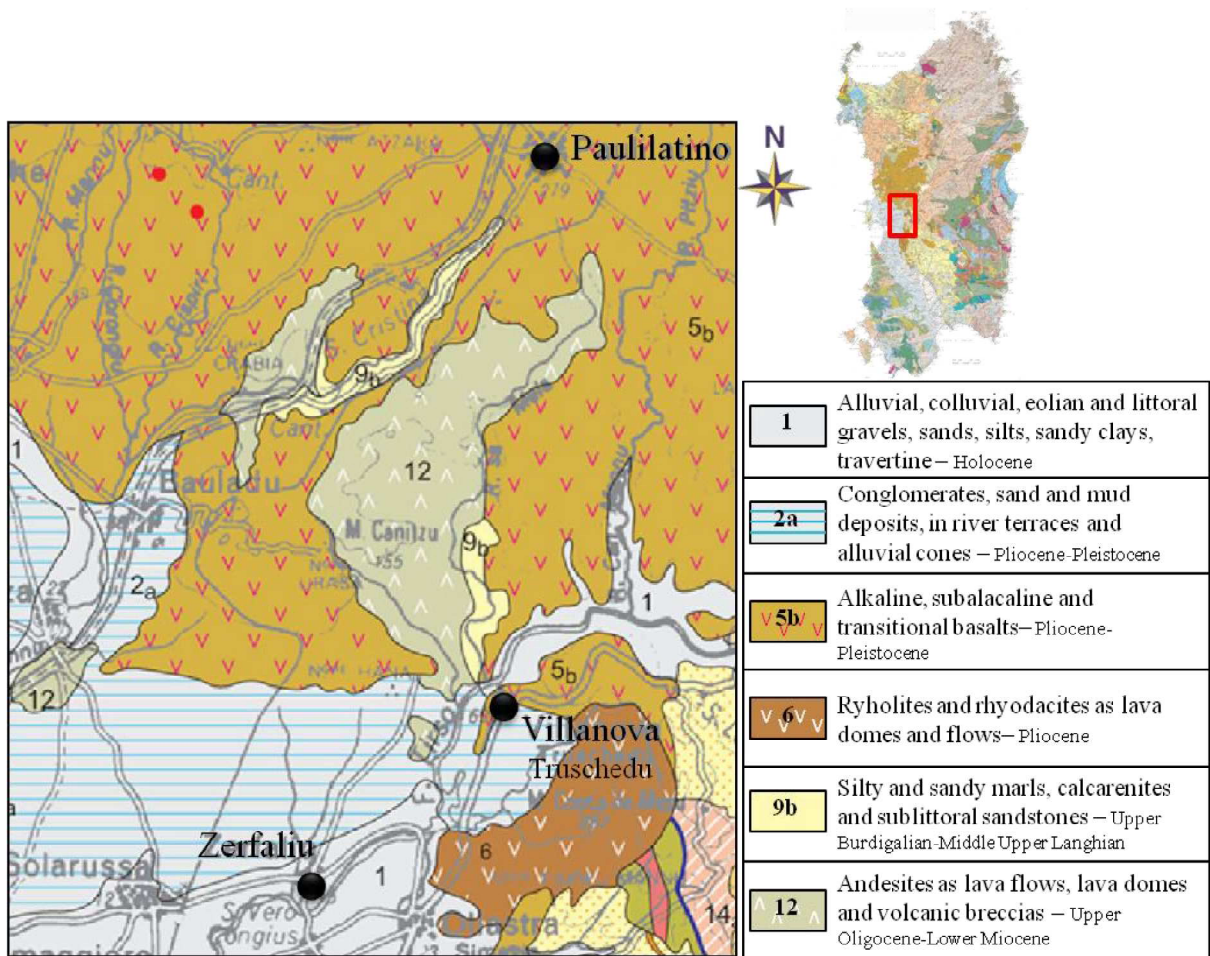
Vittorio Longo - Prospecting of Industrial Minerals: a geophysical approach -
PhD Thesis in Natural Science - University of Sassari

77

Fig. 5.2 - Extract of the Geological Map of Sardinia (Carmignani et al., 2001).

The volcanites are overlying by transgressive Miocene marine sediments (**9b**) (Odin et al., 1994).

Marine transgression is marked by sandstones, oyster calcirudites, conglomerates with calcareous cement and tuffs, indicating coastal or lagoonal environments.

The Oligo-Miocene volcanic-sedimentary succession is capped by Pliocene-Pleistocene plate basalt flows (**5b - 6**).

Extensive early Quaternary alluvial deposits (**2a**) cover most of the volcanic and Tertiary sedimentary successions. They consist of conglomerates, sands and gravels rich in clay matrix. Such alluvial deposits appear terraced and reworked at several stages.

Holocene deposits (**1**) represented by sub-actual alluvial sediments, frequently derived from reworking of the ancient alluvial deposits, are the younger rocks of the area.

Vittorio Longo - Prospecting of Industrial Minerals: a geophysical approach -
PhD Thesis in Natural Science - University of Sassari

78

5.3 - Location of Electrical Resistivity Tomographies

Five electrical resistivity profiles have been conducted using the ABEM Terrameter SAS 1000 Lund Imaging System integrated with an ES 10-64 switch unit (par. 2.1).

The Wenner-Schlumberger array with a factor n=3 has been used during the data acquisition phase.

The profiles have been placed on a Regional Technical Map (CTR 1:10000 - section 529010 "Solarussa"; section 515130 "Bauladu") using the GPS points acquired in the field (fig. 5.3A).

The ZT calibration profile, oriented 72° N, has been performed across an unpaved road, where the cinerites outcrop immediately to the east of this and are in direct contact with the Oligo-Aquitanian andesites.

In order to obtain high resolution, 64 electrodes were spaced at 3m intervals, giving a total length of 285m (roll-along technique - par. 1.5) and a maximum investigation depth of 35m.

The other 4 profiles have been positioned in the central-southern sector of the study area (fig. 5.3B). For these lines, the 64 electrodes have been arranged with an inter-electrode distance of 5m. The unit length was 315m with a maximum investigation depth of 55m.

The Z1 and Z2 profiles, oriented 87°N and 77°N respectively, have been located to the north-east of Nuraghe Lana, close to the Zerfaliu-Paulilatino road.

The Z3 profile, oriented 107°N, has been placed between Nuraghe Benas to the west and Nuraghe Santa Barbara to the east.

Finally, the Z4 profile, oriented 110°N, has been located to the south-east of Nuraghe S.Barbara, on the slope of a valley that descends towards Rio Sa Mela, a tributary to the right of the Tirso.
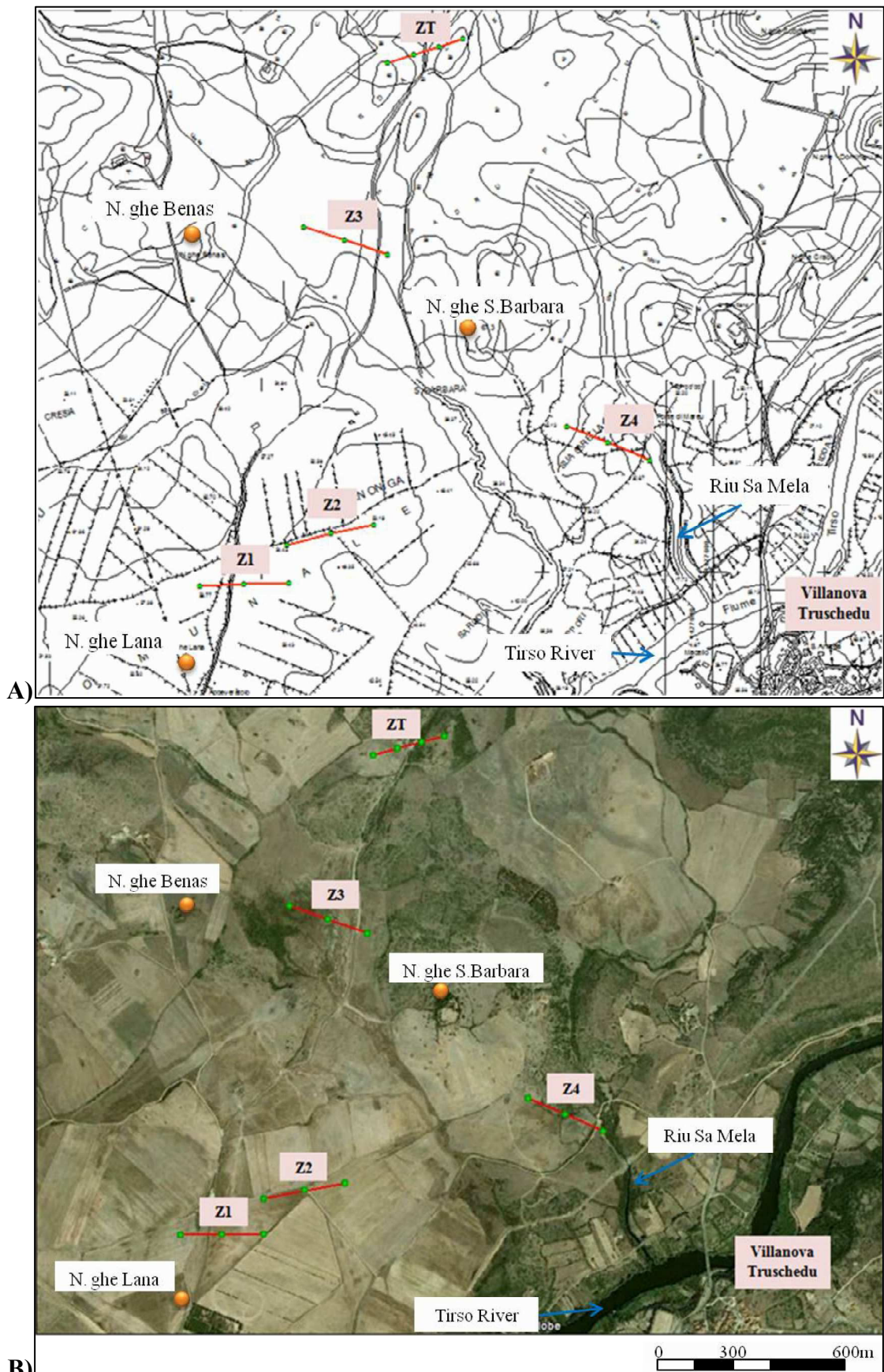
Vittorio Longo - Prospecting of Industrial Minerals: a geophysical approach -
PhD Thesis in Natural Science - University of Sassari

79

Fig. 5.3 - Location of resistivity profiles. A) CTR map and B) satellite image.

Vittorio Longo - Prospecting of Industrial Minerals: a geophysical approach -
PhD Thesis in Natural Science - University of Sassari

80

5.4 - Data processing

The apparent resistivity values measured for each electrical line have been processed using the RES2DINV inversion software (Loke, 2001).

Before performing the inversion process the "bad data points" have been removed in some cases manually and pre-inversion, in other cases automatically and post-inversion.

The *l2-norm* implementation (smoothness-constrained) based least-squares optimization method (Ellis and Oldeburg 1994) and a finer model with the cell width of half the minimum electrode spacing have been used.

Forward problem has been resolved using the finite-elements method (Silvester and Ferrari, 1990), where the nodes position has been adjusted to allow the topography to be considered in the inversion process (Loke, 2001).

The resulting section display electrical resistivity ranging from less than 2 Ω·m to more than 1000 Ω·m. The resistivity values of the Oligo-Aquitanian andesites present in the work area, are within a range that varies from approx. 40 to 250 Ω·m due to the intense fracturing and alteration.

The volcanic ash levels have low resistivity values, ranging between 2 and 8 Ω·m and show a poor compaction between the individual mineral granules, which are held together by the surrounding moisture. The moisture between the particles carries the electric current, giving electrolyte-like conductance (par. 1.1).

To the Miocene marine sediments a resistivity range between 8 and 75 Ω·m has been attributed. The volcanic-sedimentary succession in the area is overlapped by the Plio-Quaternary basalt effusive sequence. These volcanic rocks generally have micro-cavities or in any case pores characterized by poor connection: this characteristic results in higher resistivity values, even in situations where there is considerable porosity. The resistivity values observed for these lithologies are generally very high, and can exceed 1000 Ω·m.

All resistivity models have been represented using the colour scale shown in figure 5.4.

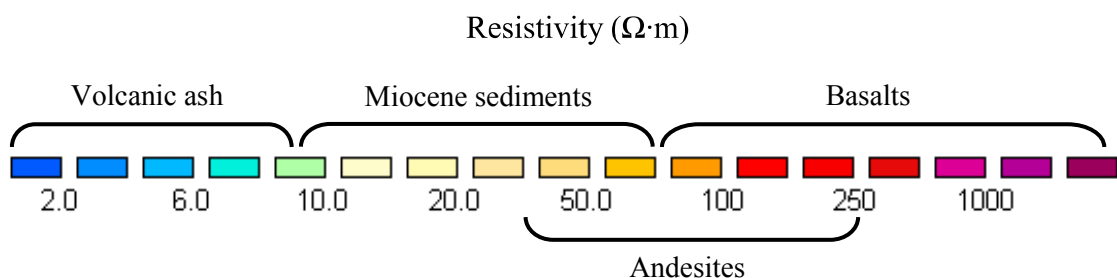Fig. 5.4 - Colour scale used to represents all resistivity models.

Vittorio Longo - Prospecting of Industrial Minerals: a geophysical approach -
PhD Thesis in Natural Science - University of Sassari

81

5.5 - Survey results

- *ZT tomography*

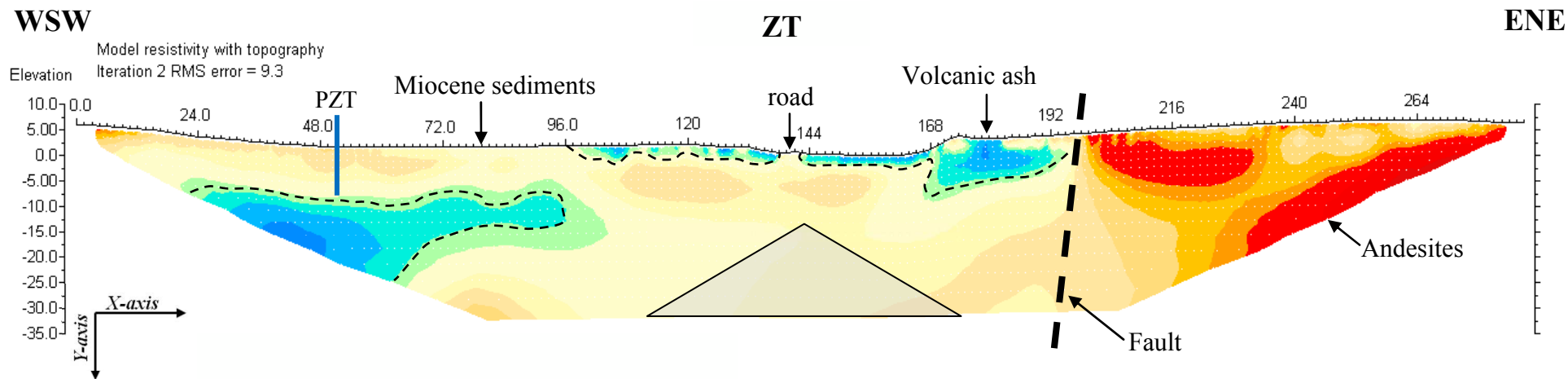| ARRAY	WENNER-SCHLUMBERGER n=3
MEASURED RESISTIVITY POINTS	1907
ARRAY LENGTH	285 m
INTERELECTRODE SPACING	3 m
MAXIMUM INVESTIGATION DEPTH	35 m
GPS POINTS	ELECTRODE 1_N 40.00900°-E 8.73554° ELECTRODE 32_N 40.00927°-E 8.73660° ELECTRODE 64_N 40.00951°-E 8.73766° ELECTRODE 96_N 40.00976°-E 8.73868°

The ZT calibration profile has been set in the northern sector of the work area (Fig. 5.3), crossing an unpaved road, where the cinerites outcrop immediately to the east of this and are in direct contact with the Oligo-Miocene andesites.

The two lithologies are in contact by a direct fault, located at chainage 195-200 metres (*x-axis*) (fig. 5.5), where a sudden change in resistivity values is observed, varying from 2-10 $\Omega \cdot m$ for the cinerites (blue-green in colour) to 50-150 $\Omega \cdot m$ for the andesites (red-orange in colour).

From the fault to the end of profile, in certain points the andesites are more altered and fractures, with resistivity values less than 100 $\Omega \cdot m$, in other points they are more compact, with values in excess of 100 $\Omega \cdot m$.

The cinerite deposit in direct contact with the fault has a thickness of approx. 5-6 metres from ground level corresponding to chainage 180 metres (*x axis*) and is bounded below by rocks with resistivity values in excess of 10 $\Omega \cdot m$.

The cinerites are exposed by a ditch that extends from the road to the escarpment adjacent to the fault at chainage 170 metres (*x-axis*), shown in the topographic profile of the tomography (fig. 5.6).

Vittorio Longo - Prospecting of Industrial Minerals: a geophysical approach -
PhD Thesis in Natural Science - University of Sassari

82

Fig. 5.5 - ZT Electrical Resistivity Tomography.

Vittorio Longo - Prospecting of Industrial Minerals: a geophysical approach -
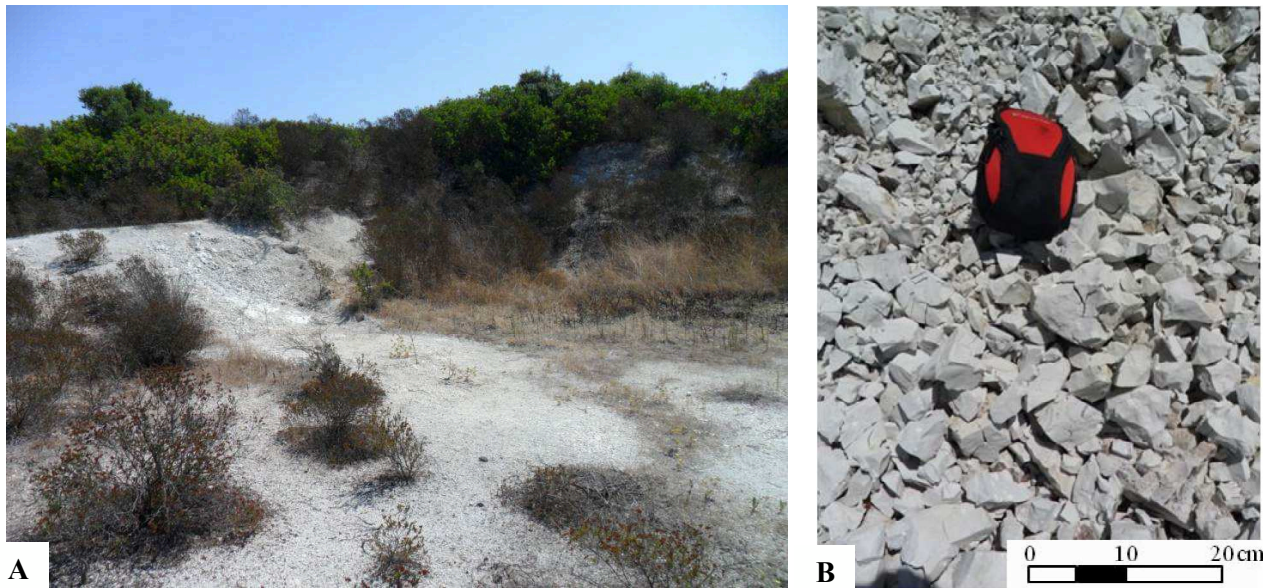PhD Thesis in Natural Science - University of Sassari

83

Fig. 5.6 - A) Volcanic ash deposit to eastern part of the road. B) Detail of volcanic ash.

From the escarpment to chainage 96 metres (*x-axis*) the cinerite layer has an average thickness of 2,5m.

Horizontally this layer is in contact with the Miocene marine sediments consisting of calcareous pebbles fossils-rich and volcanic materials.

The resistivity values of these sediments are between 10–50 $\Omega \cdot m$ and they are also observed in the central portion of the tomography below the cinerite deposits.

In the left portion of the tomography (W-SW), a conductive lens is observed at a depth of approx. 10 metres from ground level, with resistivity less than 10 $\Omega \cdot m$.

The shape of this conductive lens may not be that effectively shown by the tomography, since the data near to the margin always has a higher degree of uncertainty (Loke, 2001).

Even though, it is believed that the lateral extent (approx. 70 metres) and the mean thickness (approx. 12 metres), are elements that would support the presence of cinerite levels or possibly clay deposits that may have similar resistivity.

- *PZT borehole log*

On the 4 and 5 August 2011, a borehole was drilled at chainage 51 metres (*x axis*) of ZT profile (fig. 5.7A) in order to evaluate the nature of the lithologies present in the conductive lens located at a depth of 10 metres from ground level.

The stratigraphy column relating to the PZT borehole and the description of the lithologies at different depths are reported below (fig. 5.7B).
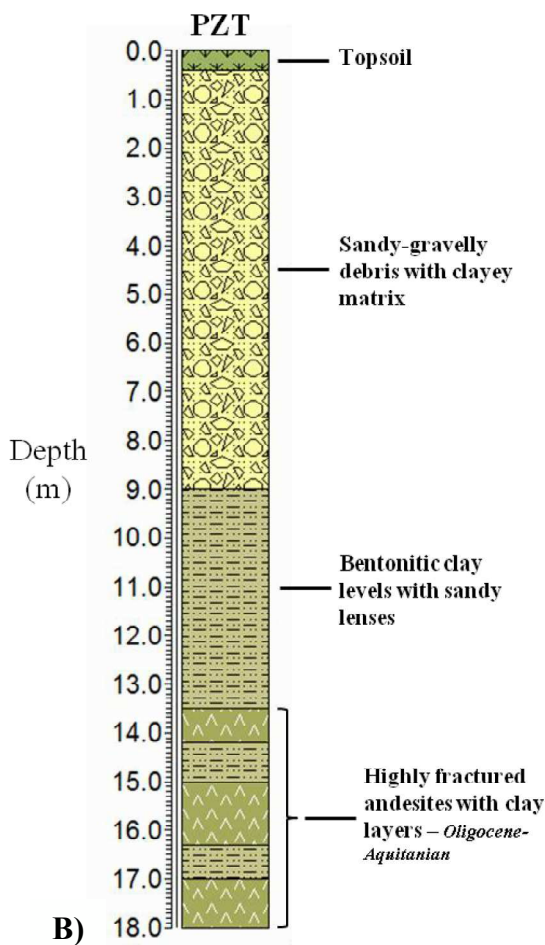
Vittorio Longo - Prospecting of Industrial Minerals: a geophysical approach -
PhD Thesis in Natural Science - University of Sassari

84
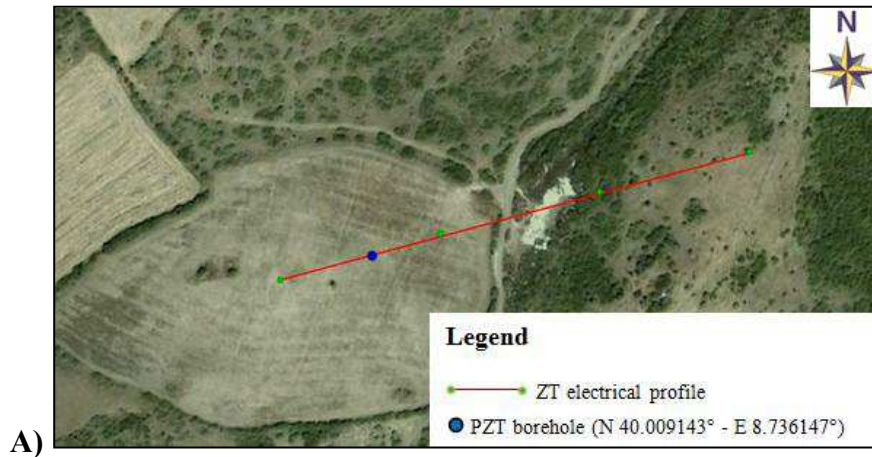
Fig. 5.7 - A) ZT profile with PZT borehole location. B) Stratigraphy column of PTZ borehole.

In the cores taken from the conductivity lens have shown the presence of clay levels with weakly bentonitised sandy sections of grey-greenish colour, associated with the alteration process of the underlying Oligo-Aquitanian andesites. These bentonitised layers show a similar resistivity range of the cinerites (1-10 Ω·m).

Vittorio Longo - Prospecting of Industrial Minerals: a geophysical approach -
PhD Thesis in Natural Science - University of Sassari

85

ARRAY	WENNER-SCHLUMBERGER n=3
MEASURED RESISTIVITY POINTS	1089
ARRAY LENGTH	315 m
INTERELECTRODE SPACING	5 m
MAXIMUM INVESTIGATION DEPTH	55 m
GPS POINTS Z1	ELECTRODE 1_N 39.99232°-E 8.72778°
	ELECTRODE 32_N 39.99239°-E 8.72961°
	ELECTRODE 64_N 39.99245°-E 8.73147°
GPS POINTS Z2	ELECTRODE 1_N 39.99366°-E 8.73141°
	ELECTRODE 32_N 39.99402°-E 8.73321°
	ELECTRODE 64_N 39.99429°-E 8.73500°

The Z1 and Z2 profiles have been located in the central-southern sector of the work area (fig. 5.3).

During the acquisition, the instrument has recorded several negative measurements, which significantly reduce the data quality, and are typically caused by poor contact between the electrodes and the soil.

During processing, the negative values and measurements with high standard deviations (> 5%) have been removed. This reduced the number of points used in the inversion process for both lines, from 1089 to 622 points in the Z1 tomography, and from 1089 to 1011 points in the Z2 tomography. RMS error value of the Z1 and Z2 tomographies is 34.2% and 22.5% respectively.

The Z1 tomography shows a polygenic conglomerate with variable thickness (4-5 metres) in the shallow portion, consisting of most saturated and conductive zones ($\rho < 10$ $\Omega \cdot$m) and least saturated and resistive zones ($\rho > 20$ $\Omega \cdot$m) (fig. 5.8A).

The conglomerate cover was also evident during the instrumentation positioning phase.

Under the conglomerates, from the start to the centre of the profile (0-160 metres *x-axis*), there is a resistive body continuing to the maximum investigation depth achieved.

The measured resistivity values are compatible with a basalt body homogeneous and compact at depth ($\rho > 1000$ $\Omega \cdot$m) and more altered towards the surface ($\rho = 100$-300 $\Omega \cdot$m).

Again under the conglomerate cover, from the centre of the profile to the end (160-315 metres, *x axis*), the distribution of resistivity values is less uniform compared to that observed previously.

At the eastern extremity of the tomography, from a depth of 6 metres from ground level to the edge of the profile, resistivity values attributable to basalts are measured ($\rho > 100$ $\Omega \cdot$m).

Vittorio Longo - Prospecting of Industrial Minerals: a geophysical approach -
PhD Thesis in Natural Science - University of Sassari

86

These values soften gradually towards lower resistivity values moving progressively towards the centre of the tomography.

A regularly shaped conductive lens is detected close to chainage 187 metres (*x-axis*) at a depth of approx. 12 metres from ground level.

It cannot be excluded the presence of a fault zone in correspondence to chainage 160 metres (*x-axis*), which could have promoted the circulation of fluids inside the basalt body and the consequent formation of clayey layers.

The Z2 tomography (fig. 5.8B) also shows the presence of a shallow conglomerate with variable thickness (5-7 metres), difficult to define in certain areas.

This conglomerate has more saturated zones at chainage 120 metres (*x-axis*) and in the end portion of the tomography (220-315 metres *x-axis*), alternating with less saturated and more resistive zones.

The high resistivity values ($\rho > 100$ $\Omega \cdot m$) are attributed to basalts, and also in this tomography are found the regularly shaped conductive lenses (ex. 200m *x-axis*, depth 30m).

Vittorio Longo - Prospecting of Industrial Minerals: a geophysical approach -
PhD Thesis in Natural Science - University of Sassari

87
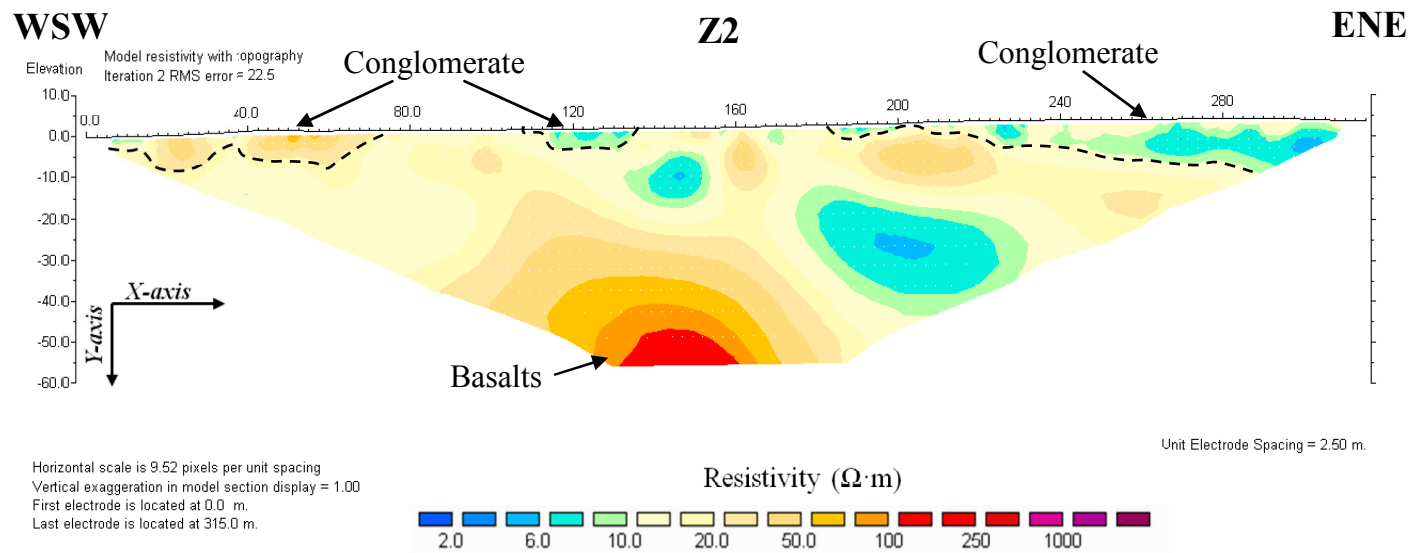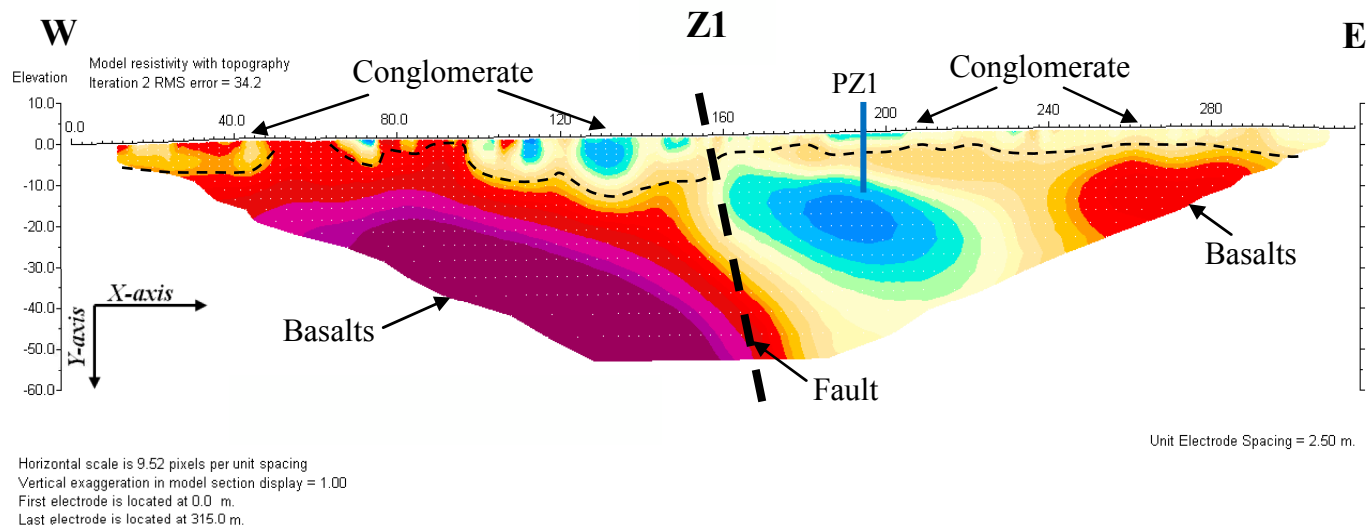
Fig. 5.8 - A) Z1 ERT with PZ1 log location. B) Z2 ERT.

Vittorio Longo - Prospecting of Industrial Minerals: a geophysical approach - PhD Thesis in Natural Science - University of Sassari

88

- *PZ1 borehole log*

On the 8 and 9 August 2011, a borehole was drilled at chainage 187 metres (*x axis*) of Z1 profile. The purpose was to define the nature of the conductive lens that starts at a depth of approx. 12 metres from ground level.

The stratigraphy column relating to the PZ1 borehole and the description of the lithologies at the various different depths is reported below
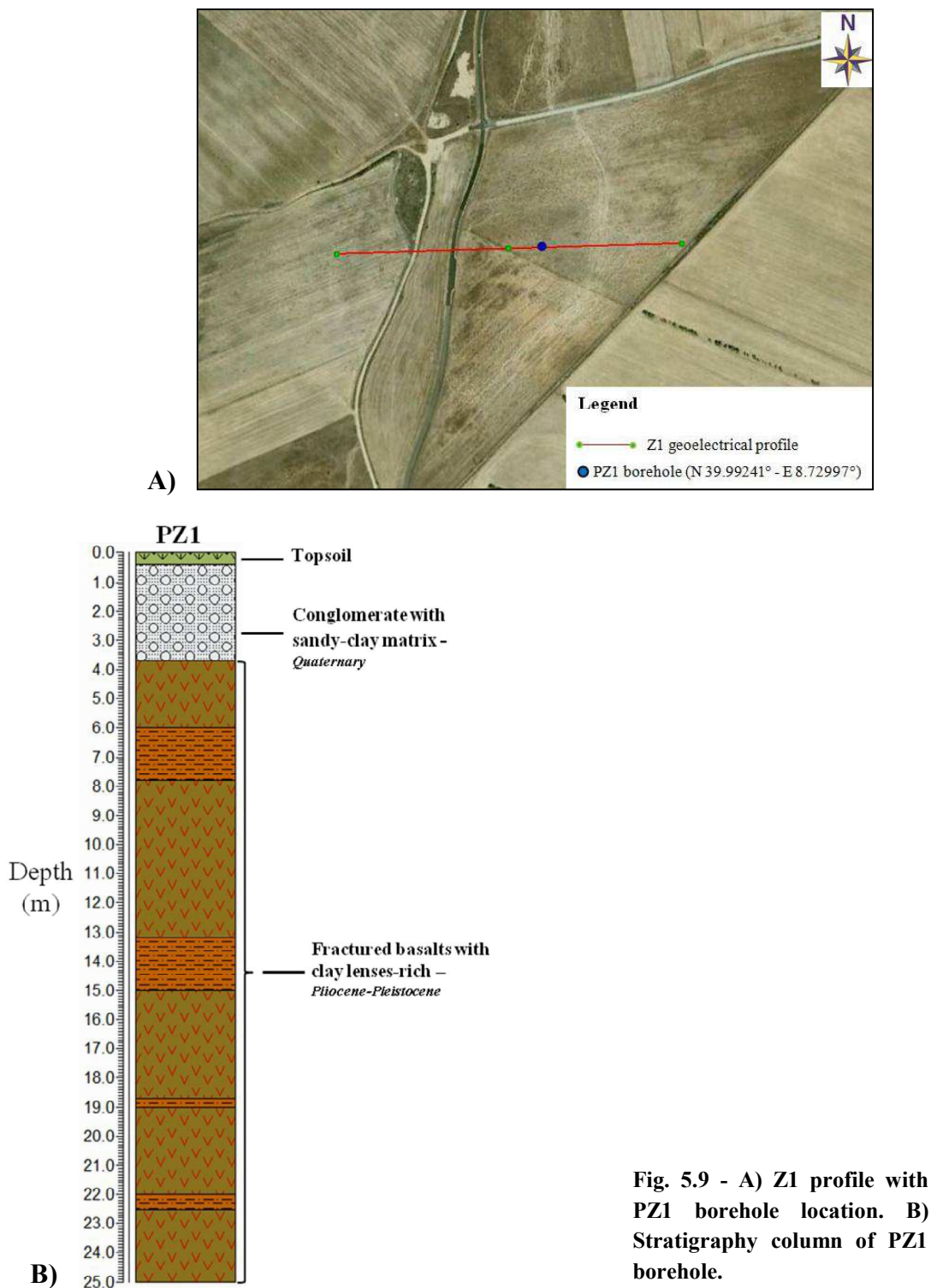

Fig. 5.9 - A) Z1 profile with PZ1 borehole location. B) Stratigraphy column of PZ1 borehole.

Vittorio Longo - Prospecting of Industrial Minerals: a geophysical approach - PhD Thesis in Natural Science - University of Sassari

89

After the first four metres of conglomerates, the core (fig. 5.9B) has shown the presence of basalt, intensely fractured with clay-rich levels, reaching to a depth of 25m. The low resistivity values of the conductive lens are not due to the cinerites, but to clay levels that, even in modest amounts, contribute towards significantly increasing the conductivity of the material in which they are found.

- *Z3 tomography*

ARRAY	WENNER-SCHLUMBERGER n=3
MEASURED RESISTIVITY POINTS	1089
ARRAY LENGTH	315 m
INTERELECTRODE SPACING	5 m
MAXIMUM INVESTIGATION DEPTH	58 m
GPS POINTS	ELECTRODE 1_N 40.003740°-E 8.732040°
	ELECTRODE 32_N 40.003340°-E 8.733770°
	ELECTRODE 64_N 40.002890°-E 8.735560°

The Z3 tomography (fig. 5.10) shows the superficial conductive clayey soil (ρ < 10 Ω·m), also observed in the field during positioning of the electrodes.

The type of soil, the slightly depressed morphology and the sand-dwelling vegetation present at the site indicate that in the past the area was most likely occupied by a lagoon or a pool of brackish water.

Beneath the soil, at chainages 200-220 metres (*x-axis*), there is an elongated conductive lens with sub-vertical direction, where the resistivity values increase from 2 to 10 Ω·m proceeding in depth. The shape of this anomaly likely identifies a fault line with a similar trending to that identified in the ZT profile. To the east of the fault, from a depth of 10 m below ground level to the maximum depth reached in the survey, the resistivity values increase (20 < ρ > 70 Ω·m), and they are compatible with Oligo-Aquitanian andesites.

Again below the superficial clay cover (from 30 to 200 metres *x-axis*) there is an elongated lens in the horizontal direction, with resistivity values greater than 10 Ω·m.

Considering the stratigraphic position, this lens might indicate the presence of Miocene sediments where the resistivity values decrease progressively proceeding downwards, due to an increased clay component or conveyed water by fault zone.

The presence of the cinerite levels in this profile cannot be entirely excluded, especially in the fault zone where the resistivity values are low (2-10 Ω·m).

Vittorio Longo - Prospecting of Industrial Minerals: a geophysical approach -
PhD Thesis in Natural Science - University of Sassari

90
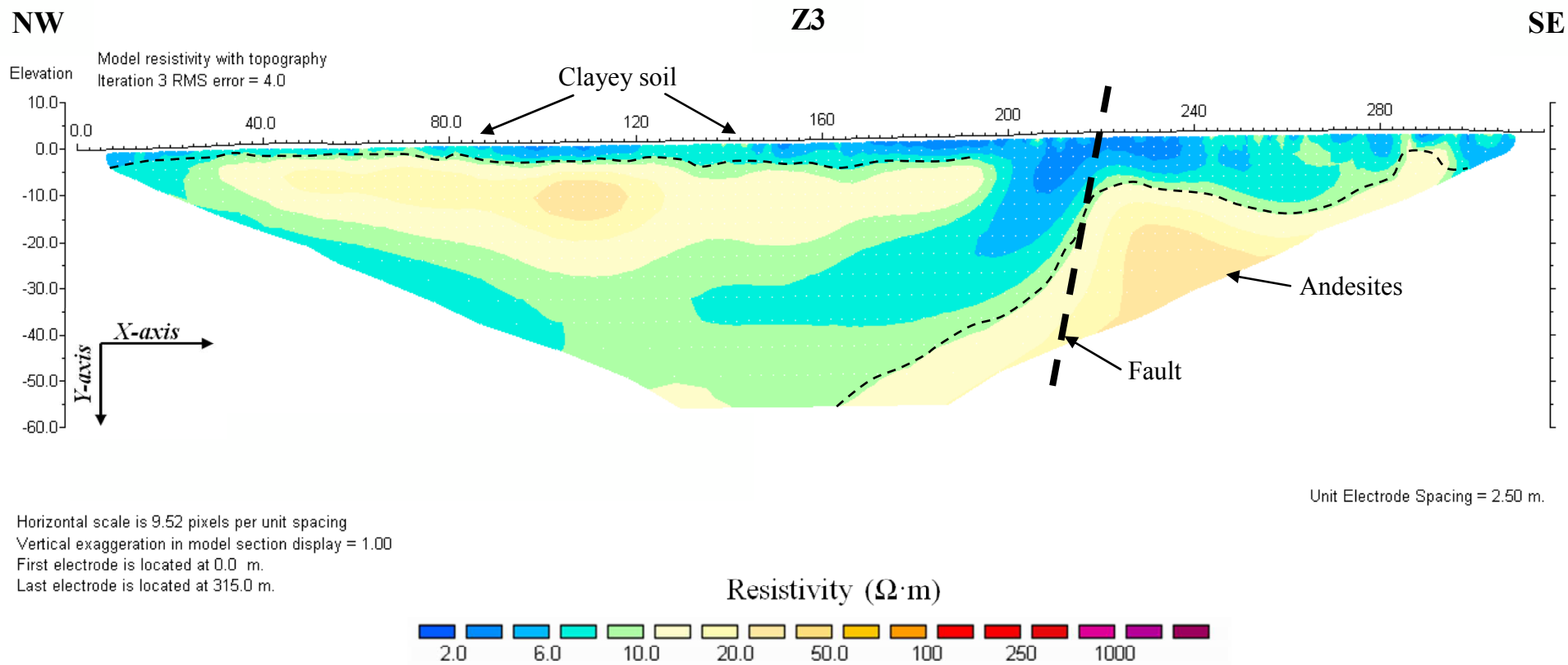
Fig. 5.10 - Z3 Electrical Resistivity Tomography.

Vittorio Longo - Prospecting of Industrial Minerals: a geophysical approach -
PhD Thesis in Natural Science - University of Sassari

91

- *Z4 tomography*

ARRAY	WENNER-SCHLUMBERGER n=3
MEASURED RESISTIVITY POINTS	1089
ARRAY LENGTH	315 m
INTERELECTRODE SPACING	5 m
MAXIMUM INVESTIGATION DEPTH	57 m
GPS POINTS	ELECTRODE 1_N 39.997450°-E 8.74298°
	ELECTRODE 32_N 39.99694°-E 8.74468°
	ELECTRODE 64_N 39.99639°-E 8.74641°

The Z4 profile has been positioned to the south-east of Nuraghe S.Barbara, on the slope of a valley that descends towards Rio Sa Mela (fig. 5.3).

In this area, the Oligocene-Aquitanian andesites outcrop close to Nuraghe S.Barbara, while the Miocene compact fossil-rich limestones outcrop near Rio Sa Mela (fig. 5.11).

The tomography (fig. 5.12) shows an extensive resistive body (red-orange in colours) with values ranging between 40 and 250 $\Omega \cdot m$, attributable to andesites already observed in the ZT calibration tomography.

The compact andesites outcrop along the slope up to chainage 170 metres (*x-axis*), after which they are found more altered and affected by fracturing at a depth of 12 metres below ground level ($\rho < 100$ $\Omega \cdot m$), reaching the maximum depth surveyed.

The shallow Miocene marine sediments cover the andesites from chainage 170 metres (*x-axis*) to the end of the profile.

This level (5-12 in thickness) consists of loose sediments with low resistivity values

Fig. 5.11 - *Ostrea* in Miocene calcarenites outcropping near Rio Sa Mela.

($\rho < 20$ $\Omega \cdot m$) derived from the breakdown of Miocene biocalcarenites. Conductive cinerite layers ($\rho < 8$ $\Omega \cdot m$), with small thickness are interbedded within these sediments.

Vittorio Longo - Prospecting of Industrial Minerals: a geophysical approach -
PhD Thesis in Natural Science - University of Sassari

92
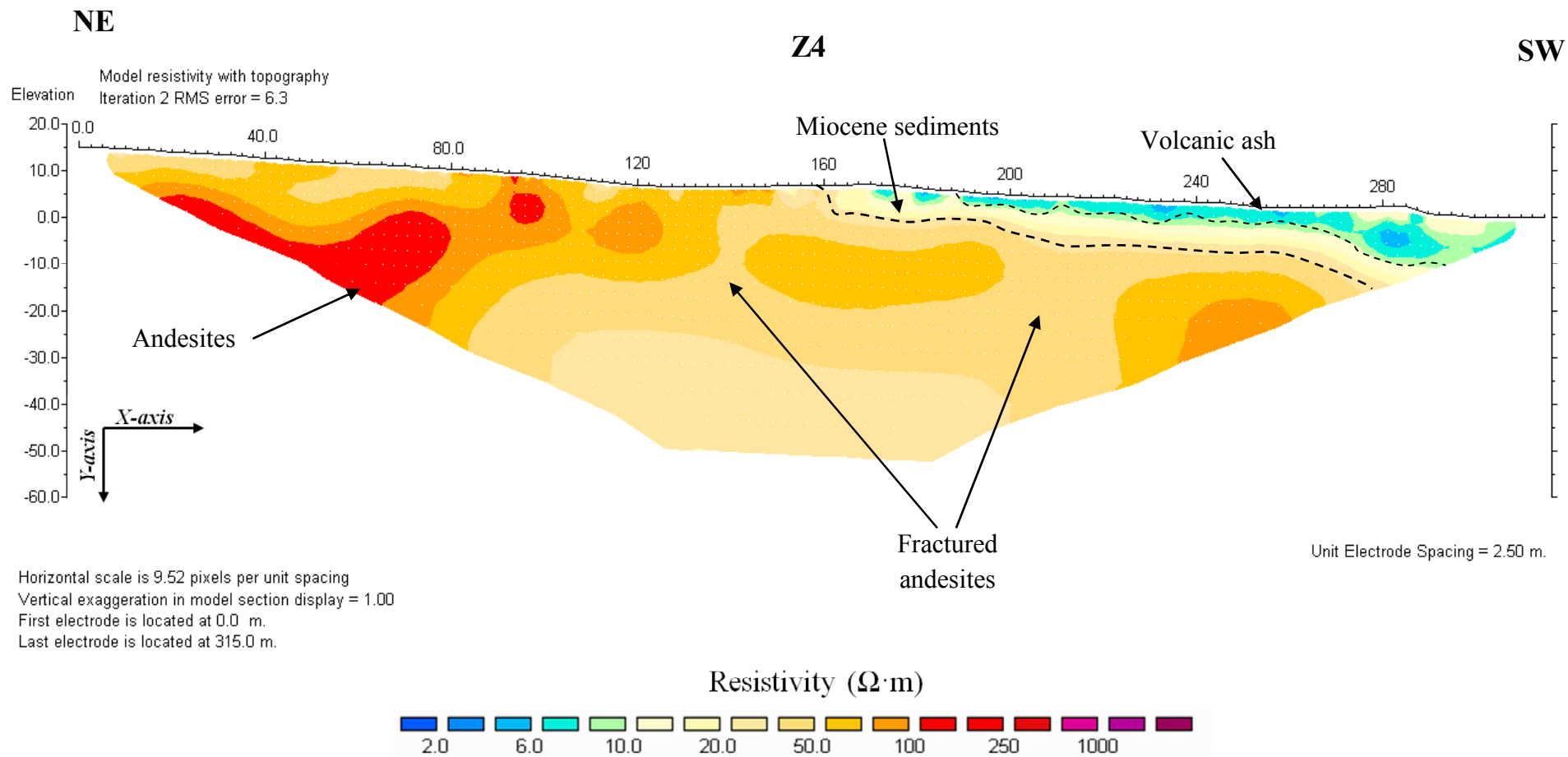
Fig. 5.12 - Z4 Electrical Resistivity Tomography.

Vittorio Longo - Prospecting of Industrial Minerals: a geophysical approach -
PhD Thesis in Natural Science - University of Sassari

93

- *PZ4 borehole log*

With the aim of identifying the thickness of the cinerite level and the most extensive Miocene sediments respect to those observed in the Z4 tomography, on 10 and 11 August 2011 a third borehole was drilled 230m to the south of Z4 profile (fig. 5.13A).

The stratigraphy column relating to the PZ4 borehole and the description of the lithologies at different depths is reported below (fig. 5.13B).
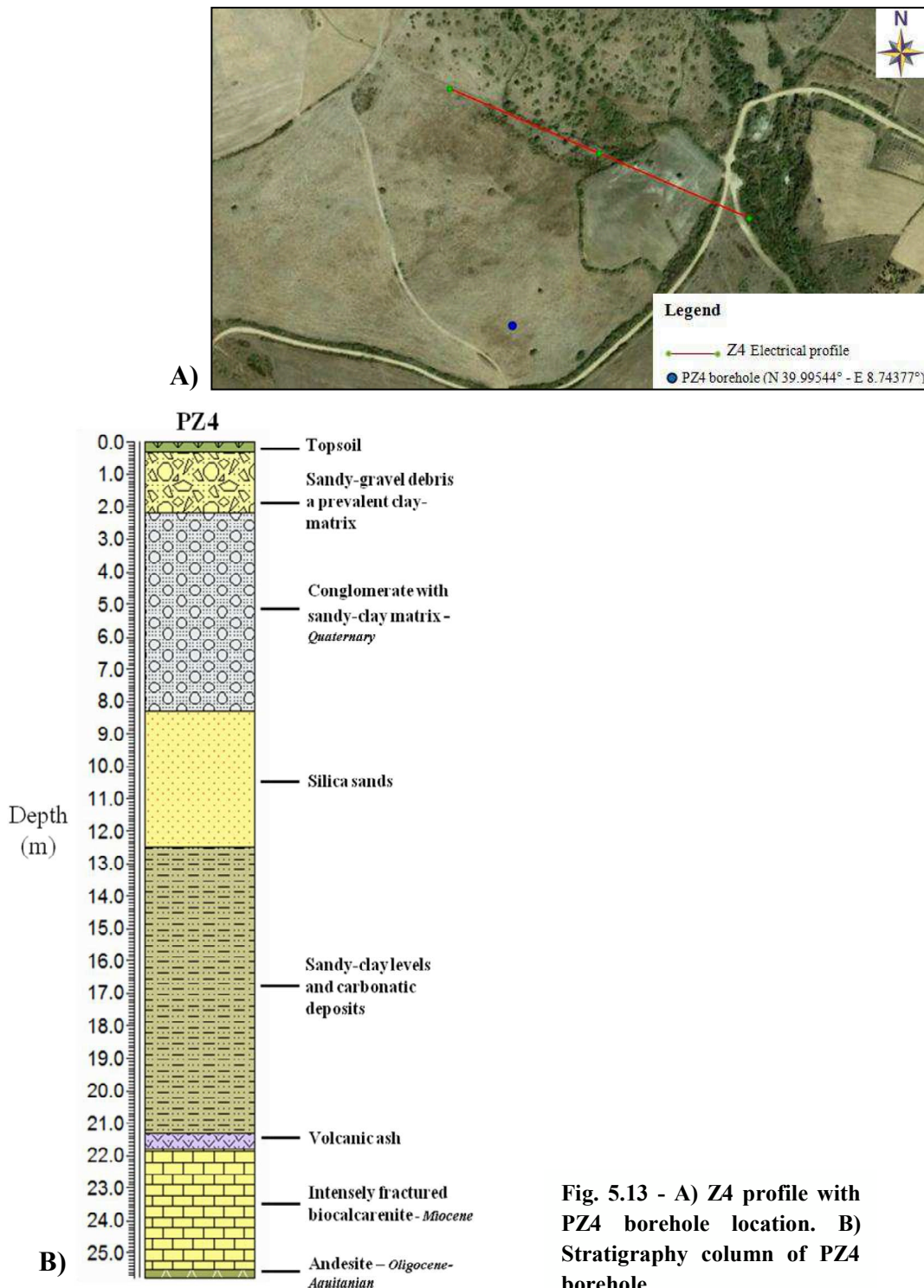

Fig. 5.13 - A) Z4 profile with PZ4 borehole location. B) Stratigraphy column of PZ4 borehole.

Vittorio Longo - Prospecting of Industrial Minerals: a geophysical approach -
PhD Thesis in Natural Science - University of Sassari

94

The cores show conglomerates in the topmost few metres, below which there are sandy deposits attributable to the Oligo-Miocene transgressive cycle.

The cinerites have a thickness of 50cm (21.3-21.8m in deep) above the compact and fossil-rich biocalcarenites.

5.6 - Conclusions

The surveys conducted near Zerfaliu have shown that the cinerites have meagre thicknesses making their extraction not economically viable.

The calibration profile has allowed to enclose the resistivity values attributed to the cinerite in a range between 2 and 8 $\Omega \cdot m$. Then this range was used as the benchmark in interpreting the subsequent tomographies.

The 5 ERTs have been examined focusing on conductive electrical anomalies that might indicate the presence of cinerite deposits.

PZT and PZ1 boreholes data have detected clayey levels in correspondence to conductive lenses identified by ZT and Z1 tomographies respectively.

Only PZ4 borehole has successfully intercepted a cineritic level with a thickness of 50cm.

However, the surveys have provided useful structural and stratigraphical information.

Some tomographies (ZT, Z1 and Z3) have highlighted a fault zone with NE-SW trending which affects the Oligo-Aquitanian andesites.

The surveys have also confirmed the stratigraphic position of the alluvial beds present in the plane close to Nuraghe Lana. These are fluvial sediments from the Tirso with abundant sandy-clay matrix (conductive), which cover the underlying basalts.

Finally, the Z4 tomography, and in particular the PZ4 log, have provided stratigraphic evidence on the Miocene succession of the area, allowing to set the cinerite beds on the Aquitanian calcarenites.

Vittorio Longo - Prospecting of Industrial Minerals: a geophysical approach -
PhD Thesis in Natural Science - University of Sassari

95

References

ASSORGIA, A., BALOGH, K., LECCA, L., IBBA, A., PORCU, A., SECCHI, F. AND TILOCCA, G., 1995. *Volcanological characters and structural context of Oligo-Miocene volcanic successions from central Sardinia (Italy).* Rapporti Alpi-Appennino Peveragno (Cn), 1994. R. Polino and R. Sacchi eds. Accademia Nazionale Scientifica, 14, 397-424.

CARMIGNANI, L., OGGIANO, G., BARCA, S., CONTI, P., SALVADORI, I., ELTRUDIS, A., FUNEDDA, A., AND PASCI, S., 2001. *Geologia della Sardegna - Note illustrative della Carta Geologica scala 1:200000. Memorie Descrittive Carta Geologica d'Italia,* LX., 283.

ELLIS, R.G., AND OLDENBURG, D.W., 1994. *Applied geophysical inversion.* Geophysics Journal Interantional, 116, 5–11.

LOKE, M.H., 2001. *Res2Dinv software users manual, version 3.4.* Geotomo Software, Penang, Malaysia, 98.

ODIN, G.S., ASSORGIA, A., BARCA, S., PORCU, A., SPANO, C., HERNANDEZ, J. AND COSCA, M., 1994. *Ar-geochronology of a Burdigalian tuff from central-northern Sardinia.* Giornale di Geologia, 56, 1, 185-197.

SILVESTER, P.P., AND FERRARI, R.L., 1990. *Finite elements for electrical engineers (2nd. ed.).* Cambridge University Press, 516.

VARDABASSO, S., 1956. *Il Quaternario della Sardegna.* Atti IV Congr. Int. Quaternario. 995-1018.

XIA, J., LUDVIGSON, G., MILLER, R.D., MAYER, L., AND HAJ, A., 2010. *Delineation of a volcanic ash body using electrical resistivity profiling.* Journal of Geophysics and Engineering, 7, 3, 267-276.

Vittorio Longo - Prospecting of Industrial Minerals: a geophysical approach -
PhD Thesis in Natural Science - University of Sassari

96

Chap.6 - ERT method as a guideline for detecting volcanic ash deposits: the Macomer case study

6.1 - Introduction

An exploitable pumice- and ash-rich layer has been identified within a composite Oligo-Miocene volcanic succession resting on the Paleozoic basement near Macomer.

The aim of surveys was to provide information regarding the position and extend of this layer, and in particular: i) to calibrate the ERT method in a sample area where epiclastites are widely outcropping; ii) to acquire and interpret the electrical resistivity models; iii) to perform the borehole in order to verify the geometry of the deposit issued from the resistivity models.

6.2 - Study area and geological setting

The study area is located in the central-western sector of Sardinia (Nuoro province).

The surveys was conducted approx. 6 km north of the town of Macomer, near the Campeda railway station, at km 151 on SS131 in loc. "Su Cadelanu" (fig. 6.1).
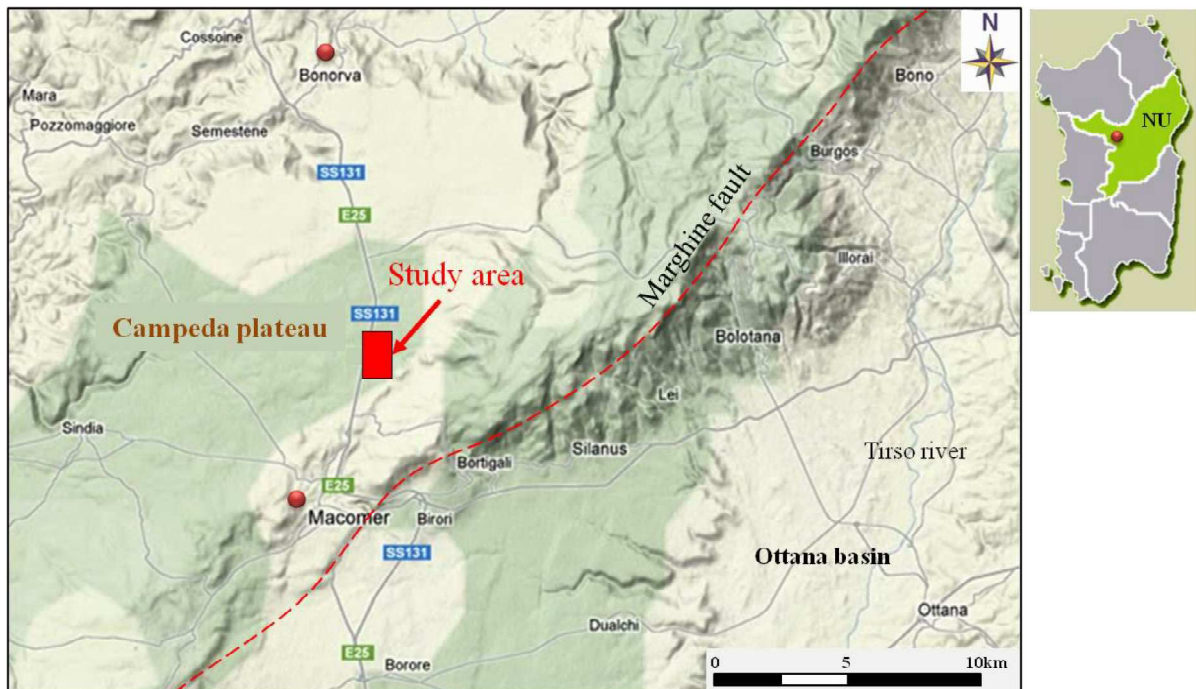

Fig. 6.1 - Location of study area.

Vittorio Longo - Prospecting of Industrial Minerals: a geophysical approach -
PhD Thesis in Natural Science - University of Sassari

97

The Oligo-Miocene volcanic successions in the study area are generally overlain by extensive Plio-Pleistocene basalts of the Campeda plateau. A fault line NE-SW trending separates this plateau from the Ottana basin.
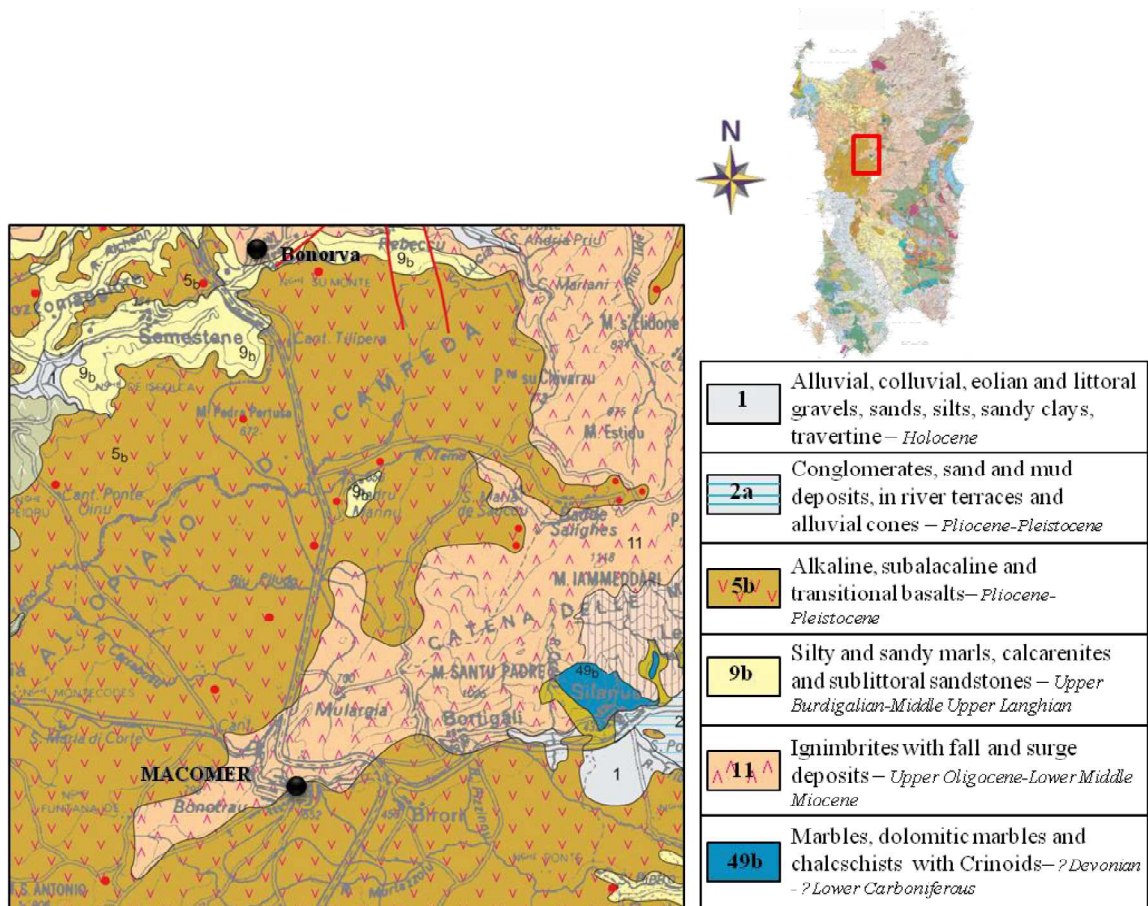

Fig. 6.2 - Extract of the Geological Map of Sardinia (Carmignani et al., 2001).

The metamorphic rocks of the Paleozoic basement outcrop at the base of Tertiary volcanites and consisting of marbles, calc-schists, phyllites and phyllitic micaschists (fig. 6.2 - **49b**).

The Tertiary volcanites (fig. 6.2 - **11**) are predominantly represented by acidic rocks ("ignimbritic series" Auct.) with thickness of hundreds metres, and they consist of welded ignimbritic units of dacitic-rhyodacitic composition, discontinuous layers of pumice-ash-rich pyroclastic flows and epiclastites containing lenses of fluvial-lacustrine deposits.

Sedimentary deposits associated with the Miocene transgression (Upper Burdigalian - Serravallian) are rare or absent in the area. These outcrop approx. 3 km to the north, in Padru Mannu locality, and are mainly represented by silty and sandy marls, calcarenites and sublittoral-epibathyal siliceous sands (fig. 6.2 - **9b**) (Carmignani et al., 2001).

The Oligo-Miocene volcano-sedimentary successions are capped by Pliocene-Pleistocene within-plate basalt (fig. 6.2 - **5b**).

Vittorio Longo - Prospecting of Industrial Minerals: a geophysical approach -
PhD Thesis in Natural Science - University of Sassari

98

6.3 - Location of Electrical Resistivity Tomographies

Three electrical resistivity tomographies have been performed in the study area using the ABEM Terrameter SAS1000 Lund Imaging System integrated with an ES 10-64 switch unit (par. 2.1).

Sixty-four stainless steel metal electrodes have been placed in the soil for each line and a hybrid Wenner-Schlumberger array with a factor n=2 has been used during the data acquisition phase.

The lines have been positioned on a Regional Technical Map (CTR 1:10000 - section 498060 "Stazione di Campeda") using the GPS points measured for each profile at the start, centre and end-point (fig. 6.3A).

ERT method has been calibrated in the southern sector, where the epiclastic layer outcrops sporadically.

In this sector, the original morphology has been modified by the activities of an old borrow-pit, the covering material of which has been partly removed for the construction of the adjacent railway line. This activity has resulted in the formation of a stagnant pool collecting water from surface streams (fig. 6.3B).

In the MT calibration profile (oriented 98°N), the electrodes were placed at 3 metres intervals, giving an overall length of 189m and a maximum investigation depth of 35m.

The M1 profile (oriented 158°N) was performed in the northern sector of the area, running parallel with the railway line at a distance of approx. 50m from it.

The M2 profile (oriented 156°N) was located 180 metres further south of M1.

For both lines the electrodes were placed at 5 metres intervals, giving an unit length of 315m and a maximum investigation depth of 55m in both cases.

Vittorio Longo - Prospecting of Industrial Minerals: a geophysical approach -
PhD Thesis in Natural Science - University of Sassari

99

Fig. 6.3 - Location of resistivity profiles. A) CTR map and B) satellite image.

Vittorio Longo - Prospecting of Industrial Minerals: a geophysical approach -
PhD Thesis in Natural Science - University of Sassari

100
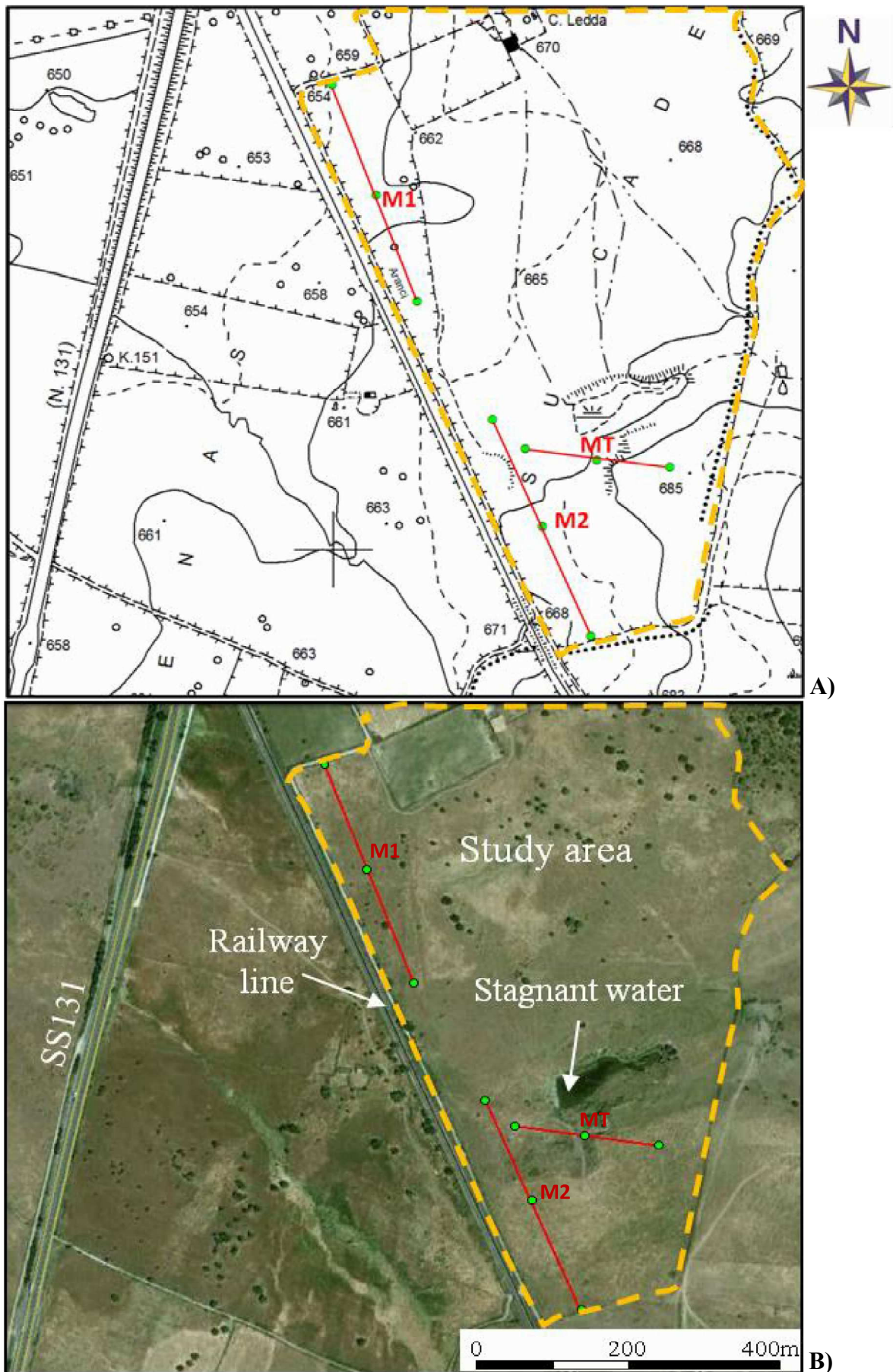
6.4 - Data processing

Apparent resistivity data were processed to generate two-dimensional resistivity models of the subsurface using RES2DINV inversion software (Loke, 2001).

The *l2-norm* implementation (smoothness-constrained) of the regularized least-squares optimization methods (Ellis and Oldeburg 1994) was applied and the forward problem was solved using the finite-element method (Silvester and Ferrari 1990).

Standard Gauss-Newton optimization methods was used, whit a convergence limit of 0.005 and the Jacobian matrix was recalculated for the first two iterations.

For all 2D resistivity dataset, the "bad data point" were removed before the inversion and the finer model with the cell width of half the minimum electrode spacing was used.

The RMS error was reduced after each iteration. It was not recommended to exceed five-six iterations because the recalculated data might differ too much from raw data and the model could become unstable. Resistivity measurements in the study area were done in a good manner, thus 2-3 iterations for profile were sufficient. Topographical data were integrated in each profiles before the inversion process.

The resulting sections display various electrical resistivities ranging from less than 2 Ω·m to more than 1000 Ω·m. Figure 6.4 shows the colour scale used to represent all the resistivity models.
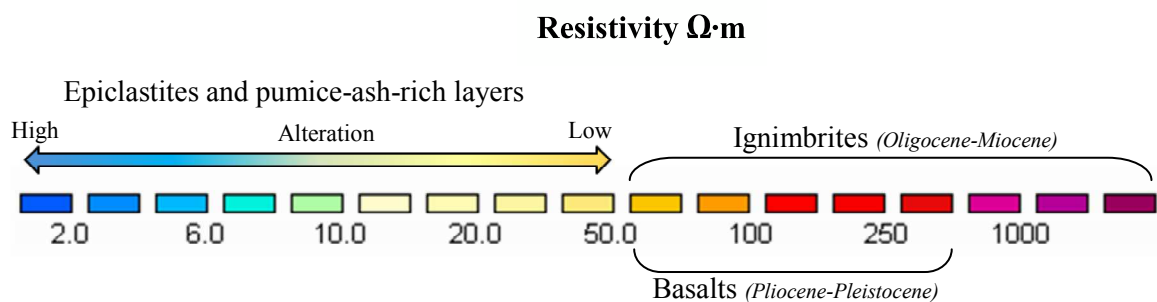
Resistivity Ω·m

Fig. 6.4 - Colour scale used to represents all resistivity models.

The welded ignimbrites, outcropping extensively in the southern sector of the site, have a very broad range of resistivity values, varying from approx. 50 to more than 1000 Ω·m, depending on the various grades of fracturation or alteration.

The pumice-ash-rich layers altered by hydrothermal fluids, are alternating with lacustrine epiclastites. By electrical method cannot be distinguished the alternating epiclastites inside the pumiceous material, therefore at this heterogeneous material have been attributed a resistivity

Vittorio Longo - Prospecting of Industrial Minerals: a geophysical approach -
PhD Thesis in Natural Science - University of Sassari

101

values range of less than 50 Ω·m. This decision is cautionary and makes it possible to "isolate" the material of interest from the overlying lithologies (ignimbrites, basalts).

Within the range of resistivity values assigned to the pumice-ash-rich layer , the lower values are caused by a higher clay component and/or an increased level of saturation (fig. 6.4).

The resistivity values relating to the Plio-Pleistocene basalts are range from 50 to approx. 500 Ω·m and thus fall within the values range already assigned to compact ignimbrites.

6.5 - Survey results

- *MT tomography*

ARRAY	WENNER-SCHLUMBERGER n=2
MEASURED RESISTIVITY POINTS	923
ARRAY LENGTH	189 m
INTERELECTRODE SPACING	3 m
MAXIMUM INVESTIGATION DEPTH	35 m
GPS POINTS	ELECTRODE1_N 40.31846°-E8.79073°
	ELECTRODE32_N 40.31832°-E8.79181°
	ELECTRODE64_N 40.31824°-E8.79291°

The MT calibration profile has been located in the southern sector of the work area, near the stagnant water where the altered pumice-ash-rich layer outcrops overlapped by the welded ignimbrites (fig.6.5).

The tomography in figure 6.6 shows resistive bodies with values greater than 50 Ω·m (red-purple in colour), identifying the Oligo-Aquitanian welded ignimbrites.

In particular, from chainage 96 metres (*x-axis*) to the end of the profile, the ignimbritic body appears compact on the surface (300 > ρ < 1000 Ω·m) and

Fig. 6.5 - Location of MT calibration line.

progressively more altered moving to depth.

The thickness of the ignimbritic body varies from 10 metres (near the escarpment) to 30 metres (at the end of the profile).

In the uppermost portion from the start of the tomography to chainage 80 metres (*x-axis*), the ignimbrites are discontinuous with meagre thickness.
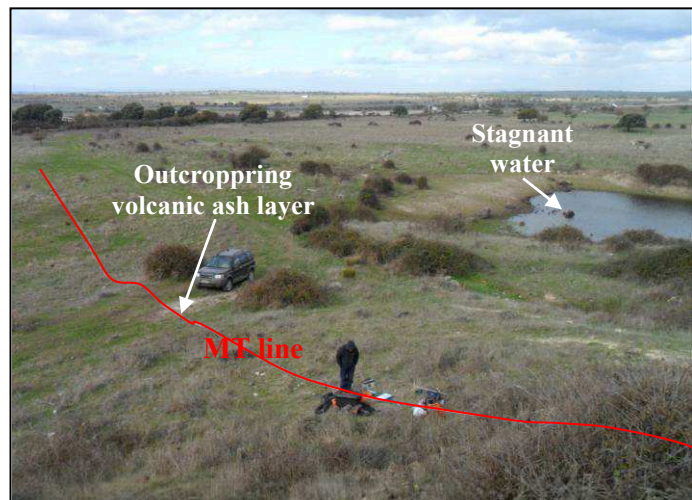
Vittorio Longo - Prospecting of Industrial Minerals: a geophysical approach -
PhD Thesis in Natural Science - University of Sassari

102

At chainage 72m (*x-axis*) the resistivity values greater than 100 Ω·m are attributable to ignimbritic boulders associated with the quarrying activities that have altered the original topography of the area (fig. 6.6 A-B).

Along the line, the pumiceous-cineritic level only outcrops below the escarpment, between chainages 80 and 90 metres (*x-axis*).

The resistivity values measured for this material are less than 50 Ω·m (yellow-blue in colour) and are observed along the entire profile below the ignimbrites described previously and down to the maximum depth achieved in the survey (35m).

More conductive zones (ρ < 10 Ω·m, green-blue in colour) can be observed inside these deposits, probably due to a higher clay content or a higher level of saturation.

Vittorio Longo - Prospecting of Industrial Minerals: a geophysical approach -
PhD Thesis in Natural Science - University of Sassari

103
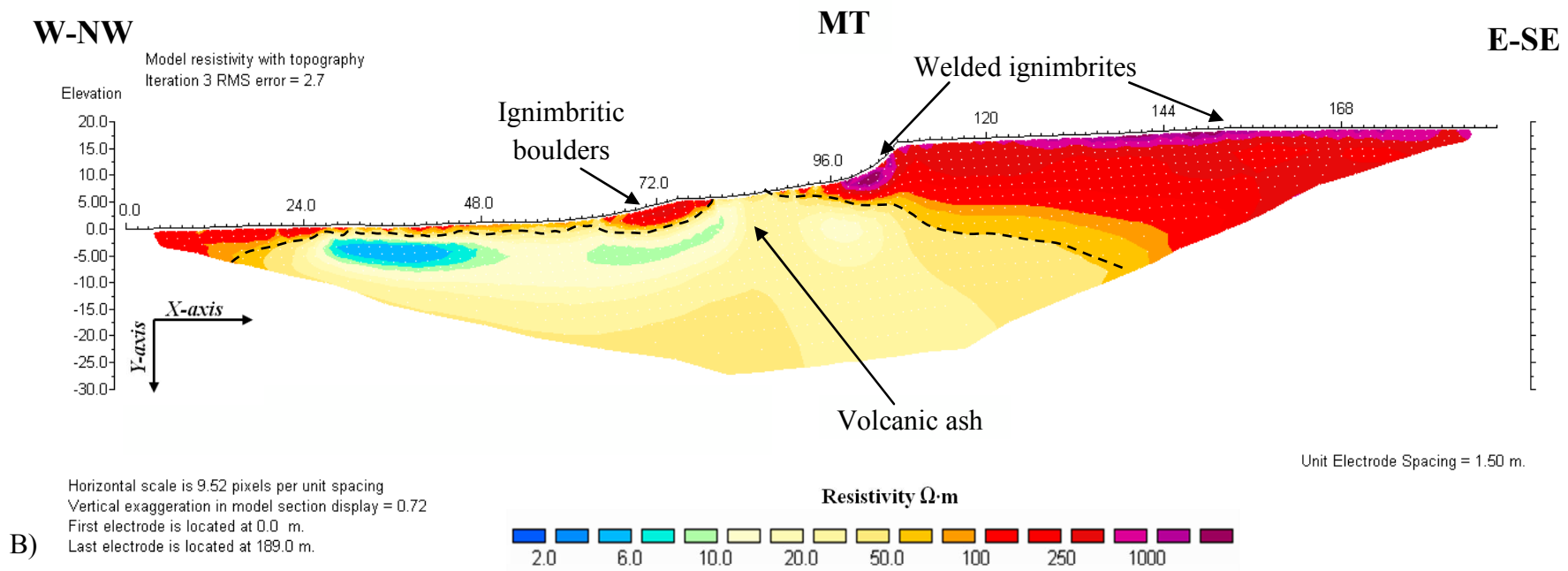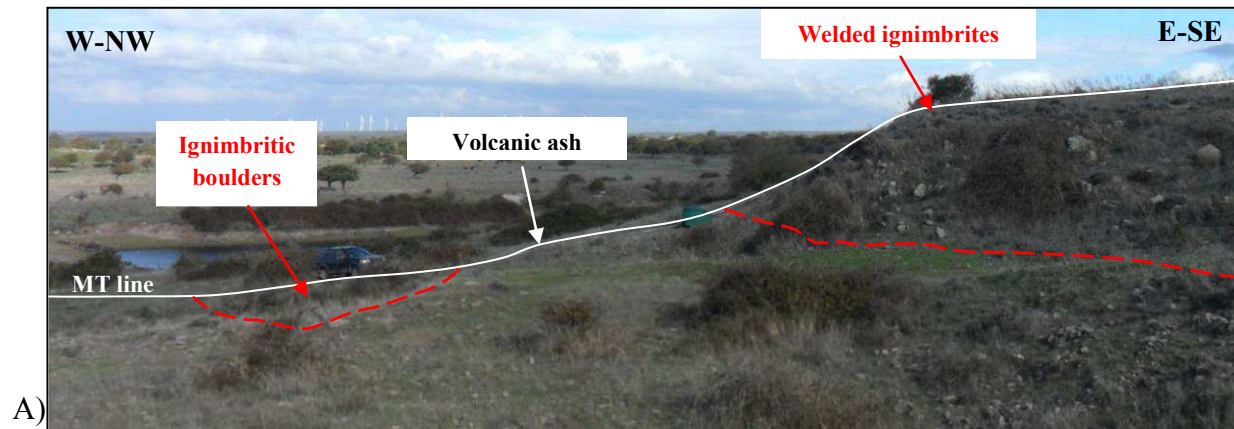
Fig. 6.6 - A) The calibration area. B) MT Electrical Resistivity Tomography.

Vittorio Longo - Prospecting of Industrial Minerals: a geophysical approach -
PhD Thesis in Natural Science - University of Sassari

104

- *M1 tomography*

ARRAY	WENNER-SCHLUMBERGER n=2
MEASURED RESISTIVITY POINTS	923
ARRAY LENGTH	315 m
INTERELECTRODE SPACING	5 m
MAXIMUM INVESTIGATION DEPTH	58 m
GPS POINTS	ELECTRODE 1_N 40.32281°-E8.78781°
	ELECTRODE 32_N 40.32149°-E8.78848°
	ELECTRODE 64_N 40.32022°-E8.78910°

The M1 tomography (fig. 6.8) shows resistivity values greater than 50 Ω·m (red-orange in colour) in the uppermost level along the entire profile and in the deepest portion between chainages 0-120 metres (*x-axis*).

The shallow level (thickness 5m) has resistivity values between 50 and 250 Ω·m, attributable to Plio-Pleistocene basalts that have different degrees of alteration.

Between chainages 180 and 220 metres (*x-axis*) there is an outcrop of compact basalt with resistivity values between 100 and 200 Ω·m (fig.6.7).

From the start to chainage 120 metres (*x-axis*) the resistive body has a thickness of approx. 25-30m.

This body shows resistivity values compatible with both Plio-Pleistocene compact basalts (as can be seen outcropping) and with Oligo-

Fig. 6.7 - Outcropping basalts at station at 200m (*x-axis*) in M1 electrical line.

Aquitanian welded ignimbrites (as observed in the MT tomography).

The presence of a fault at the station at 120 metres (*x-axis*), and possible fracture zones associated with it, should not be excluded, promoting the circulation of hydrothermal fluids.

Lower resistivity values ($\rho < 50$ Ω·m) have been measured at the south-eastern edge and in the deeper central portion of the tomography.

The pumice-ash-rich level is detected with very high probability inside this sector, since the resistivity values measured are entirely in keeping with those recorded in the calibration tomography.

Vittorio Longo - Prospecting of Industrial Minerals: a geophysical approach -
PhD Thesis in Natural Science - University of Sassari

105
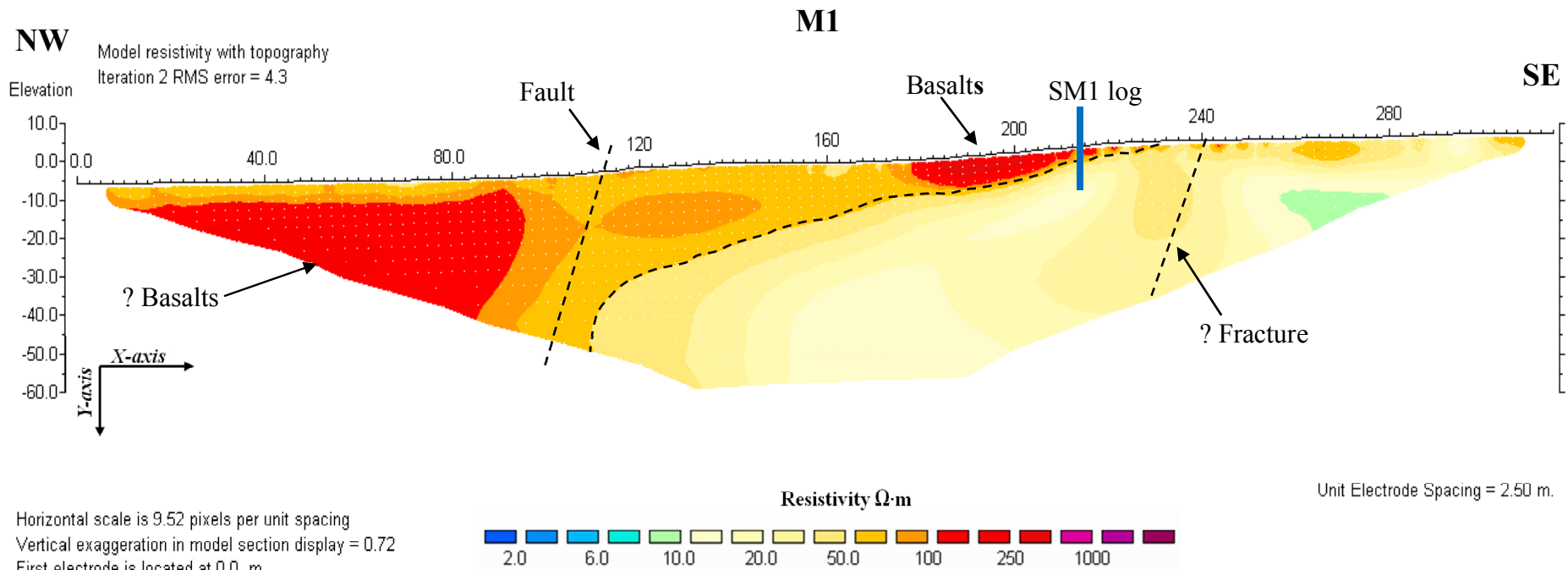
Fig. 6.8 - M1 Electrical Resistivity Tomography.

Vittorio Longo - Prospecting of Industrial Minerals: a geophysical approach -
PhD Thesis in Natural Science - University of Sassari

106

- *SM1 borehole*

On the 21 and 22 November 2011, a borehole was drilled at chainage 215 metres of the M1 profile (fig. 6.9A). The purpose was to assess the nature of the rocks with resistivity values less than 50 Ω·m. The SM1 stratigraphy column and the description of the lithologies at the different depths are reported below (fig. 6.9B).
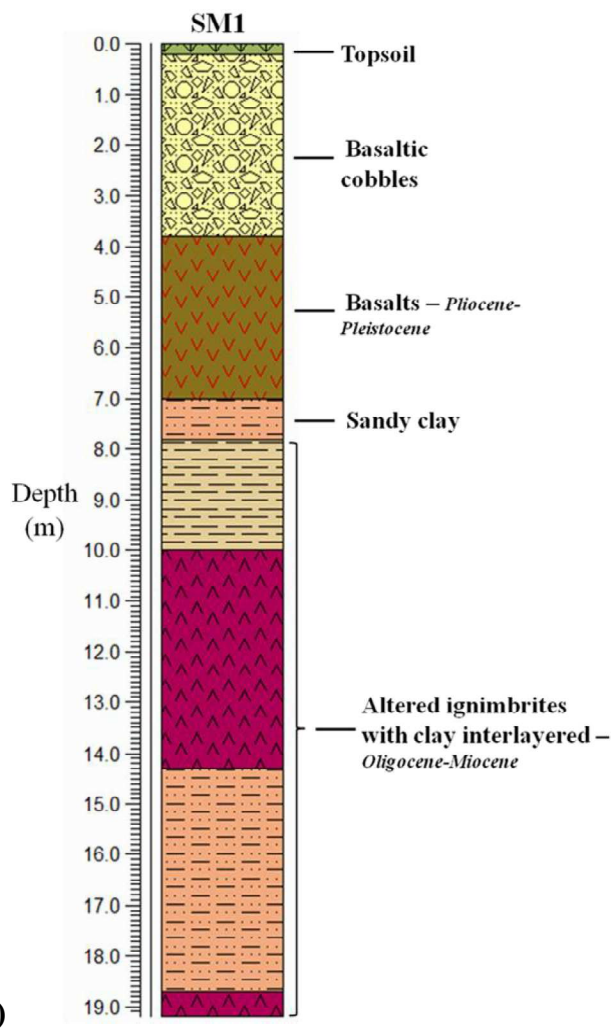
Fig. 6.9 - A) Location of SM1 borehole at 215m (*x-axis*) on the M1 profile. B) Stratigraphy column of SM1 borehole.

Vittorio Longo - Prospecting of Industrial Minerals: a geophysical approach -
PhD Thesis in Natural Science - University of Sassari

107

The cores have shown basaltic debris to a depth of 7 metres beneath surface level followed by compact basaltic-andesite. The basalt cover is in contact with a layer of brick-red sandy clay, attributable to a paleosoil with a thickness of 80cm.

This contact is highlighted by the colour change from red to yellow (depth of 7 metres) in the tomography. Beneath the paleosoil, to the base of the borehole (19.2m), are alternating strata of varicoloured bentonitised clays, associated with alteration of the pyroclastic products (ignimbrites, cinerites).

- *M2 tomography*

ARRAY	WENNER-SCHLUMBERGER n=2
MEASURED RESISTIVITY POINTS	923
ARRAY LENGTH	315 m
INTERELECTRODE SPACING	5 m
MAXIMUM INVESTIGATION DEPTH	58 m
GPS POINTS	ELECTRODE 1_N 40.31881°-E 8.79024°
	ELECTRODE 32_N 40.31752°-E 8.79099°
	ELECTRODE 64_N 40.31621°-E 8.79173°

The M2 tomography clearly distinguishes two sub-horizontal levels (fig. 6.10):

- the uppermost level, characterised by resistivity in excess of 100 $\Omega \cdot m$ (red-purple in colour);

- the deeper level with resistivity values less than 50 $\Omega \cdot m$ (yellow-blue in colour).

The uppermost resistive level identifies the welded Oligo-Miocene ignimbrites, running continuously from chainage 80m (*x-axis*) to the end of the profile, with thicknesses varying between 10 and 30m.

The ignimbritic body appears discontinuous only in the first part of the tomography.

The more conductive and deeper level follows the overlying ignimbrite trending perfectly.

In the tomography, the transition between the two bodies is sharp and well defined in the colour changes from red to orange.

The resistivity values in this layer reduce rapidly (from 50 to 10 $\Omega \cdot m$) when moving to depth, and are perfectly compatible with the pumice-ash-rich deposits of interest.

At bottom of the tomography, the minimum measured resistivity values ($\rho < 10 \ \Omega \cdot m$, blue-green in colour) identify either a higher degree of argillic alteration or the presence of saturated zones.

Vittorio Longo - Prospecting of Industrial Minerals: a geophysical approach -
PhD Thesis in Natural Science - University of Sassari

108
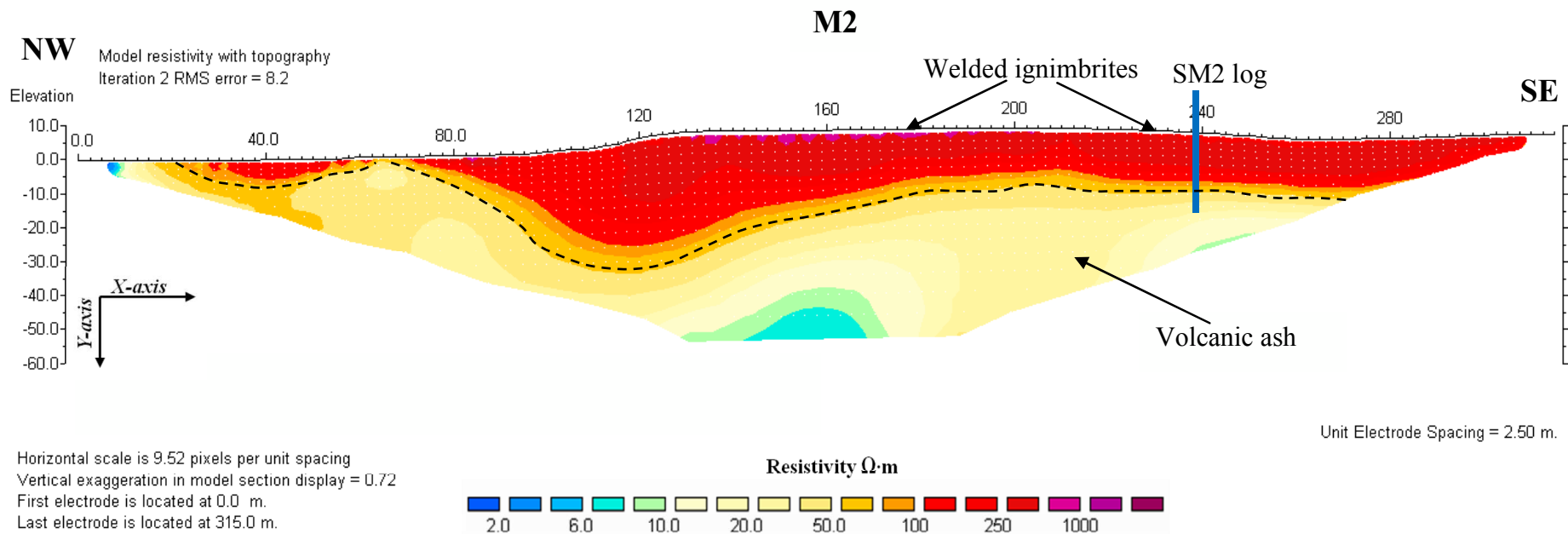
Fig.6.10 - M2 Electrical Resistivity Tomography.

Vittorio Longo - Prospecting of Industrial Minerals: a geophysical approach - PhD Thesis in Natural Science - University of Sassari

109

- *SM2 - SM3 boreholes*

Boreholes SM2 and SM3 were performed on 23-24-25 November 2011.

The location and the related stratigraphic columns are reported below (fig. 6.11A-B).

A)

B)

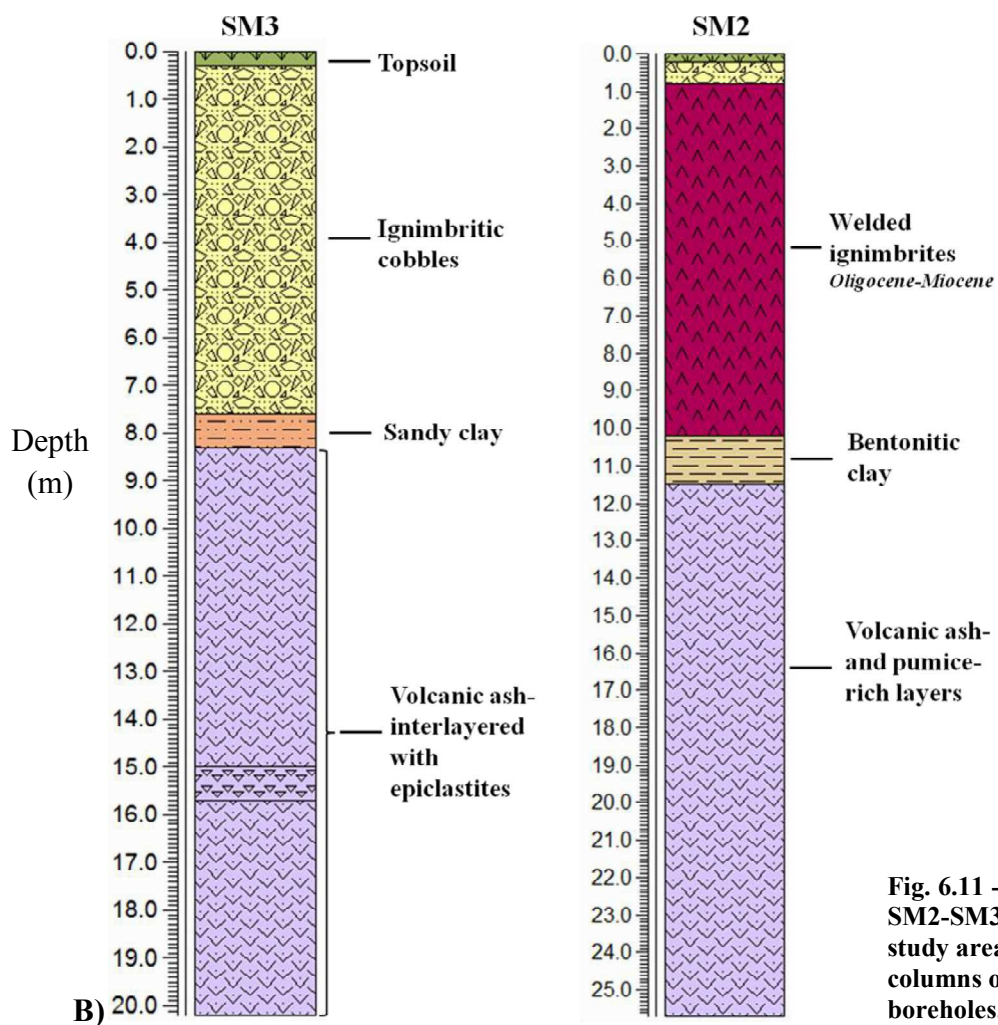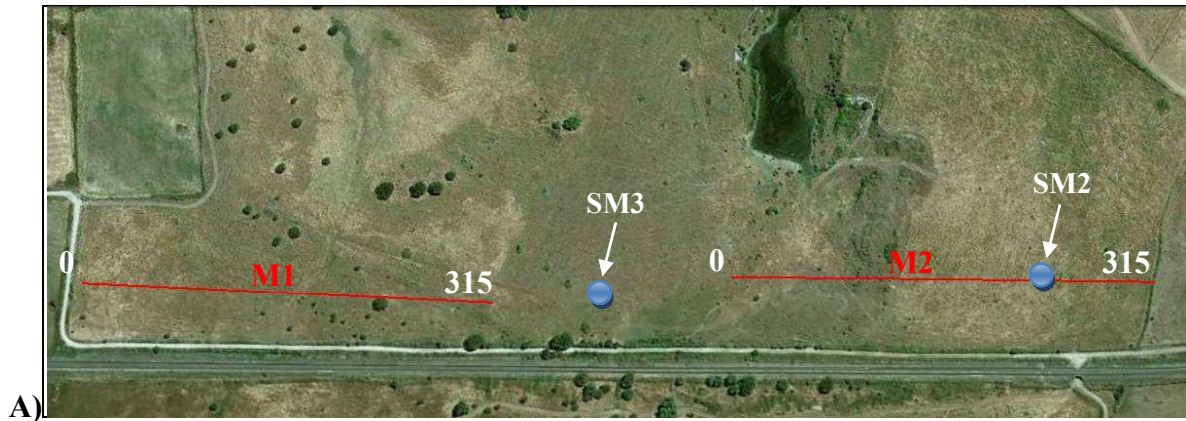Fig. 6.11 - A) Location of SM2-SM3 boreholes in the study area, B) Stratigraphy columns of SM2 and SM3 boreholes.

Vittorio Longo - Prospecting of Industrial Minerals: a geophysical approach -
PhD Thesis in Natural Science - University of Sassari

110

Borehole SM2 was drilled along profile M2 at station at 240 metres (*x-axis*), where the tomography has identified a sharp contact between the welded ignimbrites and the air-fall pyroclastic deposits at 10–12 metres deep (fig. 6.10).

The cores confirm the presence of welded ignimbrites down to a depth of 10,2m, followed by a layer of extensively bentonitised white to red coloured clays (fig. 6.12A).

The pumice-ash layer, varying from compact to altered and grey-white in colour, is located beneath of this until to the base of the borehole (25.7 metres) (fig. 6.12B).
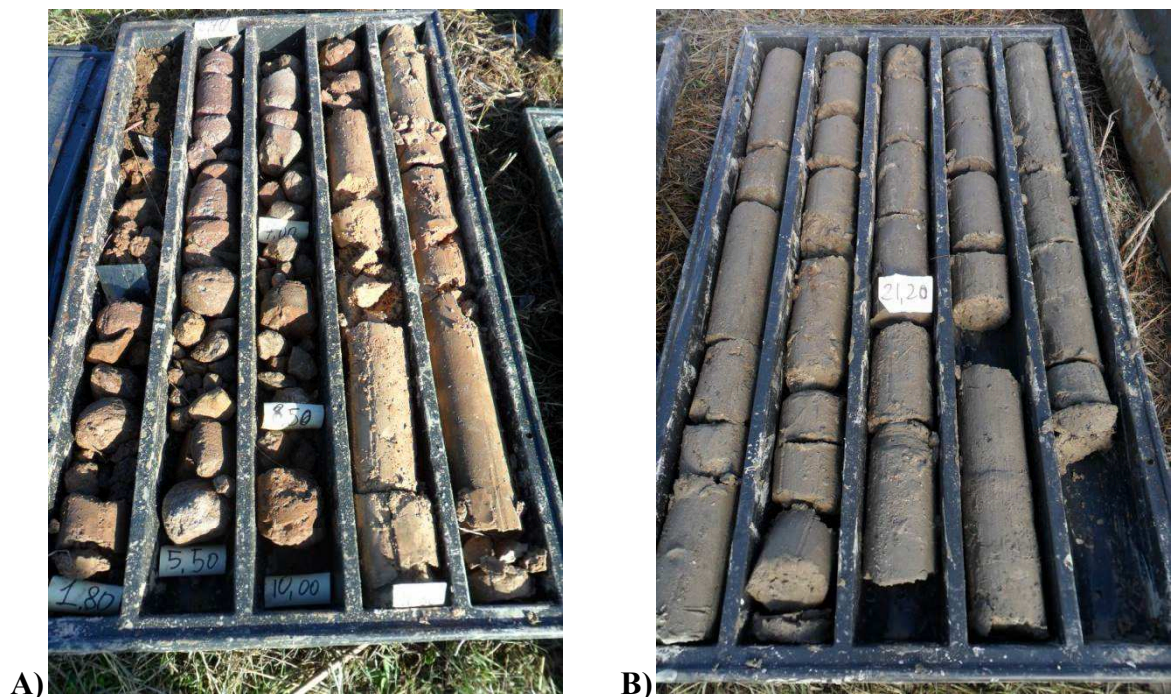

Fig. 6.12 - Cores of SM2 borehole. A) Welded ignimbrites. B) Volcanic ash- and -pumice rich layer (white and grey in colour).

Based on interpretation of the previous tomographies, borehole SM3 was located in an un-investigated area of the geoelectric surveys, approx. 90m from the end of M1 (fig. 6.11A).

The first few centimetres of SM3 log (fig. 6.11B) have ignimbritic debris followed by a reddish clay layer, comparable to the paleosoil shown in borehole log SM1.

Pumiceous-cineritic material, argillized to various extents, with interlayered epiclastic strata, is present from a depth of 8,3m to the base of the borehole (20,2m).

Vittorio Longo - Prospecting of Industrial Minerals: a geophysical approach -
PhD Thesis in Natural Science - University of Sassari

111

6.6 - Conclusions

The surveys performed near Macomer was successful in identifying the pumice- and ash-rich layer of interest.

The resistivity tomographies have provided targets for drillings, and have reduced the number of boreholes required with consequent saving in time and costs. The boreholes have confirmed the interpretation of the tomographies.

The pumice-ash-rich layer examined is altered due to the action of hydrothermal fluids conveyed by the major fracture systems. Smectite and zeolite are the main phases derived from hydrothermal alteration.

The heterogeneity of the material is confirmed by the broad range of resistivity values observed (2-50 Ω·m).

Tomography M2 and SM2 log have identified the contact between the welded ignimbrites and the conductive epiclastites at depth of approx. 10m.

The thickness of the deposit exceeds 40 metres, in fact the maximum depth investigated (55m) revealed conductivity values characteristic of the altered epiclastites.

The relationship of the thicknesses of the cover materials and the thicknesses of the deposit makes this site suitable for intensive exploitation.

References

CARMIGNANI, L., OGGIANO, G., BARCA, S., CONTI, P., SALVADORI, I., ELTRUDIS, A., FUNEDDA, A., AND PASCI, S., 2001. *Geologia della Sardegna - Note illustrative della Carta Geologica scala 1:200000. Memorie Descrittive Carta Geologica d'Italia,* LX, 283.

ELLIS, R.G. AND OLDENBURG, D.W., 1994. *Applied geophysical inversion*: Geophysical Journal International, 116, 5-11.

LOKE, M.H., 2001. *Res2Dinv software users manual, version 3.4.* Geotomo Software, Penang, Malaysia, 98.

SILVESTER, P.P., AND FERRARI, R.L., 1990. *Finite elements for electrical engineers (2nd. ed.).* Cambridge University Press, 516.

Vittorio Longo - Prospecting of Industrial Minerals: a geophysical approach -
PhD Thesis in Natural Science - University of Sassari

112

Chap.7 - Geoelectrical Prospecting for characterising the Messinian clay deposits in the Nurra region (Sardinia NW): a preliminary study

7.1 - Introduction

The results of a geoelectrical survey carried out in northern of Nurra region (Sardinia N-W) are here presented.

This study has the aim to discriminate, by Electrical Resistivity Tomography, some clay deposits compared to the underlying bedrock, and meantime to define the thickness and extension of the clayey bodies.

The examined sediments are floodplain deposits that have filled a valley formed after the Messinian Salinity Crisis.

These materials represent a continuous clayey band, topped by flooding channeled mainly composed of clast-supported conglomerates with variable thickness.

These clays, for their mineralogical and chemical characteristics are extracted for use as raw materials for bricks production. In the study area there are the disused quarries of clays, some of which have been reused as solid urban waste landfill.

The electrical acquisition lines were performed with a different resolution and were localized in several areas of the palaeovalley.

Vittorio Longo - Prospecting of Industrial Minerals: a geophysical approach -
PhD Thesis in Natural Science - University of Sassari

113

7.2 - Geological setting

NW Sardinia consists of a structural high that represents the uplifted part of a wide, tilted block. To the west, this structural high borders the eastern passive margin of the Liguro-Provencal backarc basin; to the east, it abuts the edge of a N–S-trending Miocene half-graben (the Porto Torres Basin of Thomas and Gennessaux 1986).
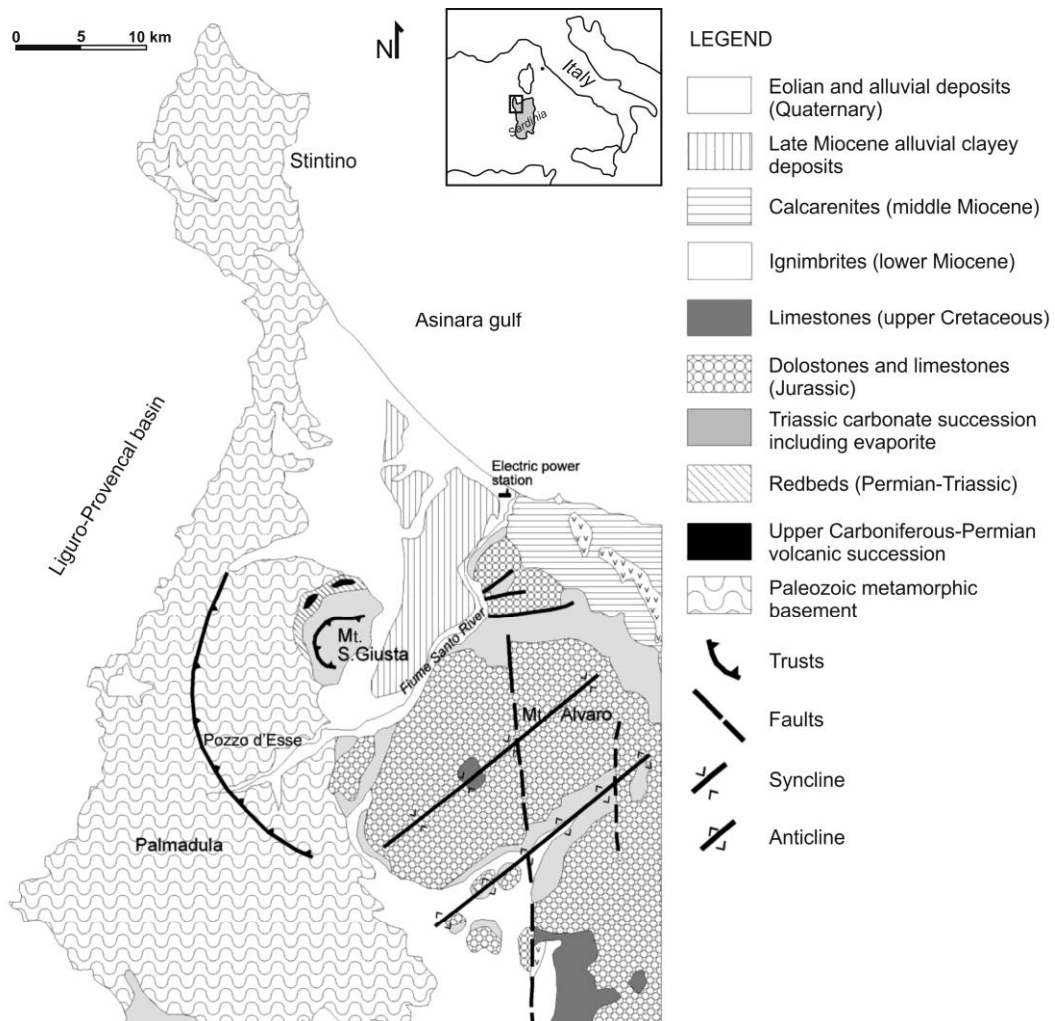

Fig. 7.1 - Geological sketch map of NW Sardinia showing the sequences from Palaeozoic to Quaternary age (Mongelli et al., 2012, mod.).

Upper Burdigalian to Tortonian carbonate marine deposits of the Porto Torres Basin onlap the structural high, where Mesozoic and Palaeozoic sequences are exposed.

The Mesozoic sequences consist of basal red beds (Buntsandstein facies), evaporites, and shallow-marine carbonate deposits, ranging in age from Middle Triassic to Cretaceous and overlying Lower–Middle Permian continental sediments and volcanites (Buzzi et al., 2008). The Permian–Mesozoic sequences unconformably overlie Variscan low-grade metamorphic

Vittorio Longo - Prospecting of Industrial Minerals: a geophysical approach -
PhD Thesis in Natural Science - University of Sassari

114

basement consisting of phyllites, quartzites, and metabasites, which are exposed along the coast (fig. 7.1). The Permian and Mesozoic successions are unconformably overlain by an alluvial (mainly clayey) deposit that has been interpreted as an alluvial fan and braided-river plain of Messinian age (Pascucci et al., 2004).

The supposed Messinian deposits occur over a wide depression between Jurassic uplands and Variscan basement, and their thickness increases towards the present shoreline.

Abbazzi et al. (2008) proposed a late Tortonian–early Messinian age for these sediments, based on the presence of a palaeofauna that includes mammals with a Tuscan affinity.

The structural framework of the Nurra area mainly reflects Tertiary tectonic events that were possibly related to Pyrenean and North Apennine tectonics (Mameli et al., 2007 and references therein).

The cover rocks are affected by NE–SW-trending folds and faults (some of the faults evolved into thrusts); evaporites commonly occur as décollement horizons and are exposed in the cores of anti-clines and in structural highs.

Since the Burdigalian, the area was subjected to an extensional tectonic regime related to the opening of the Liguro-Provencal Basin, followed by moderate uplift during the Pliocene.

Erosion in the region was controlled mainly by lithology: areas of deformed and exposed evaporites were more deeply eroded than were areas of Mesozoic limestone and metamorphic basement.

Erosion was enhanced by a drop in base level during the Messinian crisis, resulting in development of wide, shallow depressions rimmed by alluvial sediments that represent depositional surfaces dipping away from the axial culmination of the main structures (i.e. towards the Asinara Gulf and towards the Provencal Basin).

After uplift in the Pliocene, these surfaces were mildly eroded, especially at the edges of valleys. Nevertheless, one of these depositional palaeosurfaces is largely preserved in the wide and shallow palaeovalley which runs from Pozzo d'Esse to the Fiume Santo power plant (fig. 7.1).

The upper Tortonian–lower Messinian continental deposits, which infill this palaeo-erosional depression, are exposed in quarries where they are extracted for use as raw material in the manufacture of tiles.

The deposits are about 20m thick in the deepest quarry, and their thickness increases northward. The upper part of the succession, which is 1–3m thick, consists of channelized gravel deposits with rounded–subrounded clasts of metamorphic quartz, quartzites, and highly weathered rhyolite within a silty–sandy matrix.

Vittorio Longo - Prospecting of Industrial Minerals: a geophysical approach -
PhD Thesis in Natural Science - University of Sassari

115

The age of this capping horizon is probably Pliocene–Pleistocene, and the contact with underlying deposits is sharp and marked by the presence of calcrete. This gravel-dominated horizon is underlain by a 10m-thick unit of clays and sandy clays, which shows evidence of intense pedogenesis, including rhizoliths consisting of Fe-depleted zones within purple to ochre clays.

Locally, 1m-thick gravel layers are interbedded with the clays. The base of the alluvial-residual deposit is not exposed.

7.3 - Location of Electrical Resistivity Tomographies

The acquisition electrical lines were located in the southern sector of the palaeovalley enclosed by Fiume Santo river to the east and M.S.Giusta to the west, where thrust west-verging involving the outcropping Triassic sequences.

The six performed electrical lines have been placed in the 1:25000 Geological map (fig. 7.2 - Oggiano unpublished) through GPS points collected in the field.

For resistivity data acquisition was used the SAS 1000 ABEM Lund Imaging System (Dahlin, 1996), together with a relay switching unit (Electrode Selector ES 10-64), four 160-m multiconductor cables, and 64 stainless steel rod electrodes (par. 2.1).

A hybrid Wenner–Schlumberger array (Loke, 2000) was used for this study. This array arrangement is moderately sensitive to both horizontal and vertical structures and has a horizontal coverage and depth of penetration that is about 15% larger than the Wenner array.

The resistivity data were acquired in two different steps.

During the first step were collected the data relating to the S1-S2-S3 ERT lines, located in the eastern part of the work area near Fiume Santo (fig.7.2).

Particularly S1 and S2 electrical lines were placed in correspondence of the slope of the palaeovalley where the clayey body outcrops in a discontinuous way, while S3 profile was located in the central part of this.

The aims of these surveys were to measure the electrical signature of clayey body and detected the depth to bedrock. For each lines was used inter-electrode spacing of 5m, obtaining a unit length of 315m and a maximum investigation depth of 60m.

During the second step were collected the data relating to the N1-N2-N3 ERT lines nearest to M.S.Giusta (fig.7.2).

The N1 line was performed close to an outcrops of Permian continental sediments (Buntsandstein facies).

Vittorio Longo - Prospecting of Industrial Minerals: a geophysical approach -
PhD Thesis in Natural Science - University of Sassari

116

After the electrical data acquisition a borehole CS5 was drilled at 180m station in the N1 line, and the obtained stratigraphy information were correlated with resistivity values.

The N3 profile was located at south parts of M.S.Giusta, where the contact between Triassic carbonate succession and Upper Miocene alluvial clayey deposits is well exposed.

For both lines (N1 and N3) was used inter-electrode spacing of 10m, obtaining a unit length of 630m and a maximum investigation depth of 115m.

The N2 profile is located in close to the floodplain in the central part of the palaeovalley. For this survey inter-electrode spacing of 5m was used, obtaining a unit length of 315m and a maximum investigation depth of 60m.

Vittorio Longo - Prospecting of Industrial Minerals: a geophysical approach -
PhD Thesis in Natural Science - University of Sassari

117
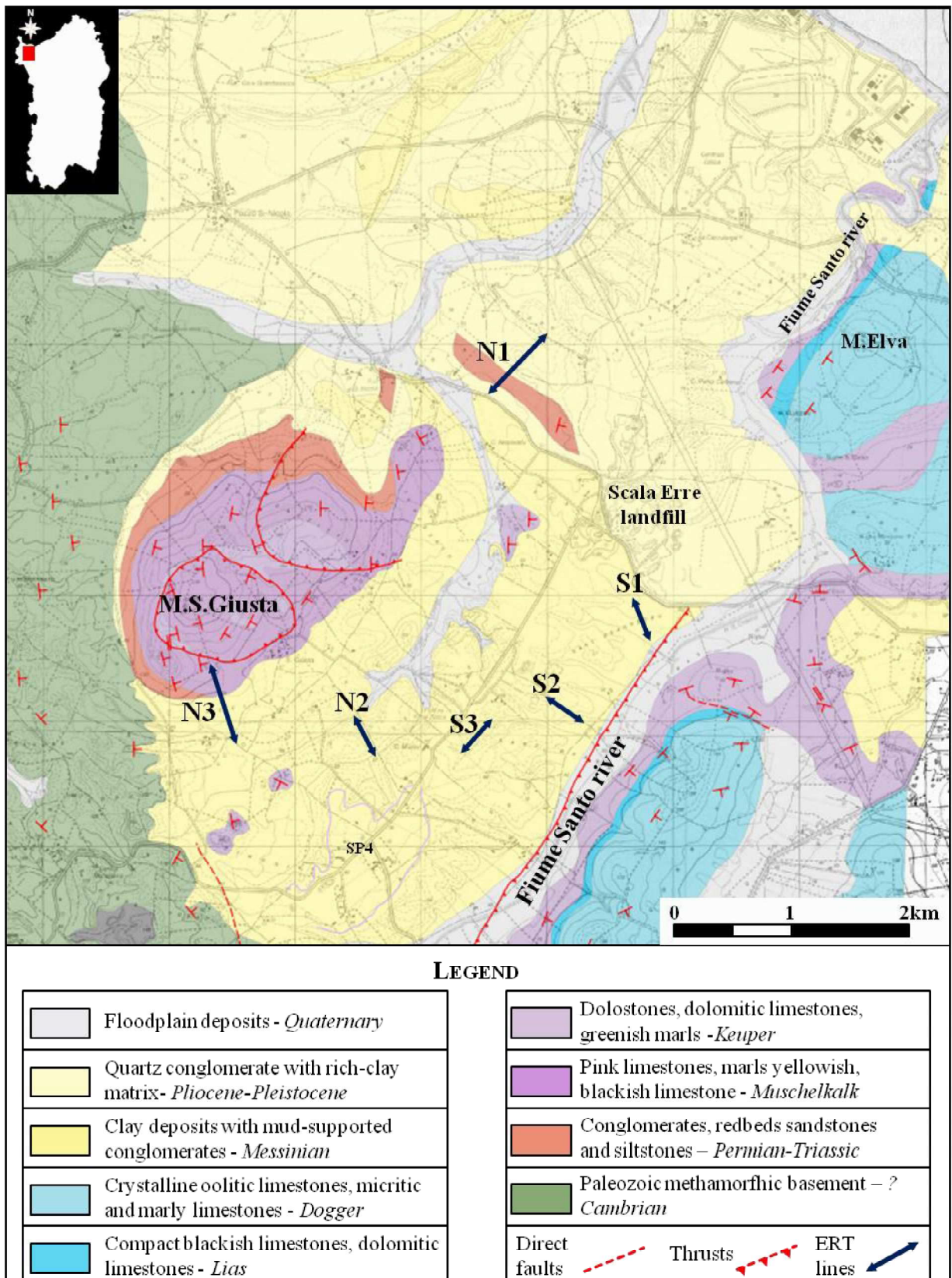
Fig. 7.2 - Extract of Geological Map of Nurra district (Sardinia) (Oggiano, unpublished, mod.).

Vittorio Longo - Prospecting of Industrial Minerals: a geophysical approach -
PhD Thesis in Natural Science - University of Sassari

118

7.4 - Data processing

The data from field surveying was exported to computer and 2D inversion and topographic correction of the pseudosections were performed using the RES2DINV software package (Loke, 2001).

The topographic corrections were carried out with measurements of elevation for each electrode position through an inclinometer.

The forward problem was solved using the finite-element method (Silvester and Ferrari 1990), in which node positions were adjusted to allow topography to be taken into account in the inversion process.

The inversion routine of RES2DINV software based on the smoothness-constrained least-squares technique (deGroot-Hedlin and Constable, 1990; Sasaki, 1992) was used for all data.

The Standard Gauss-Newton optimization methods was used, whit a convergence limit of 0.005 and the Jacobian matrix was recalculated for the first two iterations. The finer model with the cell width of half the minimum electrode spacing was used.

For all 2D resistivity dataset the "bad data points" were removed in some cases manually and pre-inversion, in other cases automatically and post-inversion (par. 2.2).

In this study five iterations were recalculated for all profiles and the better resistivity model according to expected geological models was taken.

RMS error is usually grater of 20%, probably due to heterogeneous character of the lithologies and high resistivity contrast with underlain bedrock.

The ERT resulting display various electrical resistivities ranging from less than 5 Ω·m to greater than 700 Ω·m.

Resistivity Ω·m

Clay deposits *(Upper Miocene)*   Bedrock

5.0   10.0   20.0   40.0   80.0   160   320   640

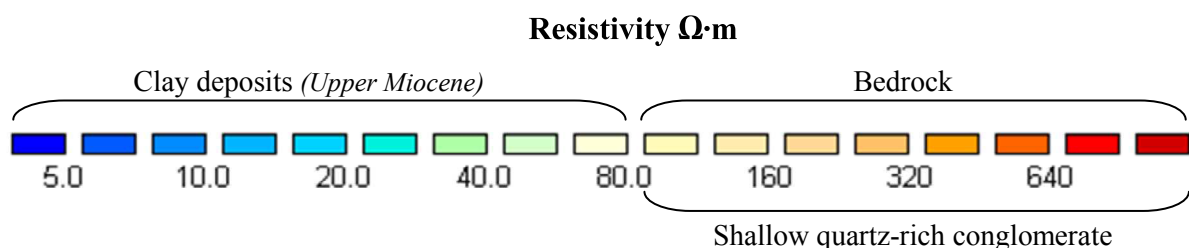Shallow quartz-rich conglomerate

Fig. 7.3 - Colour scale used to represents the resistivity models.

Observing the inversion results, we have classified the resistivity values into two range: [from less of 5 Ω·m to 80 Ω·m] represents the conductive bodies, [by 80 Ω·m to more of 700 Ω·m] represents the resistive bodies (fig.7.3).

Vittorio Longo - Prospecting of Industrial Minerals: a geophysical approach -
PhD Thesis in Natural Science - University of Sassari

119

The resistivity values of the clayey deposits (Upper Miocene) fall within the range given to the conductive bodies, while among the resistive bodies are distinguished the quartz-rich superficial conglomerates and the bedrock consisting of carbonatic rocks (Triassic succession) or redbeds sandstones (Permian).

In the tomographies, it is possible to discriminate the conglomerates from the bedrock by the different stratigraphic positions.

7.5 - ERT survey results: first step

- *S1-S2 tomographies*

ARRAY	WENNER-SCHLUMBERGER n=5
MEASURED RESISTIVITY POINTS	1071
ARRAY LENGTH	315 m
INTERELECTRODE SPACING	5 m
MAXIMUM INVESTIGATION DEPTH	60 m
GPS POINTS	S1 *ELECTRODE 1* - 40°48'20.49" N; 8°17'08.12" E *ELECTRODE 32* - 40°48'25.15" N; 8°17'05.83" E *ELECTRODE 64* - 40°48'30.05" N; 8°17'04.12" E S2 *ELECTRODE 1* - 40°47'59.07" N; 8°16'48.09"E *ELECTRODE 32* - 40°48'01.45" N; 8°16'42.34" E *ELECTRODE 64* - 40°48'03.84" N; 8°16'36.44" E

S1 and S2 tomographies, SSE-NNW and SE-NW-orientated respectively, are shown in figure 7.4. In both tomographies the topographic elevation increases moving towards NW.

The ERT models shown three sub-horizontal levels:

- A shallow resistive level (ρ = 80-500 Ω·m) assigned to clast-supported conglomerates.
- A intermediate conductive level (ρ < 40 Ω·m) compatible whit interest clays.
- A deep resistive level (ρ > 250 Ω·m) related to bedrock.

In both profiles the superficial conglomerates (yellow-orange in colour) appear discontinuous and variable in thickness.

In S1 this layer occupies the outer parts of the profile. In the first part (0-150m *x-axis*) the conglomerate has a thickness of about 8m, while in the distal portion (240-315 m *x-axis*) shows a maximum thickness of 15m.

Vittorio Longo - Prospecting of Industrial Minerals: a geophysical approach -
PhD Thesis in Natural Science - University of Sassari

120

In S2 the conglomerate has an irregular geometry and outcrops from the start of profile to the station at 160m (*x-axis*). The thickness of this layer is ranging from 5 to 10m.

In the morphologically lower areas the irregular shape of the conglomerates is due to important channeling processes.

The clayey intermediate level (blue-green in colour) appears, in both profiles, continuous and in some places outcropping.

The geometric features of this level are strongly conditioned by to the trend of underlying resistive bedrock and of the overlying conglomerates.
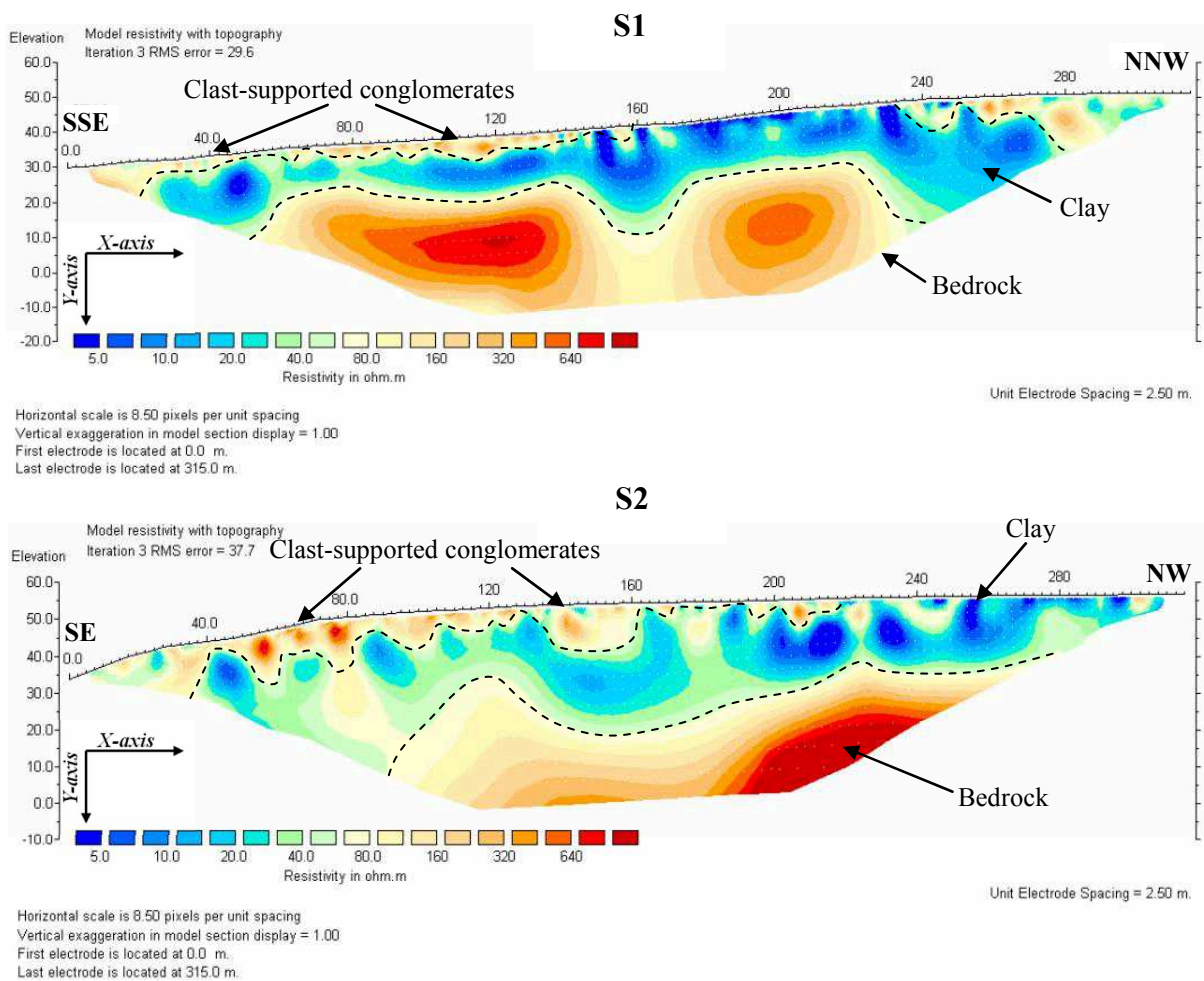

Fig.7.4 - S1 and S2 tomographies.

The clayey level outcrops only between 160-240m (*x-axis*) in S1 profile and in the end portion of S2 profile (220-315m *x-axis*). The average thicknesses for this level are approx. 15 and 20m respectively.

In either profiles, the conductive clayey level shows areas with resistivity values less than 20 $\Omega \cdot m$, index of a higher concentration of clay minerals or of a higher saturation degree.

Vittorio Longo - Prospecting of Industrial Minerals: a geophysical approach -
PhD Thesis in Natural Science - University of Sassari

121

The clay/bedrock interface is detected at 15-20m in depth of the ERTs (fig. 7.4).

The resistivity values of the bedrock are compatible both with Tertiary carbonatic rocks, that outcrop few kilometers toward est-direction (eastern bank of Fiume Santo), and with the Permian sandstones (fig. 7.2). The bedrock has an irregular trend and shows a wide resistivity range from 80 to up 700 Ω·m, in relation to the different fracturing and alteration conditions.

- *S3 tomography*

ARRAY	WENNER-SCHLUMBERGER n = 5
MEASURED RESISTIVITY POINTS	640
ARRAY LENGTH	315 m
INTERELECTRODE SPACING	5 m
MAXIMUM INVESTIGATION DEPTH	60 m
GPS POINTS	ELECTRODE 1 - 40°47'51.24"N; 8°16'06.70" E
	ELECTRODE 32 - 40°47'54.58"N; 8°16'11.68" E
	ELECTRODE 64 - 40°47'58.02"N; 8°16'16.77"E

The S3 profile, SW-NE oriented, was performed parallel to the SP4 road in the central sector of the palaeovalley (fig. 7.2), where the Messinian clays outcrop.

The tomography reported in figure 7.5 show a well developed clays deposit, which extends from the ground surface at maximum depth of 45m.
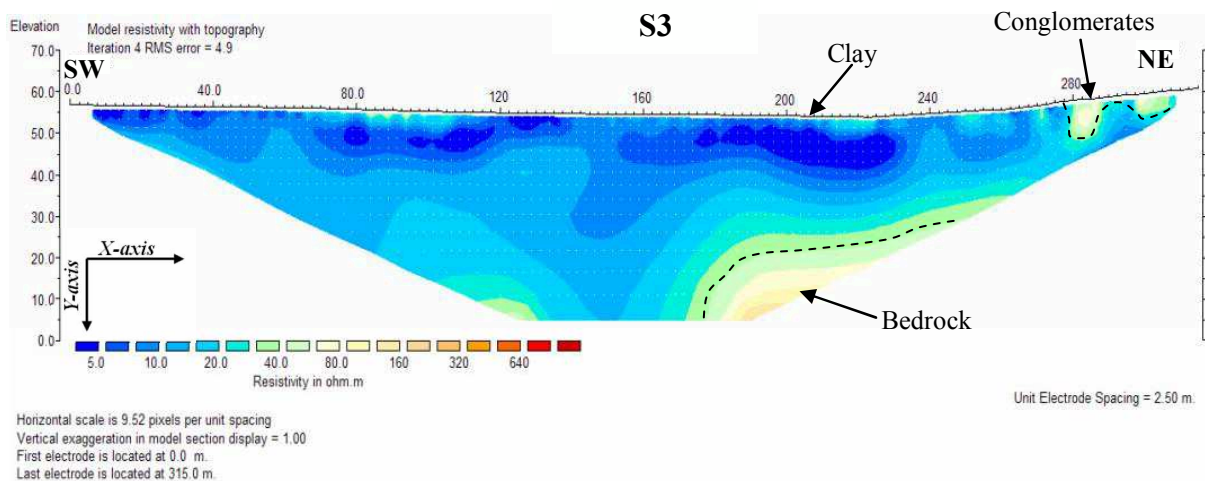

Fig. 7.5 - S3 tomography.

The resistivity values of clayey body don't exceed 30 Ω·m, and in the surface layers (down to 20m) are recorded the lowest resistivity values (less than 10 Ω·m).

The clay/bedrock interface isn't clearly identified, however the resistivity values greater than 100 Ω·m were recorded in the deeper edges of tomography. This suggest that the compact bedrock could find themselves at a greater depth of 50m.

Vittorio Longo - Prospecting of Industrial Minerals: a geophysical approach -
PhD Thesis in Natural Science - University of Sassari

122

The cover conglomerates, as noted in outcrop, are present from station 280m to the end of line (*x-axis*). This is a conglomerate rich in clay matrix with resistivity values lower than those previously observed.

The homogeneous resistivity values and the absence of thick cover conglomerates in this deposit, suggest a good quality clays similarly to those extracted in the northern sector (Scala Erre area - fig.7.2).

7.6 - ERT survey results: second step

- *N1 tomography*

ARRAY	WENNER-SCHLUMBERGER n = 3
MEASURED RESISTIVITY POINTS	967
ARRAY LENGTH	630 m
INTERELECTRODE SPACING	10 m
MAXIMUM INVESTIGATION DEPTH	100 m
GPS POINTS	ELECTRODE 1 - 40°49'24.24"N; 8°16'11.46" E
	ELECTRODE 32 - 40°49'31.62"N; 8°16'20.46" E
	ELECTRODE 64 - 40°49'39.54"N; 8°16'28.70"E

N1 tomography, SW-NE oriented, is located in the northern part of the work area, near a Permian redbeds outcrop. Using the interpretation of the lines S1-S2-S3 as a guide, the N1 ERT appears to suggest for the subsurface the same three layers model as analyzed in the eastern sector.

The superficial level of clast-supported conglomerates occupies the morphologically higher area, from the station 320m until the end of the profile (*x-axis*) (fig. 7.6A).

This has a thickness comprised from 5 to 10m and resistivity values higher than 200 Ω·m.

The conductive layer appears heterogeneous with wide resistivity range between 5-50 Ω·m.

The contact between the conductive layer and the compact arenaceous resistive bedrock is shown in the ERT to a depth of 45-50m.

After the electrical data acquisition a borehole CS5 was drilled at station 180m of N1 line (fig. 7.6A), in order to assess the nature of the conductive anomaly.
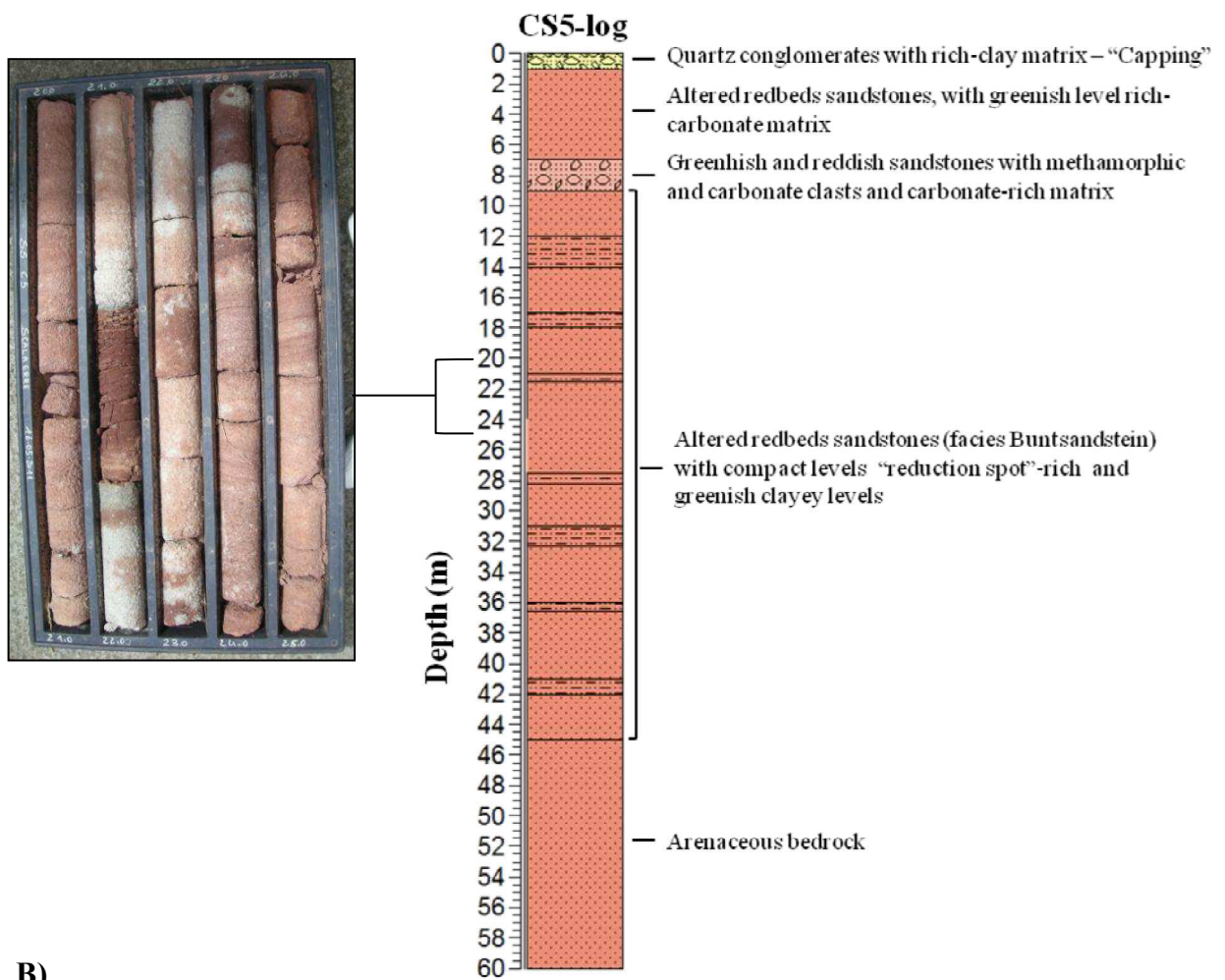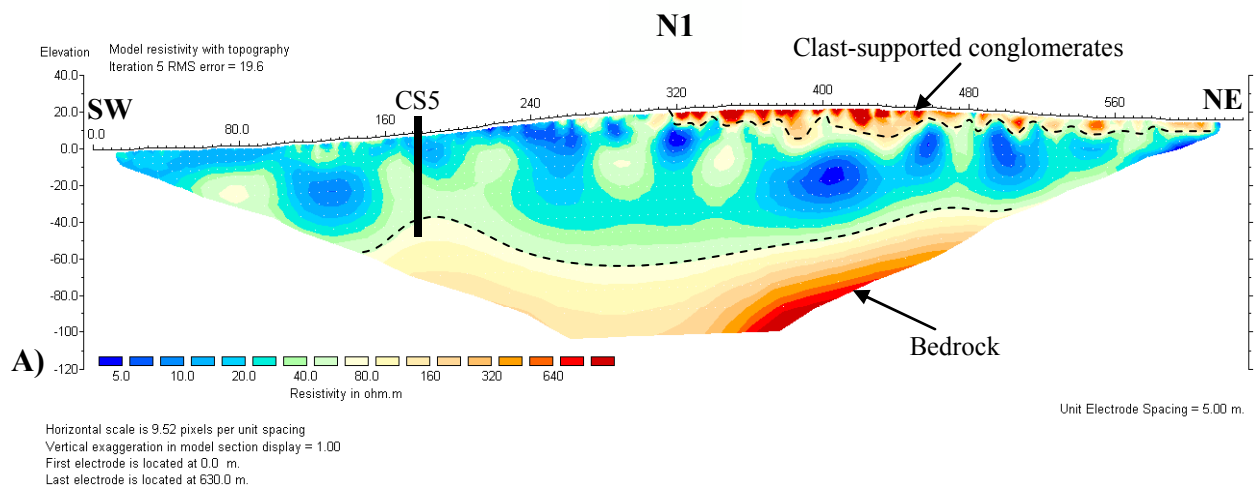
Vittorio Longo - Prospecting of Industrial Minerals: a geophysical approach - PhD Thesis in Natural Science - University of Sassari

123

Fig. 7.6 - A) N1 tomography, B) CS5 borehole log.

The cores (fig.7.6B) reveal the presence of Permian redbeds sandstones beneath a thin layer of superficial mud-supported quartz conglomerates (thick 1m).

This sandstones appear strongly altered, interlayered with clay and locally have a rich in carbonate matrix down to depths of 45m. Beneath this depth to the end of borehole, the cores show the compact sandstone (bedrock).

Vittorio Longo - Prospecting of Industrial Minerals: a geophysical approach -
PhD Thesis in Natural Science - University of Sassari

124

Comparing the borehole data with the conductive values of N1 tomography, we can say that both the Messian clays and Permian sandstones have similar resistivity values, when these sandstones are altered, satured and with clay-rich matrix.

In this case, the electrical resistivity method is not suitable to distinguish the two different lithologies. Therefore the presence of Messinian clays below the conglomerate level in the north-east portion of tomography we cannot exclude. In fact, these clays outcrop extensively northward.

- *N3 tomography*

ARRAY	WENNER-SCHLUMBERGER n = 3
MEASURED RESISTIVITY POINTS	1054
ARRAY LENGTH	630 m
INTERELECTRODE SPACING	10 m
MAXIMUM INVESTIGATION DEPTH	115 m
GPS POINTS	ELECTRODE 1 - 40°48'12.89"N; 8°14'39.88" E
	ELECTRODE 32 - 40°48'3.31"N; 8°14'43.62" E
	ELECTRODE 64 - 40°47'53.88"N; 8°14'48.37"E

The N3 line, NW-SE oriented, was situated to the SW of Monte Santa Giusta where the Tertiary carbonate successions are outcrop (fig. 7.2).

At the time of acquisition data the ground surface was moist due to rain of the previous days. Probably this altered the resistivity values of shallow levels.

The initial 240m of the profile were placed on the sub-outcropping Triassic limestones (facies Muschelkalk). The tomography (fig. 7.7A) in this sector has detected a compact resistive body with resistivity values greater than 300 Ω·m.

From the station 240m to the end of profile, the tomography shows a shallow conductive level with irregular shape. The resistivity values for this level are less than 40 Ω·m and beneath it is in contact with a resistive body.

The field evidences and the N1 survey results have allowed to create the interpretative schematic model shown in figure 7.7B.

The conductive lens, at the 320m station (*x-axis*), was interpreted as altered and saturated Permian sandstones with rich-clay matrix. In this area the Permian sandstones outcrop a few tens of meters to west of N3 profile and in a continuous semicircular band in the north-western sector of M.S.Giusta (fig. 7.2).

Horizontally the conductive lens is in contact with alluvial deposits rich in clay matrix, which occupy the last part of the profile and it is approx. 10-15m in thickness.

Vittorio Longo - Prospecting of Industrial Minerals: a geophysical approach -
PhD Thesis in Natural Science - University of Sassari

125

The deep resistivity body was interpreted as the sandstone bedrock, which is probably in contact with the underlying Paleozoic metamorphic basement.

In this case the bedrock has a irregular shape and rises upward proceeding to SE.

A normal fault that displaces the Permian sandstones was assumed at station 250m (*x-axis*), according to the tectonic trend of the area.

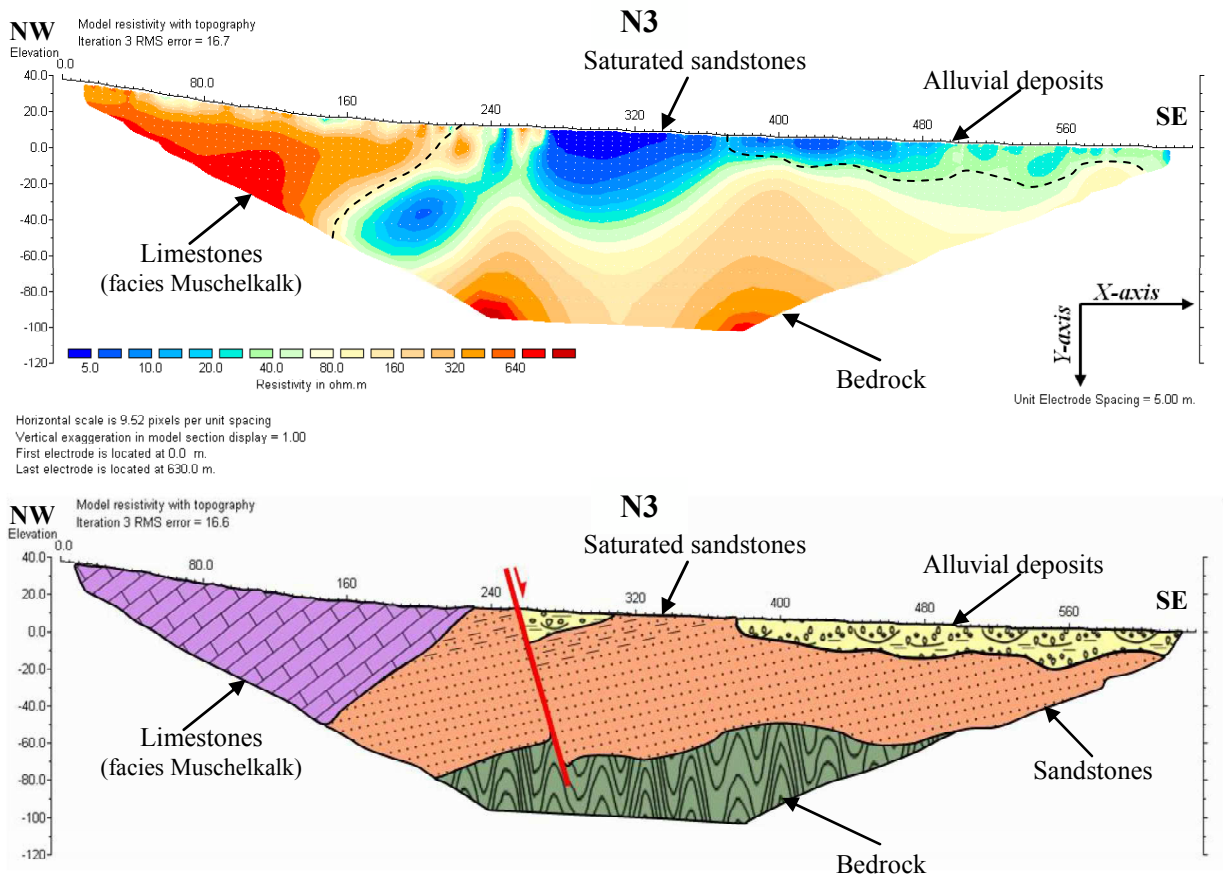**Fig. 7.7 - A) N3 electrical tomography in the western slope of palaeovalley. B) Interpretative schematic model for N3 ERT.**

Vittorio Longo - Prospecting of Industrial Minerals: a geophysical approach -
PhD Thesis in Natural Science - University of Sassari

126

ARRAY	WENNER-SCHLUMBERGER n = 5
MEASURED RESISTIVITY POINTS	**1098**
ARRAY LENGTH	**315 m**
INTERELECTRODE SPACING	**5 m**
MAXIMUM INVESTIGATION DEPTH	**60 m**
GPS POINTS	**ELECTRODE 1 -** 40°48'0.53"N; 8°15'29.44" E **ELECTRODE 32 -** 40°47'56.07"N; 8°15'32.51" E **ELECTRODE 64 -** 40°47'51.45"N; 8°15'35.66" E

The N2 profile, NW-SE oriented, was performed in the central part of the palaeovalley where the Messinian clays are outcropping (fig. 7.2).

In the tomography (fig. 7.8) the conductive clays level appears continuous and with resistivity values generally less than 20 Ω·m (blue in colour). The shallow mud-supported conglomerate was detected from the station at 70m to station at 110m (*x-axis*) only, with resistivity values less than 150 Ω·m.

The thickness of clays ranges from a minimum of 10m in the NW sector to a maximum of 25m in the SE sector of the tomography. This level has the trend of the underlying bedrock.

The resistivity values of the bedrock, ranging from 100 Ω·m to up of 500 Ω·m (yellow-red in colours), have the lowest values in the central sector due probably to the fracturing or alteration processes.

Fig. 7.8 - N2 tomography.
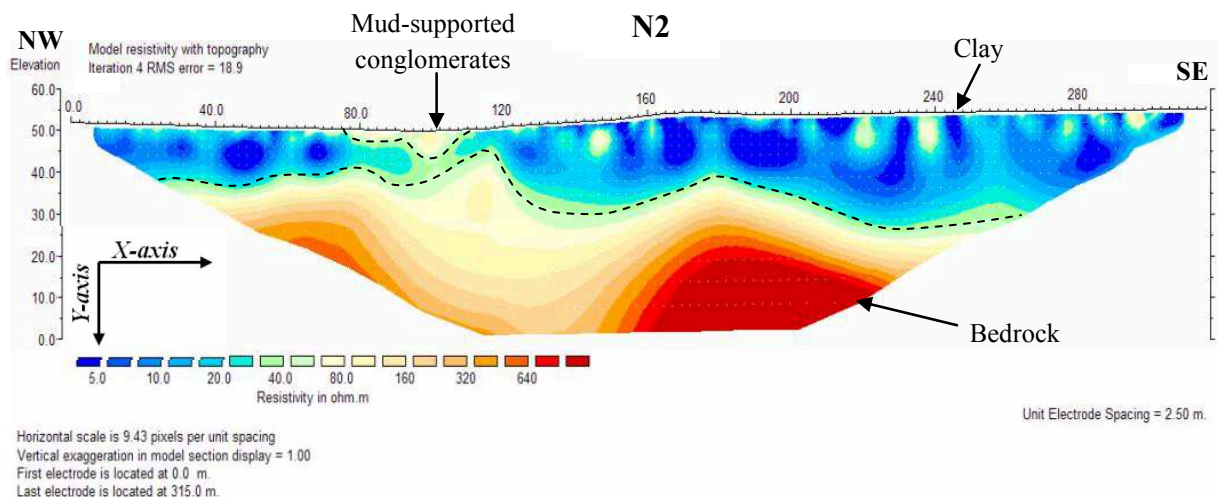
Vittorio Longo - Prospecting of Industrial Minerals: a geophysical approach - PhD Thesis in Natural Science - University of Sassari

127

7.7 - Discussion and conclusions

The resistivity models confirm the stratigraphy derived by some expeditive surveys in the area.

The Messinian clays, with resistivity values generally lower than 40 Ω·m, were discriminated by superficial conglomerates and by underlying bedrock.

The ERT models suggest that the structural setting of the area is affected by wavy and irregular bedrock, with structural highs and depressions filled by Miocene alluvial deposits.

In the eastern part of the palaeovalley, the S1 and S2 tomographies reveal a structural high oriented NE-SW (fig. 7.9), where the clays have reduced thickness of 15-20m and are capped by 5-10m metres thick conglomerates.

In the centre of the palaeovalley the thickness of the clays increases significantly, up to 45m (S3 tomography, fig. 7.5).

The westernmost tomographies, where the evaporites, limestones and redbeds cropping, were performed in order to obtain direct resistivity values on the rocks that are believed for the bedrock of the deposit elsewhere.

Particularly the N3 line started on Triassic limestones and pursued on alluvial deposits (fig. 7.7) showing thin cover of alluvial clay which increases in correspondence of post-messinian fault and toward the centre of the palaeovalley.

Of great interest was the result of the N1 ERT. The low resistivity values of this tomography was affected by high uncertain because compatible with clay or satured Permian redbeds.

The execution of borehole revealed that the resistivity values were referable to satured Permian sandstones.

Even if the central part of the palaeovalley could contain meaningful clay deposits with thickness higher than 50 metres, caution must be adopted when exploitations are planned towards the palaeovalley slopes where the occurrence of satured Permian sediments can cause mistakes in interpreting the lithology of the subsurface rocks.

Vittorio Longo - Prospecting of Industrial Minerals: a geophysical approach -
PhD Thesis in Natural Science - University of Sassari

128
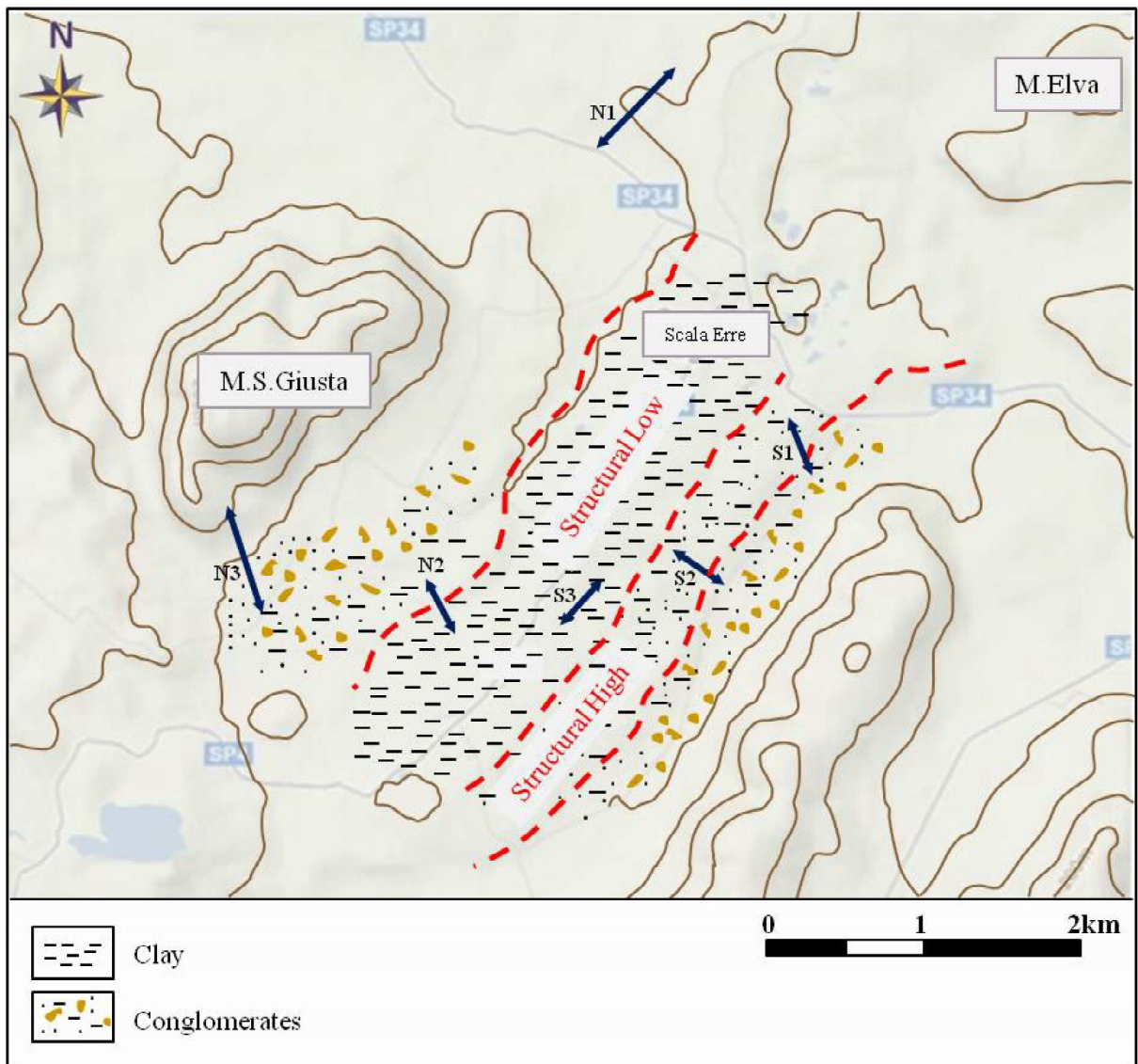
Fig. 7.9 - Interpretative scheme of the study area.

Vittorio Longo - Prospecting of Industrial Minerals: a geophysical approach -
PhD Thesis in Natural Science - University of Sassari

129

References

ABBAZZI, L., DELFINO, M., GALLAI, G., TREBINI, L., AND ROOK, L., 2008. *New data on the vertebrate assemblage of Fiume Santo (North-western Sardinia, Italy), and overview on the Late Miocene Tusco-Sardinia paleobioprovince*: Palaeontology, 51, 425–451.

BUZZI, L., GAGGERO, L., AND OGGIANO, G., 2008. *The Santa Giusta Ignimbrite (NW Sardinia). A clue for the magmatic, structural and sedimentary evolution of a Variscan segment between early Permian and Triassic*: Bollettino della Società Geologica Italiana, 127, 683–695.

DAHLIN, T., 1996. *2D resistivity surveying for environmental and engineering applications.* First Break, 14, 7, 275–283.

DEGROOT-HEDLIN, C., CONSTABLE, S., 1990. *Occam's inversion to generate smooth, two-dimensional models from magnetotelluric data.* Geophysics, 55, 1613–1624.

LOKE, M.H., 2000. *Electrical Imaging Surveys for Environmental and Engineering Studies. A Practical Guide to 2D and 3D Surveys.*

LOKE, M.H., 2001. *Res2Dinv software users manual, version 3.4.* Geotomo Software, Penang, Malaysia, 98.

MAMELI, P., MONGELLI, G., OGGIANO, G., AND DINELLI, E., 2007. *Geological, geochemical and mineralogical features of some bauxite deposits from Nurra (Western Sardinia, Italy): Insights on conditions of formation and parental affinity.* International Journal of Earth Sciences, 96, 887–902.

PASCUCCI, V., TEDDE, M., AND OGGIANO, G., 2004. *Late Messinian valley fill in the Asinara Gulf (NW Sardinia, Italy)*, in Dissertation of 4th International Congress on Environment and Identità in the Mediterranean, Corte, 19–25 July (Corsica, France).

SASAKI, Y., 1992. *Resolution of resistivity tomography inferred from numerical simulation.* Geophys Prospect, 40, 453–464.

SILVESTER, P.P., AND FERRARI, R.L., 1990. *Finite elements for electrical engineers (2nd. ed.).* Cambridge University Press, 516.

THOMAS, B., AND GENNESSAUX, M., 1986. *A two stage rifting in the basin of the Corsica-Sardinia strait*: Marine Geology, 72, 225–239.

Vittorio Longo - Prospecting of Industrial Minerals: a geophysical approach -
PhD Thesis in Natural Science - University of Sassari

130

Chap. 8 - General considerations on ERT method

Despite its obvious suitability, the mining companies do not consider the ERT method as a basic tool in prospecting industrial minerals.

This project has show the advantages that this indirect technique provides compared to conventional investigation methods.

With a conspicuous saving in times and costs the method allowed an accurate assessment of the volume and nature of clay deposits, and proved an invaluable resource in subsequent planning of mining activities.

The ERT surveys moreover evidenced cinerite deposits with significant lateral heterogeneity providing targets for drilling, and have reduced the number of intrusive sample points.

In any case the non-uniqueness or ambiguity of some resistivity models and the loss of resolution in the marginal portions of the images can lead to significant distortions, hence a careful interpretation supported by field survey must be adopted in order to avoid unwanted errors.

Vittorio Longo - Prospecting of Industrial Minerals: a geophysical approach -
PhD Thesis in Natural Science - University of Sassari

131

Ringraziamenti

Desidero ringraziare il Prof. Giacomo Oggiano, relatore di questa tesi e guida durante questi tre anni, la Dott.ssa Paola Mameli, il Dott. Guido Cerri, il Dott. Leonardo Casini, il Dott. Stefano Cuccuru, il Dott. Antonio Brundu, il Dott. Antonio Puccini e il gruppo di ricerca del Dipartimento di Scienze della Natura e del Territorio dell'Università degli Studi di Sassari per il supporto scientifico.

Un particolare ringraziamento va alla Minersarda s.p.a nelle persone di Dott. Geol. Paolo Staritta e Dott. Andrea Testa per la disponibilità nelle indagini di campo, per il materiale cartografico e i dati relativi ai sondaggi.

Infine un doveroso ringraziamento va al Prof. Luigi Carmignani e ai ragazzi del laboratorio di Geofisica e Geofisica Applicata del Centro di GeoTecnologie di San Giovanni Valdarno dell'Università degli Studi di Siena per i preziosi consigli e le nozioni di base sui metodi e sulle strumentazioni impiegate in questo progetto.

Vittorio Longo - Prospecting of Industrial Minerals: a geophysical approach -
PhD Thesis in Natural Science - University of Sassari

132